Breaking Barriers: A Quantitative Analysis of Axon Initial Segment Damage in Neurodegenerative Diseases

Merci Ngozi Best

Richmond, Virginia

M.S. in Biological and Physical Sciences, University of Virginia, 2019

B.S. in Neuroscience, The College of William & Mary, 2017

A Dissertation presented to the Graduate Faculty

of the University of Virginia in Candidacy for the Degree of

Doctor of Philosophy

Department of Pharmacology

University of Virginia

May, 2023

Abstract

Axon initial segment (AIS) damage has been implicated in several neurodegenerative diseases (NDs). Nevertheless, it is unknown whether systematic damage to the AIS is a unifying feature among Alzheimer's disease, amyotrophic lateral sclerosis, frontotemporal dementia, multiple sclerosis, and Parkinson's disease. In this dissertation, it was hypothesized that 1) AIS structural and functional damage occurs in NDs, 2) extracellular tau oligomers (xcTauO) cause damage to the AIS, and 3) xcTauOs cause AIS protein, tripartite motif-containing protein 46 (TRIM46) and lysosomal-associated membrane protein 1 (LAMP1)+ organelles to co-localize. A systematic literature review, quantitive western blots, and quantitative immunofluorescence were performed. The literature review identified 42 studies that quantified 14 AIS structural and two AIS functional parameters in five NDs. The data chapters found that xcTauOs work through intracellular tau to cause a reduction in AIS immunofluorescent intensity as a semi-quantitative measurement of localized protein abundance and AIS shortening. These same xcTauOs also increase AIS protein, TRIM46, and LAMP1 co-localization. Overall the work presented in this dissertation demonstrates that the AIS can be damaged by xcTauOs in NDs.

Dedication Page

I owe a debt of gratitude to God, my Heavenly Father, Jesus Christ, and Holy Spirit for creating me. I would also like to express my gratitude to my ancestors for preparing me. In addition, I would like to thank my family for birthing me. Moreover, my church for maturing me. I am grateful to my sponsors for funding me. I am also forever grateful to my committee for guiding me. My gratitude also extends to teachers, professors, administrators, and mentors for teaching me. I extend a special thanks to my colleagues and lab members for helping me. I also thank my friends for sharpening me. Finally, I would like to thank the STEAM kids for humbling me.

Table of Contents

List of Tables

List of Figures

Chapter One: Introduction

The aim of this introductory chapter is to lay the necessary foundations for this dissertation as a whole. Chapter one introduces the key concept of the axon initial segment (AIS), which is the main focus of this dissertation and underscores its growing importance in the field of neurodegenerative diseases (NDs). It also outlines the structure of the dissertation providing a brief overview of each of the chapters that follow.

In chapter two, there were five key themes explored. These themes include AIS damage in Alzheimer's disease (AD), amyotrophic lateral sclerosis (ALS), frontotemporal dementia (FTD), multiple sclerosis (MS), and Parkinson's disease (PD). Of these, the first AIS damage in ND study was published in 1990 on ALS. Since this early publication, numerous other scholars have followed extending this initial research. The growing interest on the AIS in the ND field is evident with the 42 publications. These studies find evidence for several changes in 14 AIS structural and two AIS functional parameters. Although AIS damage is a unifying feature among NDs, there is a lack of a consensus on whether there is no change, decrease, or increase in the AIS parameters. This is an important gap since understanding AIS damage, could lead to developing solutions to NDs.

Moreover, the majority of AIS damage in ND research efforts have been focused on providing evidence of AIS damage in AD. Despite this, there were no studies to examining extracellular tau oligomers (xcTauOs), which are used to study AD. This presented a need to explore AIS structural parameters in

mouse and human neurons in chapter three. It was found that xcTauOs cause a reduction in AIS immunofluorescent intensity as a semi-quantitative measurement of localized protein abundance and AIS shortening. The mechanism identified for this AIS damage was intracellular tau.

In chapter four, a different effect of xcTauOs was found on the AIS protein, tripartite motif-containing protein 46 (TRIM46). The xcTauOs caused an increase in the co-localization between TRIM46 and LAMP1. The mechanism suggested was phosphorylation of TRIM46 by the AIS kinase, cyclin-dependent kinase five.

The academic reasons to explore AIS damage in ND are also supported by very personal reasons. My maternal grandmother, Dorothy Joyce Sutton and my first mentor Dr. Waide Robinson both passed of NDs. Also, during the final year of my PhD, I served as one of the caregivers for my elderly cousin who was diagnosed with dementia. These personal experiences are shared with others I know who have a loved one with ND. These academic and personal experiences have sparked my interest in ND research field and have ultimately led to my choosing to focus on the AIS as a novel target for future therapeutic intervention for the current research project.

Consequently, the aim of this dissertation is to examine the extent to which AIS damage is involved in ND. This study was conducted in multiple research labs and involved immortalized cell lines, mice brain cells, and human brain tissue. More specifically, this study aims to first ascertain structural and functional parameters of AIS damage. Furthermore, the research questions that are posed in this dissertation also seek to determine a novel mechanism of AIS

damage. The study also hopes to move beyond studying NDs in isolation by investigating systematic AIS damage as a unifying feature among five NDs.

The current research project expands on the AIS damage in NDs. It provides possible parameters to quantify AIS structural and functional damage. It is hoped that this research project might trigger similar studies in other research contexts to corroborate its findings. Together, these studies might provide the necessary insights that can help determine whether AIS damage causes NDs.

In conclusion, this dissertation is organized as five total chapters. This includes Chapter one structured as an introduction. Chapter two structured as a systematic literature review. Chapter three and four structured as research papers. Finally, chapter five structured as a conclusion.

Chapter Two: A Review: Axon Initial Segment Damage in Neurodegenerative Diseases

Merci N. **Best**[a,b] and George S. **Bloom**[a,b,c,*]

[a]Department of Biology, University of Virginia, Charlottesville, VA, USA

[b]Department of Pharmacology, University of Virginia, Charlottesville, VA, USA

[c]Department of Neuroscience, University of Virginia, Charlottesville, VA, USA

[d]Department of Cell Biology, University of Virginia, Charlottesville, VA, USA

Running title: Axon initial segment damage in neurodegenerative diseases

*Correspondence to: George S. Bloom, Department of Biology, University of Virginia, PO Box 400328, Charlottesville, VA 22904-4328, USA; Tel: +1 434 243 3543; E-mail: gsb4g@virginia.edu

Abstract

A commonality among neurodegenerative diseases (NDs) is the disruption of action potential initiation and maintenance of neuronal polarity. The axon initial segment (AIS) neuronal compartment is essential for those two functions. Given that aging populations are susceptible to NDs and currently there are no FDA-approved pharmacological treatments to cure NDs, there exists an urgent need to explore shared mechanisms of NDs. Therefore, the aim of this study is to determine whether systematic damage of the AIS is a unifying feature of NDs and if so, what are mechanisms that cause AIS damage. Using the PubMed database, 42 articles at the intersection of ND and AIS were analyzed. The NDs included Alzheimer's disease, amyotrophic lateral sclerosis, frontotemporal dementia, multiple sclerosis, and Parkinson's disease. Our findings generated 14 structural and two functional AIS parameters that were quantitatively analyzed in NDs. We conclude that AIS damage is a unifying mechanism among NDs. There was however a lack of consensus in the findings including the three most commonly assessed AIS parameters 1) AIS immunofluorescent intensity as a semi-quantitative measurement of localized protein abundance, hereafter referred to as AIS intensity, 2) AIS length, and 3) AIS position. We argue that the inconsistency within and across the ND literature can be attributed to disunity in use of analysis tools. Therefore, future mechanistic studies should make every effort to identify whether AIS damage causes NDs or is a consequence of disease onset using open-access quantitative analysis tools.

Keywords

Axon Initial Segment, Neurodegenerative Disease, Alzheimer's disease, Amyotrophic Lateral Sclerosis, Frontotemporal Dementia, Multiple Sclerosis, Parkinson's Disease

Introduction

Approximately 55 million individuals around the world are diagnosed with a neurodegenerative disease (ND), many of which are fatal [1]. NDs emerge when neurons and their connections in the central and peripheral nervous systems become progressively damaged, lose function, and ultimately die [2–4]. Although there is a lack of a unifying mechanism on the exact cause of NDs, one such element shared among them is the AIS [5,6]. An essential part of the neuron, the AIS functions include action potential initiation and the maintenance of neuronal polarity [7–9]. Thus, any systematic damage to neuronal structure might be explained in part by systematic damage to the AIS.

Given that age is the greatest risk factor for NDs [1], as life expectancy continues to increase, more people may develop NDs. Although, FDA-approved therapeutics may relieve some of the physical or mental symptoms associated with ND onset, there is currently no therapy to prevent or delay neurodegeneration, and there are no known cures [1]. Because these NDs are debilitating, research into understanding their causes is urgent and important [1]. The AIS is a strong candidate for further study because it may be damaged in many NDs as the loss of neuronal structural integrity is a key element of ND pathogenesis [10]. As a result, there is potential that AIS damage could serve as a target of therapeutic intervention for NDs. However, no reviews have been published on AIS damage in NDs.

In this review, we conducted a literature search on the PubMed database with the search terms (AD, AIS, ALS, Alzheimer’s disease, amyotrophic lateral sclerosis, axon initial segment, FTD, frontotemporal dementia, MS, multiple

sclerosis, neurodegenerative disease, neurodegenerative disorder, Parkinson's disease, PD). Our search yielded several studies that quantified the AIS in Alzheimer's disease (AD), amyotrophic lateral sclerosis (ALS), frontotemporal dementia (FTD), multiple sclerosis (MS), and Parkinson's disease (PD). To be as comprehensive as possible, unpublished thesis, dissertations and preprint articles were included. After the 42 sources were identified, we generated 14 AIS structural parameters and two AIS functional parameters shared among AD, ALS, FTD, MS, and PD. The three most common unifying features were AIS intensity, length, and position. Additionally, several mechanistic connections of how damage to the AIS is involved in NDs and potential interventions were identified. These findings suggest that AIS damage is a unifying feature of ND.

Main text

Axon initial segment structure

Most neurons have three major cytoplasmic regions: the dendrites, the soma, and the axon [11–13]. The AIS occupies 20-60 μm of the axon that is most proximal to the soma [6]. The localization of components at the AIS depends on ankyrin-G, a protein that functions as a cytoskeletal scaffold and major regulator of membrane domains [14]. The AIS also structurally includes voltage gated ion channels, actin filaments, actin-binding proteins, cell adhesion molecules, microtubules, and microtubule-associated proteins [6]. In this review the following 16 proteins will be discussed as explicit markers of the AIS: 1) a

disintegrin and metalloproteinase 22 (ADAM22), 2) ankyrin-G, 3) βIV spectrin, 4) calcium/calmodulin-dependent protein kinase II (CAMKII), 5) end-binding protein 1 (EB1), 6) EB3, 7) fibroblast growth factor 14 (FGF14), 8) glycogen synthase kinase 3 beta (GSK3β), 9) voltage-gated potassium channel 7.3 (Kv7.3), 10) voltage-gated sodium channel 1.1 (Nav 1.1), 11) Nav 1.2, 12) Nav 1.6, 13) neurofascin-186 (NF-186), 14) pan Nav, 15) pan neurofascin, and 16) tripartite motif-containing protein 46 (TRIM46) (Figure 1). In this study the literature on AIS structure was divided into the following 14 parameters: 1) branching, 2) density, 3) gene levels, 4) intensity = immunofluorescent intensity as a semi-quantitative measurement of localized protein abundance, 5) length, 6) localization, 7) lysosomes, 8) mitochondria, 9) neurofilaments, 10) position, 11) protein levels, 12) smooth endoplasmic reticulum, 13) synapse size, and 14) width.

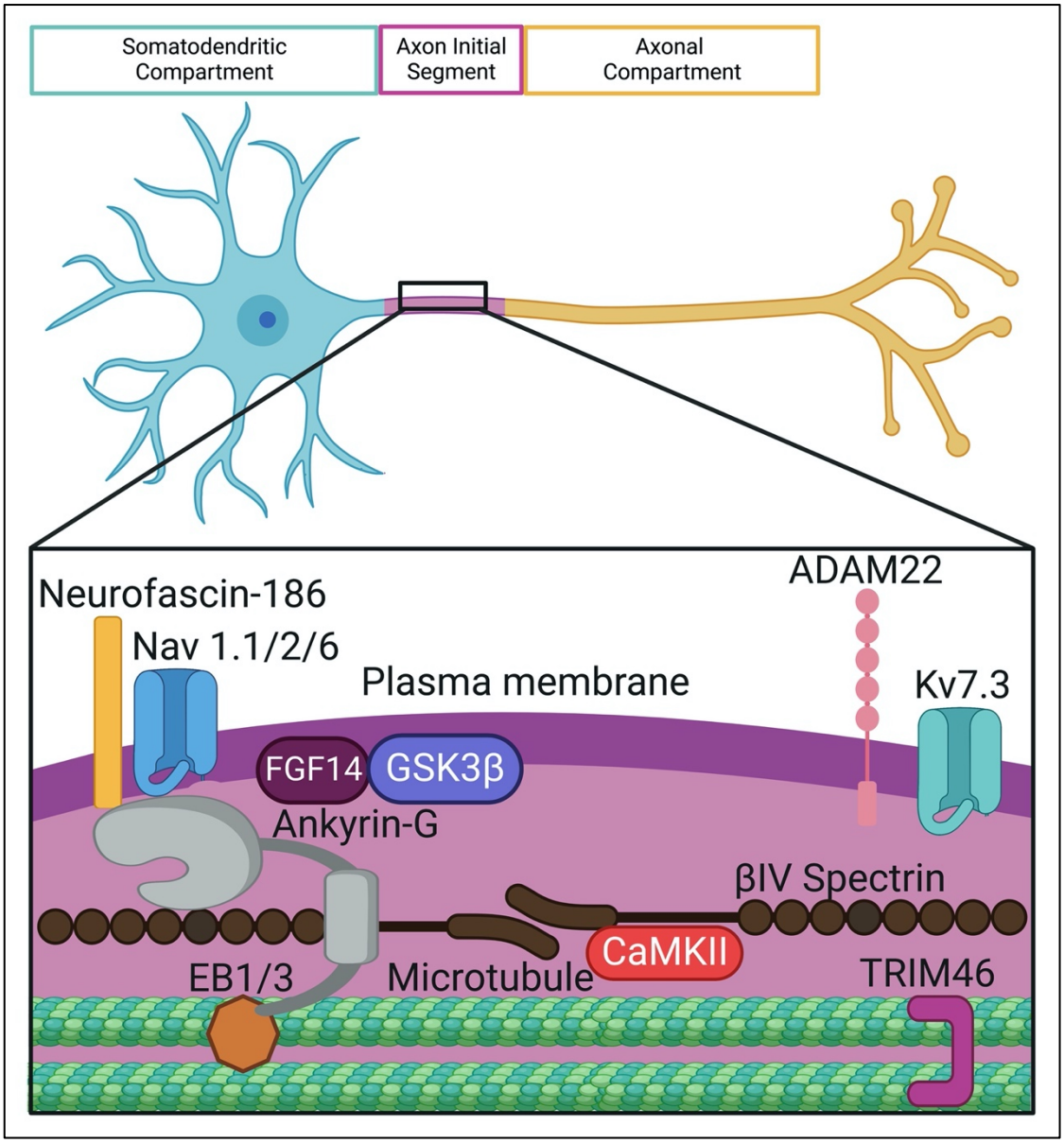

Figure 1. Schematic of a neuron featuring the AIS proteins discussed in this review.

Most healthy neurons are segmented into three distinct compartments the – somatodendritic compartment (cyan), axon initial segment (magenta), axonal compartment (yellow). This model of the AIS includes (from left to right) neurofascin-186 (yellow), Nav 1.1/2/6 (blue), EB1/3 (orange), FGF14 (maroon), ankyrin-G (gray), GSK3β (purple), CaMKII (red), βIV spectrin (brown), ADAM22 (pink), TRIM46 (magenta), and Kv7.3 (cyan).

Axon initial segment function

The AIS has two main roles. The first relates to the neuronal function since the AIS regulates input integration, action potential initiation, propagation, and modulation [15]. At the AIS, inputs from the somatodendritic compartment are converted to generate action potentials [16]. The second relates to the neuronal structure as the AIS is a neuronal barrier that maintains axonal dendritic polarity, thereby ensuring that proteins are trafficked and restricted in their proper locations [9,17]. There is a likely interplay between AIS structure and function because the AIS exhibits signalling- and activity-dependent structural plasticity [18–22]. In this study the literature examining AIS function was divided into the following two categories: 1) action potential initiation and 2) maintenance of neuronal polarity.

Due to the location and structure of the AIS, its disruption has the potential to be implicated in NDs. In fact, the dysregulation or downregulation of AIS-enriched components have been implicated in the pathogenesis of many neurological disorders [23]. Therefore, the aim of this review is to determine whether AIS damage is a unifying feature in NDs. To address this aim, the guiding questions for this review are 1) is the AIS examined in ND field's literature, and 2) if so, what are the parameters and 3) which parameters are most common among NDs? To address these questions, the literature that examines AIS integrity in five NDs: AD, ALS, FTD, MS, and PD will be discussed. Within each ND, these papers were categorized by AIS structural and AIS functional parameters.

Alzheimer's disease

Sporadic or early-onset AD is the most common neurodegenerative disorder [24]. It is typically associated with progressive memory deficits and cortical neurodegeneration in the temporal and parietal lobes [10,25–29]. The characterization of AD includes formation of extracellular amyloid-β (Aβ) plaques and intraneuronal neurofibrillary tangles [25,30–34]. Although the exact cause of AD is unknown, there are over 20 genetic risk factors associated with AD [35]. For those diagnosed with AD, there are seven FDA-approved therapeutics available to treat symptoms [36]. These treatments include three cholinergic inhibitors (donepezil, galantamine, and rivastigmine), one N-methyl D-aspartate receptor antagonist (memantine), a combination of donepezil and memantine, and most recently, two monoclonal anti-Aβ antibodies (Aducanunab and Lequembi) [36]. Unfortunately, none of these drugs have been shown to prevent, delay, or cure AD. Therefore, the AD pharmacological research field could benefit from investigating novel targets such as the AIS.

In AD, the AIS structure has been examined (Table 1). The most common structural parameter analyzed was AIS length. With regards to AIS length, some research suggests that it may not change in AD. These studies used several proteins as markers of the AIS, such as 1) ankyrin-G [37,38], 2) βIV spectrin [37], and 3) neurofascin-186 [39]. This may suggest that AD models fail to modulate AIS length in response to stimuli, an example of the lack of plasticity [38]. In contrast, several studies provide evidence for AIS shortening using the following markers 1) ankyrin-G [37,39–42], 2) βIV spectrin [37,42,43], 3) EB3 [42], 4) Nav 1.2 [39], and 5) TRIM46 [44]. The mechanisms identified

for decrease in AIS length include 1) internalized acetylated tau-induced aggregation [42], 2) intracellular tau [44], and 3) loss of serotonin receptor [39]. A handful of other studies conclude that the AIS lengthens using some of the same AIS markers 1) ankyrin-G [45], 2) βIV spectrin [46], and 3) neurofascin-186 [47]. The mechanisms identified for increase in AIS length include 1) increase in serotonin receptor [47] and 2) soluble β-amyloid [45]. These studies have even identified potential therapies to restore AD model AIS length to control including 1) serotonin receptor antagonist [47] and 2) alpha tubulin deacetylation inhibitor [45].

Table 1. Twenty-four Alzheimer's disease field papers on the axon initial segment

Paper number	Citation	AIS structure										AIS function	
		Branching	Density	Gene levels	Intensity	Length	Localization	Lysosomes	Position	Protein levels	Synapse size	Action potential initation	Maintenance of neuronal polarity
1	Best 2023				↓	↓	↑		–	–			↓
2	Le 2023					↓			–				
3	Antón 2022					↑			↓				
4	Ma 2022		–, ↓			–, ↓			–, ↑	↓			
5	Martinsson 2022				–	↓						↑	
6	Chen 2021					↓			–, ↑			–, ↓	
7	Stroobants 2021							↑					
8	Sun 2021					–, ↓			–, ↑	–		↑	
9	Tiago 2021					–			↓, ↑			↓	
10	Wang 2021				↓								
11	Sos 2020										↑		
12	Butler 2019												↓
13	Hsu 2017				–, ↓, ↑							↓	
14	Hu 2017	↑				↑			↓				
15	Zempel 2017				↓								↓
16	Marin 2016		↓			↓							
17	Sohn 2016									↓			↓
18	Wang 2016				↑					↑		↑	
19	Tsushima 2015					↑	↑					↑	
20	Sun 2014, Cell Reports				↓					↓			
21	Sun 2014, PNAS						↓			↓			
22	Sanchez-Mut 2013			↓						↑			
23	Santuccione 2013				↑		↑			↑			
24	Li 2011												↓
Key: – = no change, ↓ = decrease, ↑ = increase													

In many of these same studies on AIS length, AIS position was also analyzed, with some research suggesting that AIS position does not change using 1) ankyrin-G [37,41,42], 2) neurofascin-186 [39], 3) TRIM46 [44]. Others, however, suggested that AIS position decrease as the start became more proximal using 1) ankyrin-G [38], 2) βIV spectrin [46], 3) neurofascin-186 [47]. The mechanisms that lead to a decrease in AIS position include 1) loss of phospholipids [38] and 2) an increase in serotonin receptor [47]. The potential

therapies identified that could restore AD model AIS position to control include 1) exogenous lipids [38], 2) increase kinase activation [38], 3) serotonin receptor antagonist [47]. In addition, AIS position is suggested to increase because the start of the AIS becomes more distal starting further down the axon using the markers 1) ADAM22 [38], 2) ankyrin-G [37–39,41], 3) βIV spectrin [37] 4) FGF14 [38], 5) pan Nav [38], 6) Nav 1.2 [39]. The only mechanisms identified for the increase in AIS position is loss of serotonin receptor [39].

The next largest category of studies focused on AIS intensity. Two studies suggested that AIS intensity does not change using two markers that were not previously analyzed for length and position 1) CaMKII [40] and 2) FGF14 [48]. Most studies on AIS intensity suggest a decrease using 1) ankyrin-G [49–51], 2) Nav 1.2 [50]), 3) pan Nav [48], and 4) TRIM46 [44]. The only mechanisms identified for a decrease in AIS intensity included extracellular tau oligomers working through intracellular tau [44]. In contrast, other studies suggest that AIS intensity increases using 1) ankyrin-G [48,52] and 2) Nav 1.6 [50]. The mechanisms identified for an increase AIS intensity include 1) phosphorylation of an AIS kinase, which can be attenuated using an FDA-approved treatment for diabetes [48].

In addition to AIS intensity, AIS protein levels have been examined in the literature. Several studies have found that AIS protein levels do not change using 1) ankyrin-G [39], 2) Nav 1.2 [39], 3) TRIM46 [44]. Other studies analyzing the main two AIS structural proteins 1) ankyrin-G [37,51,53,54], 2) βIV spectrin [54] find that AIS protein levels decrease. The only mechanisms identified for decrease in AIS protein levels include micro-RNA induced reduction in ankyrin-G expression [51]. In contrast, the same AIS proteins and others were found to

increase in other studies using 1) ankyrin-G [52], 2) βIV spectrin [55], 3) pan Nav [50], 4) Nav 1.6 [50] – yet no mechanisms have been identified.

A handful of other papers examine other AIS structural parameters. For example, AIS protein localization has been both suggested to decrease using 1) Nav 1.6 [53] and increase using 1) ankyrin-G [45,52], 2) EB3 [45], and 3) TRIM46 [44]. On the other hand, it increases with1) soluble Aβ [45] and 2) tau oligomers [44]. The only potential therapeutic identified to restore AD model AIS protein localization to control is an alpha tubulin deacetylation inhibitor [45]. AIS density has been suggested to either not change using 1) ankyrin-G [37] and 2) βIV spectrin [37] or decrease using βIV spectrin [37,43].

Only one paper each examined the remaining AIS structural parameters. One suggests a decrease in AIS gene levels using βIV spectrin [55]. In contrast, increases were suggested in AIS branching using neurofascin-186 [47]. In this study expression of serotonin receptor was responsible for this increase and could be attenuated by a serotonin receptor antagonist [47]. AIS synapse size [56] and lysosomes [57] were both suggested to increase. While no mechanism has been identified for the synapse size, genetic variants were demonstrated to lead to increase in lysosomes [57].

Changes in AIS structure are hypothesized to reflect changes in AIS function – namely in action potential initiation and maintenance of neuronal polarity. Only one paper suggests the contrary that AIS action potential initiation does not change [41]. Two papers suggest that AIS action potential initiation decrease but lack a mechanism [38,41]. Many papers suggest that AIS action potential initiation increase [39,40,45,50] likely due to two mechanisms: 1) loss of serotonin receptor [39] and 2) soluble Aβ [45]. The potential therapies

identified for AIS action potential initiation increase include 1) an alpha tubulin deacetylation inhibitor [45], 2) inhibitory receptor antagonist [40].

All studies in AD literature as it relates to the AIS suggest that maintenance of neuronal polarity is decreased [44,45,49,53,54,58,59]. Several mechanisms have been identified for decrease in AIS maintenance of neuronal polarity 1) genetic variant [58], 2) loss of AIS protein [49,60], 3) micro-RNA [53], 4) over activation of AIS kinase [49], 5) tau acetylation [54], 6) tau phosphorylation [59], and 7) soluble Aβ oligomer [45,49]. The potential therapies include 1) an alpha tubulin deacetylation inhibitor [45], 2) exogenous ankyrin-G [53,60], and 3) microtubule stabilizer [54]. There have even been two reports that these agents that repair the AIS contribute to recovery of cognitive impairment in AD models [47,53].

Although there is no full consensus yet about whether AIS structure and function changes occur before or after AD onset, these results suggest that AIS disruption could be an early-stage therapeutic target for AD-associated cognitive impairment. To provide insight into whether the AIS should be a therapeutic target or not, direct studies are needed to understand how AIS disruption alters neuronal function in specific AD models. These findings would move the field from association and establish causality.

Amyotrophic lateral sclerosis

Sporadic or familial-type ALS are NDs with an early age of onset. ALS is characterized by progressive loss of motor neurons, which leads to numerous motor deficits [61,62]. ALS can be caused by several risk factors [63], such as

genetic alterations, including a mutation in the superoxide dismutase 1 (SOD1) gene [61,64]. There are five FDA-approved ALS drugs: edaravone, riluzole, riluzole oral suspension, riluzole oral film, and dextromethorphan/ quinidine [61,65–67]. Unfortunately, none of these five drugs can prevent, delay, or cure ALS. There is hope for a new experimental drug, NU-9 [68] – yet considering these limitations, ALS drug discovery efforts could centralize the investigation of novel targets such as the AIS.

In, ALS, there are several papers that explore AIS structure and function with the vast majority assess AIS length (Table 2). Two reports using ankyrin-G as a marker suggest that AIS length does not change [69,70]. This lack of change may corroborate, on article that suggest an overall reduction in AIS plasticity [71]. There are however numerous findings of AIS shortening and lengthening, which suggest a shared mechanism whereby genetic variants in models of ALS can contribute to different effects on AIS length and action potential initiation – even within the same manuscript [71,72]. AIS length is suggested to decrease using 1) ankyrin-G [69,71,72] and 2) Nav 1.6 [73]. In contrast, AIS length increases using the same markers 1) ankyrin-G [69,71] and 2) Nav 1.6 [64,73].

Table 2. Eleven amyotrophic lateral sclerosis field papers on the axon initial segment

Paper number	Citation	AIS structure									AIS function
		Gene levels	Intensity	Length	Lysosomes	Mitochondria	Neurofilaments	Position	Smooth endoplasmic reticulum	Width	Action potential initation
1	Bos 2022		–	↓							↓
2	Harley 2022	↓, ↑	↑	↓, ↑				–, ↑			↓, ↑
3	Kiryu-Seo 2022		↓	–		↓					
4	Jorgensen 2021			↑				–		↓	↑
5	Stroobants 2021				↑						
6	Bonnevie 2020			↓, ↑				–, ↑		–, ↓, ↑	–,
7	Smerdon 2019			–, ↓, ↑							↓, ↑
8	Sasaki 2007					↑					
9	Sasaki 2005					↑	↑				
10	Sasaki 1992					↑	↑		↑	↑	
11	Sasaki 1990						↑			↑	
Key: – = no change, ↓ = decrease, ↑ = increase											

Many of the previous papers assessing AIS length connected their findings to changes in AIS function, namely action potential initiation. In essence AIS shortening was reflective of hypoexcitability, whereas AIS lengthening was reflective of hyperexcitability [64,69,71,72]. In some models AIS action potential initiation does not change [64,72,73]. In other studies, AIS action potential initiation is suggested to either decrease [69,71,72] or increase [69,71].

There are only two parameters for AIS position and gene levels. In the case of AIS position, studies suggest no change using 1) ankyrin-G (Harley 2022), 2) Nav 1.6 [64,73] or increase using 1) ankyrin-G [71] or 2) Nav 1.6 [73]. In the case of AIS gene levels studies suggest both – decrease in 1) Nav 1.1 and 2) Nav 1.6 [71] and an increase in 1) ankyrin-G, 2) Nav 1.1, and 3) Nav 1.6 [71]. The mechanisms identified for increase in AIS position and either decrease or increase in AIS gene levels is genetic variants [71].

There are all three parameters for AIS intensity using ankyrin-G – no change [72], decrease [70], and increase based on the genetic variant mechanism [71]. AIS width has not been studied in the context of AD, however in ALS it has been suggested to show all three parameters no change using Nav 1.6 [73], decrease using the same marker [64,73], and increase using either 1) electron microscopy [74,75] or 2) Nav 1.6 [73].

A subset of the AIS in ALS literature utilizes electron microscopy approaches to analyze AIS structure. Only one paper suggest that AIS mitochondria decrease [70]. However, the others suggest that AIS mitochondria increase [74,76,77], AIS smooth endoplasmic reticulum increase [74], AIS neurofilament increase [74,75,77], and AIS lysosomes increase [57]. Similarly, to the previously identified mechanisms, the mechanisms identified for increase

in AIS lysosomes is genetic variants discussed previously in the AD section [57].

Collectively, these studies provide a small but convincing body of evidence that genetic variants are related to changes in both AIS structure and function. To build on this foundational work, the ALS field could benefit from additional studies using both cell and mouse models of ALS to better determine which mouse models are most reflective of humans with ALS and build the case for robust analysis of the AIS structure in post-mortem human brain tissue.

Frontotemporal dementia

FTD is a group of NDs in which the behaviour, language, executive and often motor function regions of the frontal and/or temporal lobes degenerate to a varying degree [78,79]. These regions often have intraneuronal NFT [78,79]. Although, most cases of FTD are sporadic, there are direct disease-causing pathogenic mutations in genes, including MAPT and TMEM106B [79,80]. Currently, there are no FDA-approved therapies intended specifically for FTD. Several emerging potential therapies are still being developed or tested during clinical trials to prevent intellectual decline, behavioral problems, sleep related issues, associated medical problems, and abrupt decline [81,82]. Due to the lack of specific FTD FDA-approved therapeutics, the FTD field could benefit from exploring the AIS as a novel target.

The FTD literature on the AIS is limited assesses both AIS structure and function (Table 3). Most of the AIS structure studies examine AIS lysosomes and suggest no change using 1) ankyrin-G [83] and 2) βIV spectrin [83] or

increase using 1) ankyrin-G [57,83], 2) βIV spectrin [83], and 3) neurofascin [84]. The mechanism identified for an increase in AIS lysosomes is consistent across three studies genetic variants [57,83,84]. Two other parameters AIS intensity and position suggest there is no change or an increase. In the same study using two different markers Sohn (2019) suggests that AIS intensity does not change using ankyrin-G but increases using EB3 [85]. The mechanisms identified for an increase in AIS intensity is genetic variants [85]. The potential therapies are a reduction in protein levels [85]. While Sohn (2019) suggest that AIS position does not change using 1) ankyrin-G [85], Hatch (2017) suggest that AIS position increases using 1) ankyrin-G [86], 2) βIV spectrin [86], and 3) Nav 1.6 [86]. The mechanisms identified for an increase in AIS position is genetic variants [86]. The same study identified microtubule stabilizers as a potential therapy that could restore FTD AIS position to the control [86]. In contrast, the conflicting reports on AIS length both using ankyrin-G suggest no change [86] or a decrease [85].

Table 3. Six frontotemporal dementia field papers on the axon initial segment

Paper number	Citation	AIS structure				AIS function	
		Intensity	Length	Lysosomes	Position	Action potential initation	Maintenance of neuronal polarity
1	Stroobants 2021			↑			
2	Feng 2020			↑			
3	Lüningschrör 2020			–, ↑			
4	Butler 2019						↓
5	Sohn 2019	–, ↑	↓		–	–, ↓, ↑	
6	Hatch 2017		–		↑	↓	
Key: – = no change, ↓ = decrease, ↑ = increase							

Three studies have examined AIS function in FTD. AIS action potential initiation is suggested to not change [85], decrease [85,86], and increase [85]. The mechanisms identified for a decrease or increase in AIS action potential

initiation is genetic variants [85,86]. The potential therapies identified are 1) microtubule stabilizers [86] and 2) reduction in protein levels [85], respectively. The other AIS functional parameter AIS maintenance of neuronal polarity has been suggested to decrease with a mechanism of genetic variants that was previously discussed in the AD section [58].

Although both AIS functional parameters have been examined in the FTD literature, several AIS structural parameters have yet to be examined. A few FTD studies provide evidence that genetic variants are associated with AIS damage. Future studies should make every effort to examines the AIS in human samples as the incorporation of this data would provide the human relevance needed to strengthen the rationale that the AIS damage is involved in FTD pathogenesis.

Multiple sclerosis

MS is a neurological disease that attacks central nervous system myelinated axons, which causes brain lesions that can lead to severe physical or cognitive disability and neurological defects [87–89]. The two forms of MS include chronic autoimmune and inflammatory [88]. Several factors can contribute to the development of MS, including exposure to infectious viral agents that can lead to immune system events, neuronal death, nerve demyelination, and neuronal dysfunction [87,88]. If these risk factors contribute to MS onset, there are eight anti-inflammatory and immunomodulatory FDA-approved MS therapeutics [87]. These include beta interferons (Avonex, Betaseron, Rebif, Extavia); a glatiramer acetate (copaxone); mitoxantrone (noanthrone); recombinant

humanized immunoglobulin monoclonal antibody natalizumab's (tysabri); and fingolimod [88]. Because these only treat symptoms, the MS field needs careful examination of the AIS as a novel target for therapeutic investigation.

There are only four papers that investigate the AIS in the MS field (Table 4). Surprisingly, this small body of literature has used human samples, transgenic mouse, and computational models of MS to investigate both AIS structure and function. Most of these studies investigated AIS length and suggest all three parameters no change, increase, and decrease in AIS length. The studies that suggest no change in AIS length used 1) ankyrin G [90–92], 2) βIV spectrin [90], and 3) pan Nav [90]. In contrast, AIS length is suggested to decrease using 1) ankyrin-G [92] and 2) Nav 1.6 [90] or increase using 1) ankyrin-G [91] and 2) Kv7.3 [90]. As a potential therapy, demyelination has been suggested in one study to restore models of MS AIS length to control using 1) βIV spectrin, 2) Kv7.3, and 3) Nav 1.6 [90]. Hamada (2015) connects changes in AIS length and position to reduction in action potential initiation. This is the only paper in the MS field to examine an AIS function parameter and suggest that AIS action potential initiation decrease [90].

Table 4. Four multiple sclerosis field papers on the axon initial segment

Paper number	Citation	AIS structure				AIS function
		Density	Length	Position	Protein levels	Action potential initation
1	Senol 2022		–, ↑	↑		
2	Hamanda 2015		–, ↓, ↑	–, ↓		↓
3	Mathey 2007				↑	
4	Thummala 2015	–, ↓	–, ↓		↓	
Key: – = no change, ↓ = decrease, ↑ = increase						

Moreover, AIS position has been suggested to not change, decrease, and increase. One study using Kv7.3 suggest that the AIS position does not change [90]. In that same study using two different markers of the AIS βIV spectrin and Nav 1.6 AIS position was suggested to decrease [90]. In a different study using ankyrin-G, AIS position was suggested to increase [91]. The remaining two AIS structures examined were AIS density and protein levels. AIS density using ankyrin-G was suggested in the same study to not change in a mouse model yet decrease in post-mortem human brain tissue [92]. In contrast, the AIS protein level findings span across two papers and use two different markers of the AIS. Thummala's (2015) findings using ankyrin-G suggest AIS protein levels decrease, while Mathey's (2007) findings using neurofascin-186 suggest that AIS protein levels increase [92,93].

Collectively, these studies provide limited evidence of AIS structural and functional damage in MS. There was, however, one study that presented a potential therapeutic intervention that warrants further investigation. Nevertheless, it is still unclear what mechanisms are responsible for this damage as none of the four studies provided any mechanistic data.

Parkinson's disease

Parkinson's disease (PD) is the second most common ND after AD [94]. It is typically associated with both physiological and cognitive difficulties. PD is caused by the degeneration of neurons in the substantia nigra (SN), which causes a deficiency in striatal dopamine [94–96]. The characterization of PD includes the formation of intracellular alpha synuclein inclusions [96]. There are

numerous PD risk factors [96]. There are two FDA-approved therapeutics at hand to treat PD symptoms. These include a dopamine agonist (levodopa) and a selective adenosine A2A receptor antagonist (istradefylline) [94,97]. Currently, these therapeutics are unable to prevent, delay, or cure PD. Therefore, PD pharmacological research could be advanced by exploring novel targets such as the AIS.

Only three papers on AIS structure and function in PD were identified (Table 5). In brief, the findings that suggest no change in AIS length, likely due to a lack of plasticity [38]. There was a suggested decrease in 1) AIS position because of phospholipid loss that can be restored with exogenous lipids [38], 2) AIS action potential initiation [38], and 3) AIS maintenance of neuronal polarity due to a genetic variant [58]. In contrast there was an increase in 1) AIS position – yet the mechanism remains unidentified [38] and 2) AIS lysosomes due to genetic variants [57].

Table 5. Three Parkinson's disease field papers on the axon initial segment

Paper number	Citation	AIS structure			AIS function	
		Length	Lysosomes	Position	Action potential initation	Maintenance of neuronal polarity
1	Stroobants 2021		↑			
2	Tiago 2021	–		↓, ↑	↓	
3	Butler 2019					↓
Key: – = no change, ↓ = decrease, ↑ = increase						

Collectively, these studies provide some mechanistic evidence to suggest that genetic mutations influence AIS damage in PD and even provide a potential therapeutic intervention for further study. Considering this body of work

currently lacks any data using human samples, more research must be conducted to determine whether AIS disruption occurs in PD humans.

Concluding section

In this review we found 42 papers that suggest that systematic damage of the AIS is a unifying feature of five NDs AD, ALS, FTD, MS, and PD (Table 6). The practical implications of this work include the identification of several shared AIS structural and functional parameters, mechanisms, and pharmacological interventions. However, there were several limitations. There was a lack of consensus in the use of analytical tools to measure the most commonly assessed parameters. Additionally, not all NDs had studies that explicitly measured AIS structural or functional parameters.

To build a more cohesive understanding of AIS structure and function across the NDs discussed in this review, it is recommended that future NDs studies focus on the parameters of the AIS structure and/or function that have yet to be analyzed in the literature. In doing so, future AIS studies should prioritize research questions that uncover mechanism to determine whether AIS damage causes NDs or is a consequence of disease onset.

Table 6. Forty-two neurodegenerative disease field papers on the axon initial segment

Paper number	Citation	ND	AIS Structure														AIS function	
			Branching	Density	Gene levels	Intensity	Length	Localization	Lysosomes	Mitochondria	Neurofilaments	Position	Protein levels	Smooth endoplasmic reticulum	Synapse size	Width	Action potential initation	Maintenance of neuronal polarity
1	Best 2023	AD				↓	↓	↑				–	–					↓
2	Le 2023	AD					↓					–						
3	Antón 2022	AD					↑					↓						
4	Bos 2022	ALS				–	↓										↓	
5	Harley 2022	ALS			↓, ↑	↑	↓, ↑					–, ↑					↓, ↑	
6	Kiryu-Seo 2022	ALS				↓	–			↓								
7	Ma 2022	AD		–, ↓			–, ↓,					–,↑	↓					
8	Martinsson 2022	AD				–	↓										↑	
9	Senol 2022	MS					–, ↑					↑						
10	Chen 2021	AD					↓					–, ↑					–, ↓	
11	Jørgensen 2021	ALS					↑					–				↓	↓	
12	Stroobants 2021	AD, ALS, FTD, PD							↑									
13	Sun 2021	AD					–, ↓					–, ↑	–				↑	
14	Tiago 2021	AD, PD					–					↓, ↑					↓	
15	Wang 2021	AD				↓												
16	Bonnevie 2020	ALS					↓, ↑					–, ↑				–, ↓, ↑	–,	
17	Feng 2020	FTD							↑									
18	Lüningschrör 2020	FTD							–, ↑									
19	Sos 2020	AD													↑			
20	Butler 2019	AD, FTD, PD																↓
21	Smerdon 2019	ALS					–, ↓, ↑										↓	
22	Sohn 2019	FTD				–, ↑	↓					–					–, ↓, ↑	
23	Hatch 2017	FTD					–					↑					↓	
24	Hsu 2017	AD				–, ↓, ↑											↓	
25	Hu 2017	AD	↑				↑					↓						
26	Zempel 2017	AD				↓												↓
27	Marin 2016	AD		↓			↓											
28	Sohn 2016	AD											↓					↓
29	Wang 2016	AD				↑							↑				↑	
30	Hamanda 2015	MS					–, ↓, ↑					–, ↓					↓	
31	Thummala 2015	MS		–, ↓			–, ↓						↓					
32	Tsushima 2015	AD					↑	↑									↑	
33	Sun 2014, Cell Reports	AD				↓							↓					
34	Sun 2014, PNAS	AD						↓					↓					
35	Sanchez-Mut 2013	AD			↓								↑					
36	Santuccione 2013	AD				↑		↑					↑					
37	Li 2011	AD																↓
38	Mathey 2007	MS											↑					
39	Sasaki 2007	ALS								↑								
40	Sasaki 2005	ALS								↑	↑							
41	Sasaki 1992	ALS								↑	↑			↑		↑		
42	Sasaki 1990	ALS									↑					↑		
Key: – = no change, ↓ = decrease, ↑ = increase																		

Chapter Three: Extracellular Tau Oligomers Damage the Axon Initial Segment[1]

Merci N. **Best**[a,b], Yunu **Lim**[a], Nina N. **Ferenc**[a], Nayoung **Kim**[a], Lia **Min**[c], Dora Bigler **Wang**[a], Kamyar **Sharifi**[a], Anna E. **Wasserman**[a], Sloane A. **McTavish**[a], Karsten H. **Siller**[d], Marieke K. **Jones**[e], Paul M. **Jenkins**[c,f], James W. **Mandell**[g] and George S. **Bloom**[a,h,i,*]

[a]Department of Biology, University of Virginia, Charlottesville, VA, USA

[b]Department of Pharmacology, University of Virginia, Charlottesville, VA, USA

[c]Department of Pharmacology, University of Michigan Medical School, Ann Arbor, MI, USA

[d]Research Computing, University of Virginia, Charlottesville, VA, USA

[e]Claude Moore Health Sciences Library, University of Virginia, Charlottesville, VA, USA

[f]Department of Psychiatry, University of Michigan Medical School, Ann Arbor, MI, USA

[g]Department of Pathology, University of Virginia, Charlottesville, VA, USA

[h]Department of Cell Biology, University of Virginia, Charlottesville, VA, USA

[i]Department of Neuroscience, University of Virginia, Charlottesville, VA, USA

---

[1] Chapter three was accepted for publication in the Journal of Alzheimer's Disease

Running title: Tau oligomers damage the axon initial segment

*Correspondence to: George S. Bloom, Department of Biology, University of Virginia, PO Box 400328, Charlottesville, VA 22904-4328, USA; Tel: +1 434 243 3543; E-mail: gsb4g@virginia.edu

Abstract

Background: In Alzheimer's disease (AD) brain, neuronal polarity and synaptic connectivity are compromised. A key structure for regulating polarity and functions of neurons is the axon initial segment (AIS), which segregates somatodendritic from axonal proteins and initiates action potentials. Toxic tau species, including extracellular oligomers (xcTauOs), spread tau pathology from neuron to neuron by a prion-like process, but few other cell biological effects of xcTauOs have been described.

Objective: Test the hypothesis that AIS structure is sensitive to xcTauOs.

Methods: Cultured wild type (WT) and tau knockout (KO) mouse cortical neurons were exposed to xcTauOs, and quantitative western blotting and immunofluorescence microscopy with anti-TRIM46 monitored effects on the AIS. The same methods were used to compare TRIM46 and two other resident AIS proteins in human hippocampal tissue obtained from AD and age-matched non-AD donors.

Results: Without affecting total TRIM46 levels, xcTauOs reduce the concentration of TRIM46 within the AIS and cause AIS shortening in cultured WT, but not TKO neurons. Lentiviral-driven tau expression in tau KO neurons rescues AIS length sensitivity to xcTauOs. In human AD hippocampus, the overall protein levels of multiple resident AIS proteins are unchanged compared to non-AD brain, but TRIM46 concentration within the AIS and AIS length are reduced in neurons containing neurofibrillary tangles (NFTs).

Conclusion: xcTauOs cause partial AIS damage in cultured neurons by a mechanism dependent on intracellular tau, thereby raising the possibility that

the observed AIS reduction in AD neurons *in vivo* is caused by xcTauOs working in concert with endogenous neuronal tau.

Keywords

Axon Initial Segment, Alzheimer's Disease, tau Proteins, TRIM46 protein, neurofascin protein, ankyrin-G protein

Introduction

A hallmark of Alzheimer's disease (AD) is the accumulation in neurons of neurofibrillary tangles (NFTs) in neurons, which correspond to tightly packed filament bundles of tau, a microtubule-associated protein normally enriched in axons [98–100]. Prior to NFT formation, misfolded forms of tau, including monomers, oligomers, and short filaments, can escape from diseased neurons, and then enter nearby neurons provoking toxic misfolding of their endogenous tau [101–105]. This prion-like mechanism of tau misfolding may explain how secreted tau propagates intracellular tau pathology from neuron to neuron [106–111].

While the mechanisms of inter-neuronal tau exchange have been extensively studied, knowledge of how neuronal structure and behavior are affected by this process is limited. What is known, however, points to profound effects on neuronal polarity and neurotransmission. For example, we previously showed that one conspicuous effect of extracellular tau oligomers (xcTauOs) on cultured mouse cortical neurons is the accumulation of endogenous tau in the somatodendritic compartment [112]. Prior studies have demonstrated that excess somatodendritic tau can cause hyperexcitability of NMDA receptors, synapse loss and neuron death [113–117], and that xcTauOs can alter action potential dynamics, disrupt synaptic transmission, and impair neuronal plasticity [118].

The loss of endogenous tau polarity caused by xcTauOs [112] prompted us to test the hypothesis that the axon initial segment (AIS) is a target of xcTauOs. The AIS serves two major functions. It is the site of action potential initiation,

and it serves as a diffusion barrier that helps to segregate somatodendritic from axonal molecules and organelles [5,7,59,119,120]. The AIS is located within the first 20-60 μm of the proximal end of the axon, and its length and distance from the soma are instrumental for initiating and shaping action potentials [43,121,122]. The AIS is organized by the sub-membranous cytoskeletal proteins, ankyrin-G [119,123–129] and βIV-spectrin [130–133]; the transmembrane cell adhesion protein, neurofascin-186 (NF-186) [120,134–136]; and the microtubule-associated protein, TRIM46 [134,137–139]; among other proteins. Notably, depletion of AIS structural proteins results in AD-like tau accumulation in the somatodendritic compartment [49,137].

Dysregulation or partial loss of the AIS, as evidenced by even small morphometric changes in AIS structure, has been implicated in various adverse effects both *in vitro* in cultured neurons and *in vivo* in brain [43,45,46,49,51,53,54,59,140]. However, evidence regarding AIS integrity in AD human brain is contradictory. Sohn and colleagues reported that AIS structure is reduced in AD neurons [54], whereas Antón-Fernández and colleagues provided evidence that hyperphosphorylated tau in AD neurons correlates with a longer AIS [46]. One reason this discrepancy has not been resolved is that direct effects of tau aggregates, like xcTauOs and filaments, on AIS protein content and morphology had never been investigated to the best of our knowledge. Accordingly, we decided to address the following questions: 1) Is AIS morphology affected by xcTauOs? 2) Are AIS protein levels downregulated in AD hippocampus? 3) Is AIS length correlated with the presence of NFTs in the same neuron?

To address these questions, we quantified AIS protein content and morphology in primary mouse cortical neuron cultures and post-mortem human hippocampal tissue using quantitative western blotting and immunofluorescence microscopy. For cultured neurons, we found that xcTauOs cause a reduction of the TRIM46 concentration within the AIS and AIS shortening from its distal end, but no changes in overall TRIM46 protein levels. Similarly, in human AD hippocampus, we found that the overall levels of multiple resident AIS proteins are unchanged compared to non-AD brain, but TRIM46 concentration within the AIS and AIS length are reduced in NFT-containing neurons. Collectively, these findings prompt the hypothesis that xcTauOs work in concert with endogenous intraneuronal tau to degrade the AIS *in vivo* AD brain.

Materials and methods

Mice

Wild type (WT; C57/BL6J, https://www.jax.org/strain/000664) and tau knockout (KO, https://www.jax.org/strain/007251) mice were used for this study. Animals were maintained, bred, and euthanized in compliance with all policies of the Animal Care and Use Committee of the University of Virginia.

Cultured neurons

Primary mouse cortical neuron cultures were prepared from WT and tau KO E16.5 embryonic brains using a standard protocol [141]. Briefly, brain cortices

were dissected from embryos and minced with a scalpel in Hank's balanced salt solution (HBSS, Gibco 14175-095) containing 0.25% trypsin (Gibco 15090-046) and deoxyribonuclease I (Worthington LK003170). The minced tissue suspension was incubated at 37°C for 30 minutes, the dissociated tissue was then pelleted in a clinical centrifuge, re-suspended in HBSS, and triturated using a plastic P1000 pipette tip or a glass Pasteur pipette. After centrifugation at 900 RPM for 10 minutes, the cells were suspended in Neurobasal medium (Gibco 21103-049) supplemented with 5% fetal bovine serum (Optima FBS, R&D Systems S12450), B-27 (Gibco 17504-044) or B-27+ (Gibco A35828-01), 2 mM L-glutamine (Gibco 25030-081), 50 µg/ml gentamicin (Gibco 15710-064), and 15 mM D-(+)-glucose monohydrate (Sigma-Aldrich 16301). The cells were then plated at a density of 1.125 million cells/cm^2 on #1 thickness, 12 mm round glass coverslips (Chem Glass CLS-1760-012) in 24-well dishes (Corning 353504), or without coverslips in 12-well (Costar, Cat# 3513) or 6-well (CELLSTAR 657-160) plates following coating of the cell attachment surfaces with poly-D-lysine hydrobromide (Sigma-Aldrich P0899). Cultures were placed in a humidified incubator maintained at 37°C and 5% CO_2, the following day the medium was replaced with a fresh medium that lacked serum, and finally the cells were grown for a total of 7-22 days with 50% medium changes at least once per week. Primary cortical neurons were treated at 6-21 days *in vitro* for 24 hours with xcTauOs diluted to 125 nM total tau or with vehicle.

Tau lentivirus

Lentiviral particles encoding WT human 2N4R tau were prepared using the TRIPZ Trans-Lentiviral Open Reading Frame kit [142] in conjunction with the pBOB-NepX or pLKO.1 expression plasmids, and the packaging vectors, pSPAX2 and pMD2.G (Addgene plasmids 12260 and 12259, respectively; deposited by Dr. Didier Trono, École Polytechnique Fédérale de Lausanne). These collective plasmids were transfected using Lipofectamine 3000 (Thermo Fisher Scientific L3000-015) into HEK293T cells grown in Dulbecco's Modified Eagle Medium (Gibco 11965-092) supplemented with Cosmic Calf Serum (HyClone SH30087.03) to 10% and gentamycin to 50 µg/ml. Lentivirus-conditioned medium was collected 48 hours and 72 hours after the start of transfection. The lentiviral particles were pelleted out of medium using a Beckman Coulter Optima LE-80K Ultracentrifuge and an SW28 rotor spun at 23,000 RPM for 2 hours at 4ºC. The final pellet was resuspended in 400 µl Neurobasal medium, dispensed into 40 µl volumes, and stored at -80ºC.

Primary cortical neuron cultures derived from tau KO mice were transduced with the tau-encoding lentivirus. Experimental manipulations of the cultures were begun 48 hours after initial exposure to lentivirus.

Purification and oligomerization of recombinant human tau

BL21 *E. coli* cells were transformed with expression vectors for 1N4R or 2N4R WT human tau, each with a C-terminal his tag (kindly provided by Nicholas Kanaan of Michigan State University). Tau was purified out of soluble extracts

of transformed BL21 cells using TALON Metal Affinity Resin (TaKaRa 635502) and imidazole (Sigma-Aldrich I-0125) according to the vendors' instructions. The purified 1N4R and 2N4R solutions were concentrated in Amicon Ultra-4 Centrifugal Filters 10K (Sigma-Aldrich UFC801024) spun in a clinical centrifuge at 3,000 RPM at 4°C for 15 minute-intervals until the concentrate volume was ~500 µl [143]. Dithiothreitol (DTT, GE Healthcare 17-1318-02) was added to 1 mM, and the tau was then dispensed into 40-50 µl aliquots that were stored at -80°C. The protein concentration was measured using reducing agent-compatible BCA Protein Assay Kit (Abcam 207003).

The 1N4R and 2N4R oligomers were made as previously described [143] and summarized here. First, the buffer in which the purified tau was dissolved was changed to 0.1 M phosphate at pH 7.4 using Amicon Ultra-4 Centrifugal Filters 10K (Sigma-Aldrich UFC801024) according to the manufacturer's instructions. Next, the tau was diluted to 8 µM into a solution of 5 mM DTT, 100 mM NaCl, 10 mM HEPES (Gibco 15630-080) at pH 7.6, 0.1 mM EDTA and 300 µM arachidonic acid (Cayman Chemical Company 90010.1) and was incubated in the dark at room temperature for 6-18 hours. Vehicle controls were prepared identically, except that 0.1 M phosphate buffer was used in place of tau.

Protein electrophoresis and western blotting

Primary and secondary antibodies are listed in Table 7, and all blots were scanned using a LI-COR Odyssey infrared imager.

Tau oligomer aliquots were mixed 3:1 with 4X NuPAGE LDS Sample Buffer (Thermo Fisher Scientific NP0007) and stored at -20°C. Thawed

samples were electrophoresed in NuPAGE 4-12% Bis-Tris Gels (Thermo Fisher Scientific NP0323) using 1X MES running buffer (Thermo Fisher Scientific NP0002). After electrophoresis, gels were transferred for 1.5 hours at 100 V to 0.2 μm pore size nitrocellulose membranes (Bio-Rad 1620112) at 4°C. The membranes were then blocked with Intercept Blocking Buffer TBS (TBS blocking buffer, LI-COR 927-60001) at room temperature for 1 hour and incubated at 4°C overnight with the pan-tau mouse monoclonal antibody, Tau-5. Next, blots were washed twice with TBS/Tween 20 (TBST, VWR 0777) for 10 minutes each and incubated at room temperature for 1 hour with secondary antibody: IRDye 800 CW goat anti-mouse IgG. Following two more 10-minute washes in TBST and one rinse with TBS, blots were scanned.

Cultured neurons were collected in NuPAGE LDS Sample Buffer and 25% glycerol (Sigma-Aldrich G7893), and samples were stored at -20°C until use. Electrophoresis and western blotting were performed as described above for tau oligomers, except for the primary and secondary antibodies that were used. Primary antibodies were chicken polyclonal anti-TRIM46 and rabbit polyclonal anti-βIII-tubulin, and secondary antibodies were Alexa Fluor Plus 680 goat anti-chicken IgY (H+L) and IRDye 800 CW goat anti-rabbit IgG.

Human hippocampus samples were classified as non-AD or AD based on criteria of the Consortium to Establish a Registry for Alzheimer's Disease (CERAD), Braak staging or both. Unfractionated tissue lysates were prepared as described [123]. Tissue was homogenized manually using a plastic pestle (VWR 47747-358) in 10 ml/g tissue mass of a solution of 8M urea (Sigma-Aldrich U5378), 5 mM N-ethylmaleimide (Sigma-Aldrich E3876), 5% SDS, and 1:100 HALT protease inhibitor cocktail (Thermo Fisher Scientific 78430). The

homogenate was mixed 1:1 with 5X PAGE buffer (5% SDS, 25% sucrose, 50 mM Tris at pH 8.5, 1 mM EDTA, 30 mg/ml DTT and bromophenol blue as a tracking dye). ***Ankyrin-G blots*** were made as described earlier [123] using 3.5-17.5% gradient gels in 1X Tris buffer, pH 7.4. Gels were transferred overnight at 4°C at 300 mA to 0.45 µm pore size nitrocellulose membranes in 0.5X Tris buffer with 0.01% SDS. Membranes were blocked in TBS containing 5% BSA for 1 hour followed by incubation overnight with primary antibody (rabbit anti-ankyrin-G [144] plus mouse monoclonal anti-α-tubulin), and then for 1 hour with secondary antibodies (IRDye 800 goat anti-rabbit IgG and IRDye 680 goat anti-mouse IgG diluted into TBST supplemented with 5% bovine serum albumin - BSA, Sigma-Aldrich A3803). Blots were washed 3 times in TBST for 15 minutes each after each antibody step, and finally once each in TBS and H_2O after the secondary antibodies. The ***Tau$_{(pS202/T205)}$*****, Tau-5,** ***neurofascin-186***, ***TRIM46*** and ***mouse monoclonal anti-βIII-tubulin (clone Tuj1)*** blots were processed as described above for tau oligomers and cultured neurons. Secondary antibodies for these blots were IRDye 680RD goat anti-rabbit IgG and IRDye 800 CW goat anti-mouse IgG.

Immunofluorescence microscopy

Primary and secondary antibodies are listed in Table 7. ***Primary mouse neuron cultures*** grown on 12 mm glass coverslips in 24-well plates were fixed in PBS containing 4% paraformaldehyde for 15 minutes. The cultures were then washed sequentially with the following ice-cold solutions: twice in PBS for 2 minutes each, once in PBS containing 0.1 M glycine for 5 minutes and once in

PBS for 2 minutes. Next, the fixed cells were permeabilized and blocked for 1 hour in PBS containing 1% BSA, 0.05% saponin (Sigma-Aldrich 84510), and 0.1% normal goat serum (Southern Biotech 0060-01). Then, they were incubated with various combinations of primary antibodies (chicken polyclonal anti-TRIM46, chicken polyclonal anti-MAP2, rabbit polyclonal anti-TRIM46, and mouse monoclonal anti-tau clone Tau-5) followed by secondary antibodies (Alexa Fluor 568 goat anti-chicken IgY, Alexa Fluor 647 goat anti-rabbit IgG, Alexa Fluor 488 goat anti-mouse IgG) for 1 hour. Following each antibody step the coverslips were washed twice in PBS containing 0.05% saponin for 2 minutes each. Immediately prior to sealing the coverslips to glass slides with Fluoromount G (Southern Biotech 0100-01), the cells were incubated with 0.2 µg/ml Hoechst 33342 trihydrochloride trihydrate (Thermo Fisher Scientific H3570) in PBS for 2 minutes, then with H_2O to remove excess dye and salts.

Table 7. Primary and secondary antibodies used in chapter three

Antigen	*Host/ Label*	*Application(s)*	*Stock Concentration*	*Dilution(s)*	*Source/ Catalog #*
Primary Antibodies					
Ankyrin-G	Mouse (Monoclonal)	ICC	1 mg/mL	1:1000	NeuroMab/ N106/36
Ankyrin-G	Rabbit	WB	800 ug/ml	1:5000	P Jenkins/ University of Michigan
Tau (pS202/ pT205)	Rabbit (Monoclonal)	WB	Not Reported	1:1000	Cell Signaling/ 30505
α-tubulin	Mouse (Monoclonal)	WB	Not Reported	1:1000	Cedarlane/ CLT9002
βIII-tubulin (Clone Tuj1)	Mouse	WB	0.7 mg/mL	1:5000	T Spano and T Frankfurter/ University of Virginia
βIII-tubulin	Rabbit	WB	1 mg/mL	1:2500	Sigma/ T3952
Glial Fibrillary Acidic Protein (GFAP)	Mouse (Monoclonal)	ICC	0.2 mg/mL	1:500	Invitrogen/ MA5-12023
Tau	Mouse (Monoclonal, clone Tau-12)	WB, ICC, IHC	0.25 mg/mL	1:200, 1:500, 1:2500	LI Binder/ Northwestern University
Tau	Mouse (Monoclonal, clone Tau-5)	ICC	1 mg/mL	1:500	N Kanaan/ Michigan State University
TRIM46	Chicken	WB, ICC	1 mg/mL	1:1000, 1:2500	Synaptic Systems/ 377-006
TRIM46	Rabbit	WB, ICC, IHC	500 ug/mL	1:400, 1:500, 1:1000	Proteintech/ 21026-1-AP
MAP2	Chicken	ICC, IHC	Not Reported	1:2000	Abcam/ Ab92434
Neurofascin-186	Rabbit	ICC, WB	0.14 mg/mL	1:250, 1:2000	Invitrogen/ PA5-78668
Secondary Antibodies					
Chicken-IgG	Alexa Fluor Plus 680	WB	1 mg/mL	1:5000	LiCor/ A32934
Mouse-IgG	IRDye 680	WB	1 mg/mL	1:5000	LiCor/ 926-68070
Mouse-IgG	IRDye 800	WB	1 mg/mL	1:5000	LiCor/ 926-32210
Rabbit-IgG	IRDye 680	WB	1 mg/mL	1:5000	LiCor/ 926-68071
Rabbit-IgG	IRDye 800	WB	1 mg/mL	1:5000	LiCor/ 926-32211
Chicken-IgG	Alexa FluorTM 568	ICC, IHC	2 mg/mL	1:1000	Invitrogen/ A-11041
Mouse-IgG	Alexa FluorTM 488	ICC, IHC	2 mg/mL	1:1000	Invitrogen/ A-11029
Mouse-IgG2a	Alexa FluorTM 488	ICC	2 mg/mL	1:1000	Invitrogen/ A-21131
Rabbit-IgG	Alexa FluorTM 647	ICC, IHC	2 mg/mL	1:1000	Invitrogen/ A-21244
WB: Western Blot, ICC: Immunocytochemistry (Cultured Cells), IHC: Immunohistochemistry (Brain)					

Antibody-labeled neuron cultures were observed on an inverted Nikon Eclipse Ti microscope equipped with a Yokogawa CSU-X1 spinning disk confocal head, a Hamamatsu Flash 4.0 scientific C-MOS camera, a Nikon 40X oil 1.4 NA Plan Apo objective, and 405 nm, 488 nm, 561 nm, and 640 nm lasers. From each coverslip, 20 unique fields of cells with at least 20 cells per treatment group were imaged. All analyses were performed by 4 examiners (MNB, YL, NNF, and NK) blinded to the treatments using the FIJI version of ImageJ. More specifically, we analyzed: 1) the shortest distance between the nucleus and the AIS (nucleus-AIS gap) measured using the “straight line tool”; 2) mean TRIM46 immunofluorescence intensity within the AIS measured using an “AIS Analysis” plugin (https://github.com/ksiller/aisanalyzer) created by KHS; and 3) AIS length (region-of-interest; ROI outlining the AIS thresholded at 50%

fluorescence intensity of a skeletonized line measuring the length of the AIS) measured using the “AIS Analysis” plugin. The plugin processes pairs of fluorescent images and corresponding FIJI/ImageJ ROI files. The output includes automated nucleus and AIS ROIs that aid in the quantification of AIS morphometric parameters (Figure 2).

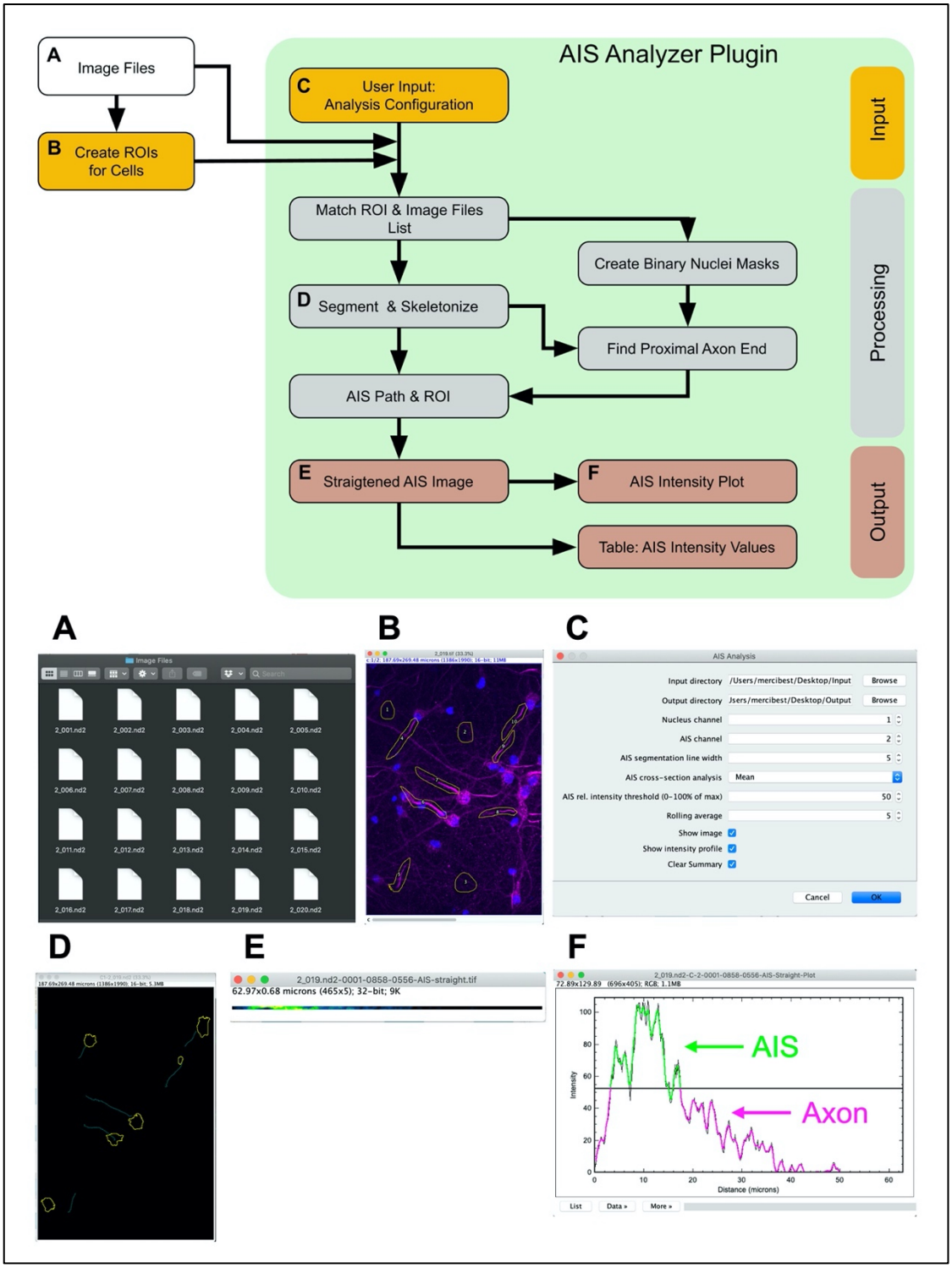

Figure 2. Semi-automated image analysis with the AIS analyzer plugin

This plugin measures nucleus-AIS gap, immunofluorescence intensity for a protein of interest (TRIM46) within the AIS, and AIS length. The plugin requires the following inputs: (A) a list of image files, (B) ROIs defining individual cells and background regions, (C) user input to configure analysis parameters. Automatic processing includes matching of ROIs and image files, creation of

binary nuclei masks, (D) segmentation and skeleton creation of the AIS, definition of proximal axon ends, calculation of AIS path and ROI. The created analysis output includes (E) an image representation of the straightened AIS, (F) creation of an intensity plot for the protein of interest along the axon path with highlighting of the AIS segment, and a CSV formatted table with measured fluorescence intensity values along the AIS path.

Human brain hippocampus sections were first examined by JWM to assess quality of fixation. Brains that did not show autolysis by loss of nuclear integrity were embedded in paraffin and cut into 4 μm thick sections from coronal blocks. The sections were deparaffinized using xylenes (Fischer Chemical X5-4), and antigen retrieval was accomplished using antigen unmasking solution, citrate-based (Vector Laboratories H-3300-250), and heat, according to the vendor's instructions. After cooling, the sections were washed twice in PBS for 5 minutes each, and then were permeabilized and blocked as described above for cultured mouse neurons. The primary antibodies included chicken polyclonal anti-MAP2, rabbit polyclonal anti-TRIM46 and Tau-5, and the secondary antibodies were as described above for cultured mouse neurons. The sections were washed twice in PBS for 5 minutes each after the primary and secondary antibody steps. Immediately prior to sealing the slides to glass coverslips with fluoromount G, lipofuscin autofluorescence was eliminated using the autofluorescence eliminator reagent (Sigma-Aldrich 2160) following the vendor's protocol.

The brain tissue sections were imaged with a Lecia Thunder Microscope equipped with a 40X dry objective, and 488 nm, 568 nm, and 640 nm lasers. All images were acquired using the same camera settings and laser intensity for consistent image analysis. From the CA1 region of each brain, 55 single plane widefield images were captured and stitched together and accounted for

an average of 72 neurons per brain. All images were analyzed using FIJI software. All analyses were done with the investigator blinded to the age, sex, and neuropathological diagnosis of the case. First, image files were loaded into FIJI. Second, image files were evaluated according to inclusion criteria: neuronal somas (MAP2 channel = 568 nm) and connecting AIS (TRIM46 channel = 647 nm) in the field of view. If criteria were met, the image was saved as a TIFF file for further analyses. Third, using the TRIM46 channel, background fluorescence intensity levels were measured as the average median gray value of three ROIs in areas void of AIS channel signal using “Measure” option under the drop-down menu labeled “Analyze”. Fourth, on the same image the freehand line tool was used to generate a manual tracing of the full AIS. The plot profile of the tracing was displayed using “Plot profile” option under the drop-down menu labeled “Analyze”. The plot values were displayed, and the distance (microns) and gray values were copied into a spreadsheet. Fifth, the Tau-5 antibody, which recognizes all tau isoforms independently of aggregation state or any post-translational modifications they may harbor, was used to determine whether each neuronal soma associated with an AIS contained “no tau accumulation” (absence of Tau-5 signal), “tau accumulation without NFTs” (diffuse Tau-5 signal) or “NFTs present” (Tau-5 positive, perinuclear flame-shaped structure that does not occupy the entirety of the cell; Figure 3). The data from all the neurons in an individual brain section were aggregated into a single spreadsheet that was exported into R for statistical analysis (as described below: statistics).

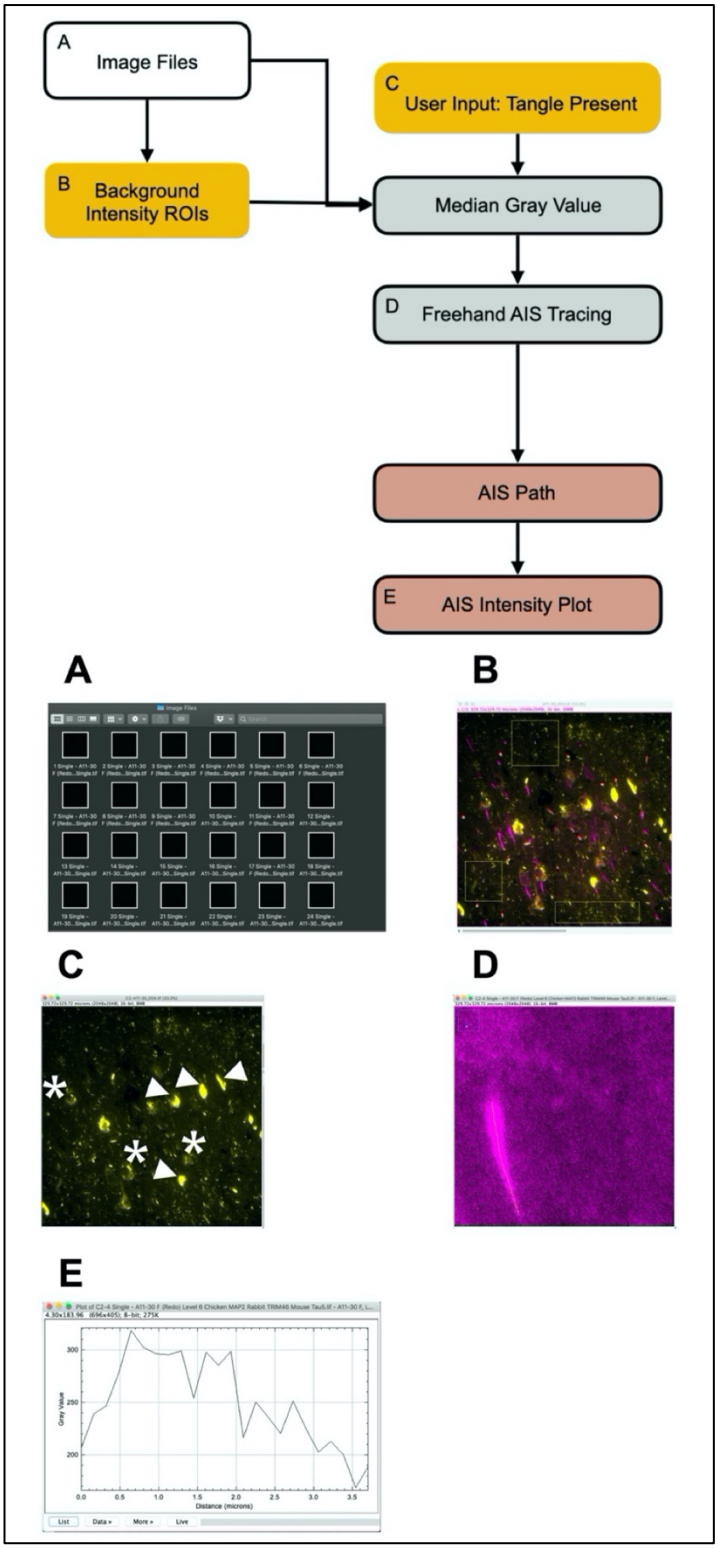

Figure 3. Manual image analysis for processing of AD and non-AD datasets in Figure 11

(A) Image files. (B) Background intensity ROIs. (C) User input: tangle present. Median gray value. (D) Freehand AIS tracing; AIS path. (E) AIS intensity plot.

Plugins for FIJI/ImageJ

The “AIS Analysis” (https://github.com/ksiller/aisanalyzer) and statistical analysis (https://github.com/mariekekjones/Alzheimer_AIS_data_analysis) codes are available online at the websites indicated here.

Statistics

Statistical analyses were performed in GraphPad Prism or in R. For cell culture western blots, data were analyzed across vehicle and xcTauOs groups using two-tailed independent Student’s t-tests, pooled variance. For cell culture immunocytochemistry, data were analyzed at the neuron level using linear mixed effects models that consider the measurement of several neurons within each coverslip. AIS morphometric parameters were explained by treatment condition (vehicle and xcTauOs) and the interaction term. Human brain tissue sample selection was based on tissue availability, and experiments were completed with 5-9 biologically distinct samples per group. For human brain western blots, the data were analyzed across non-AD and AD groups using two-tailed independent Student’s t-tests, unpooled variance. For human brain immunohistochemistry, data were analyzed at the neuron level using linear mixed effects models that consider the measurement of several neurons within each brain. AIS morphometric parameters were explained by disease state (non-AD and AD), tau pathology (“no tau accumulation”, “tau accumulation without NFTs” or “NFTs present”), and the interaction term. Because neurons

from both non-AD and AD brains had tau accumulation and tangles, it was critical to analyze our data at the neuron level.

Results

xcTauOs cause partial AIS loss in cultured neurons

Considering the evidence that xcTauOs cause accumulation of endogenous tau in the somatodendritic compartment [112,117], a likely sign of AIS functional impairment [45,49,53,54,59], we tested the hypothesis that AIS structure is compromised by xcTauOs. To do so, we exposed primary mouse cortical neuron cultures to xcTauOs made from purified recombinant human 1N4R or 2N4R tau (Figure 4) and used immunofluorescence microscopy and western blotting as quantitative morphometric and biochemical readouts, respectively, to monitor effects on the AIS. For the experiments described here, we used xcTauOs made from 1N4R and 2N4R tau interchangeably since both affected the AIS indistinguishably without any obvious effects on overall neuronal morphology, the density of axons and dendrites, or cell viability (see, for example, Figures 5A and 7A).

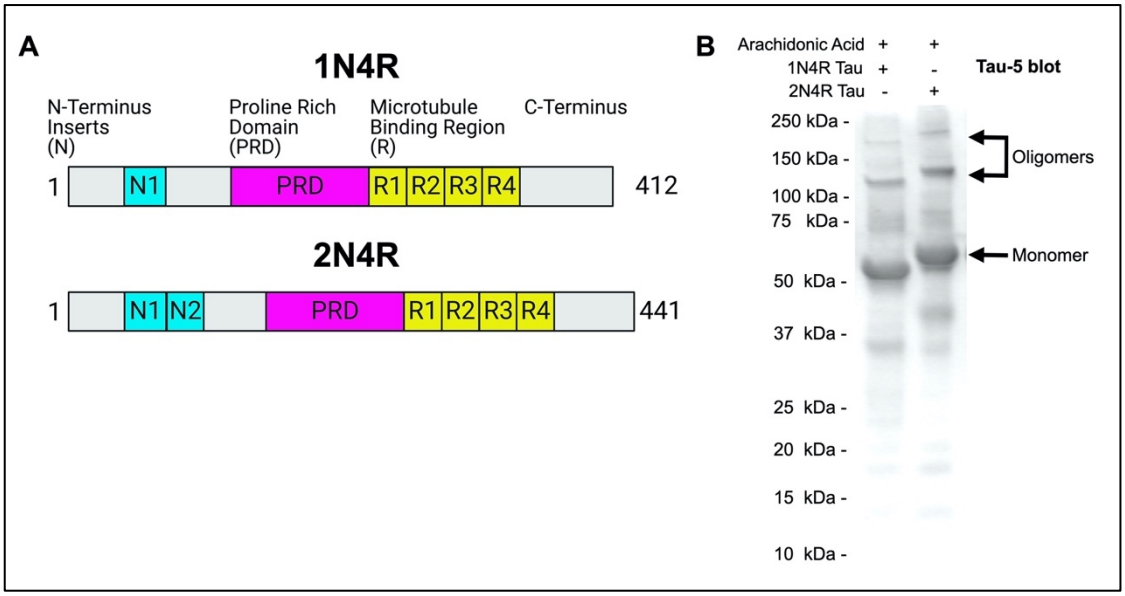

Figure 4. Characterization of Tau Oligomers

(A) Diagrams of the recombinant human 1N4R and 2N4R tau that were expressed in *E. coli*, purified, and used for making xcTauOs. (B) Western blotting of xcTauOs with the pan-tau antibody, Tau-5.

Robust immunofluorescence labeling of the AIS in primary neurons was observed with anti-TRIM46 (Figure 5A). Exposing the cells to xcTauOs at a total tau concentration of 125 nM for 24 hours resulted in the modest accumulation of tau and of punctuate TRIM46 in the somatodendritic compartment of neurons. xcTauOs did not alter the intraneuronal TRIM46 protein levels (Figure 5B), nor the shortest distance between the nucleus and proximal end of the AIS (Nucleus-AIS gap; Figure 5C). By contrast, xcTauOs induced an ~60% decrease in the average TRIM46 staining intensity within the AIS (Figure 5D). Similarly, xcTauOs induced an ~19% decrease in AIS length, from an average of 17.1 µm to an average of 13.8 µm (Figure 5E). It is possible that this loss of TRIM46 from the AIS reflects the corresponding appearance of somatodendritic TRIM46 puncta in xcTauO-treated neurons. It is important to note that only ~1/3

of the total extracellular tau was in the form of oligomers (see Figure 4B), predominantly putative dimers and trimers [145], so the true concentration of tau oligomers was in the range of 10-20 nM. Thus, we conclude that while low nanomolar concentrations of xcTauOs do not reduce the overall neuronal protein levels of TRIM46, they cause an ~19% decrease in AIS length and an ~60% reduction of TRIM46 concentration within what remains of the AIS. These data extend previous findings that AIS intensity and length can be modulated by external stimuli [18,49,146] and provide the first evidence of AIS sensitivity to xcTauOs.

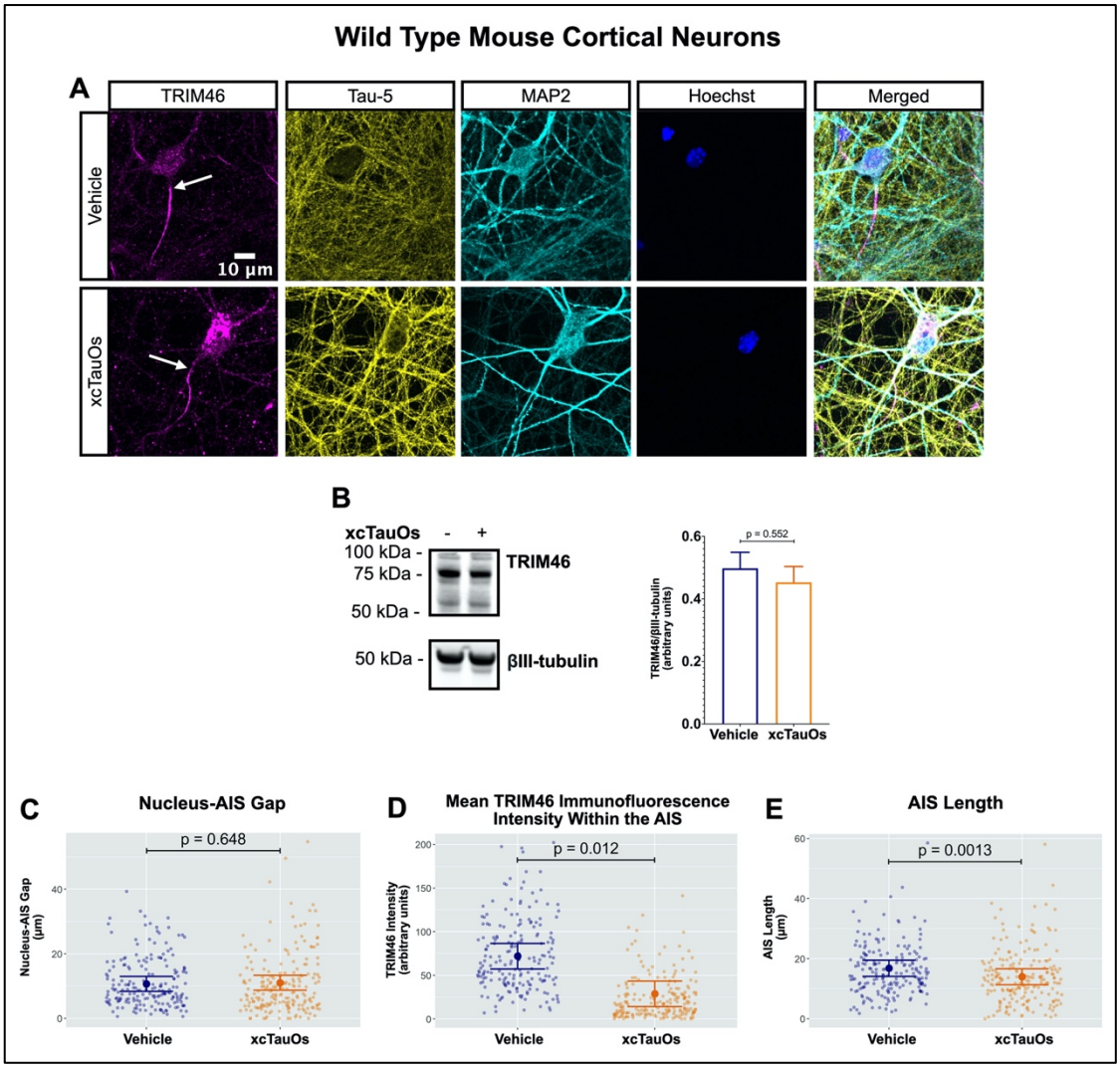

Figure 5. xcTauOs reduce clustering of TRIM46 within the AIS and AIS length

(A) Localization of TRIM46 (white arrows indicate proximal AIS ends), tau (Tau-5), somatodendritic compartment (MAP2), and nuclei (Hoechst) in primary WT mouse cortical neuron cultures. (B) Quantitative western blotting of unfractionated WT cultures probed with anti-TRIM46, and as a loading control, the neuron-specific anti-βIII-tubulin. p-value is based on two-tailed unpaired t-tests, pooled variance. Bar graph with mean and error bars represent ± standard error of the mean. (C-E) Plots of (C) Nucleus-AIS gap; (D) mean TRIM46 immunofluorescence intensity within the AIS, a surrogate measure of TRIM46 concentration; and (E) AIS length. Graph data were measured from 3-5 biological replicates (independent neuronal culture preparations). Immunofluorescence was performed with 1 technical replicate (independent coverslip) each, which accounted for a total of ~200 neurons per treatment condition (vehicle or xcTauOs). p-values from mixed model linear regression are indicated. Large dot indicates the predicted mean and error bars represent the 95% confidence interval.

Intriguingly, xcTauOs also induced perinuclear puncta of TRIM46 in the astrocytes that were present in primary mouse brain cell cultures, even though TRIM46 was undetectable in astrocytes that had not been exposed to xcTauOs (Figure 6). We do not know if the TRIM46 in xcTauO-treated astrocytes had been synthesized by those cells, or originated in neurons before being taken up by astrocytes.

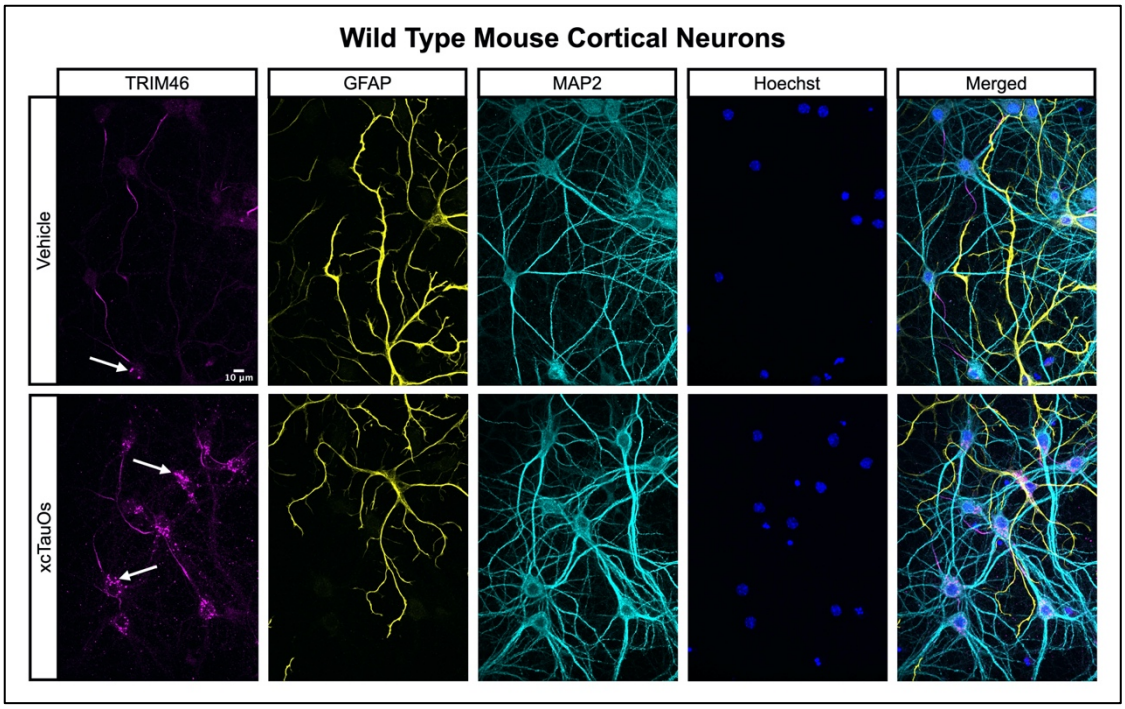

Figure 6. xcTauOs cause accumulation of TRIM46 puncta in the somatodendritic compartment of neurons and in astrocytes

Localization of TRIM46 puncta (white arrows), astrocytes (GFAP), neuronal somatodendritic compartment (MAP2), and nuclei (Hoechst) in primary WT mouse cortical neuron cultures.

Tau is necessary for xcTauO-induced AIS damage

One of the most conspicuous targets of extracellular tau aggregates, like short filaments and xcTauOs, is intracellular tau, which responds by aggregating in the cytoplasm. We therefore hypothesized that intracellular tau is required for

the partial AIS breakdown caused by xcTauOs. To test our hypothesis, we repeated the experiments shown in Figure 5 using primary cortical neurons derived from tau KO mice [147]. As shown in Figure 7, treatment of tau KO neurons with xcTauOs at a total tau concentration of 125 nM for 24 hours did not significantly alter the cellular level of TRIM46, the distance between the nucleus and the proximal boundary of the AIS, the length of the AIS, or the concentration of TRIM46 within the AIS. When WT human 2N4R tau was expressed in tau KO neurons by lentiviral transduction, however, sensitivity to xcTauOs was restored for AIS length, but not for the TRIM46 concentration within the remainder of the AIS (Figure 8). In such cells, the AIS shortened by an average of ~24%, from 20 μm to 15.3 μm (Figure 8E). Although the average expression level of lentiviral-encoded human tau in tau KO mouse neurons was ~1.3-fold higher than endogenous tau in WT mouse neurons, that difference was not statistically significant (Figure 9). Taken together, these results are consistent with the hypothesis that xcTauOs cause partial disassembly of the AIS by a mechanism dependent on intracellular tau.

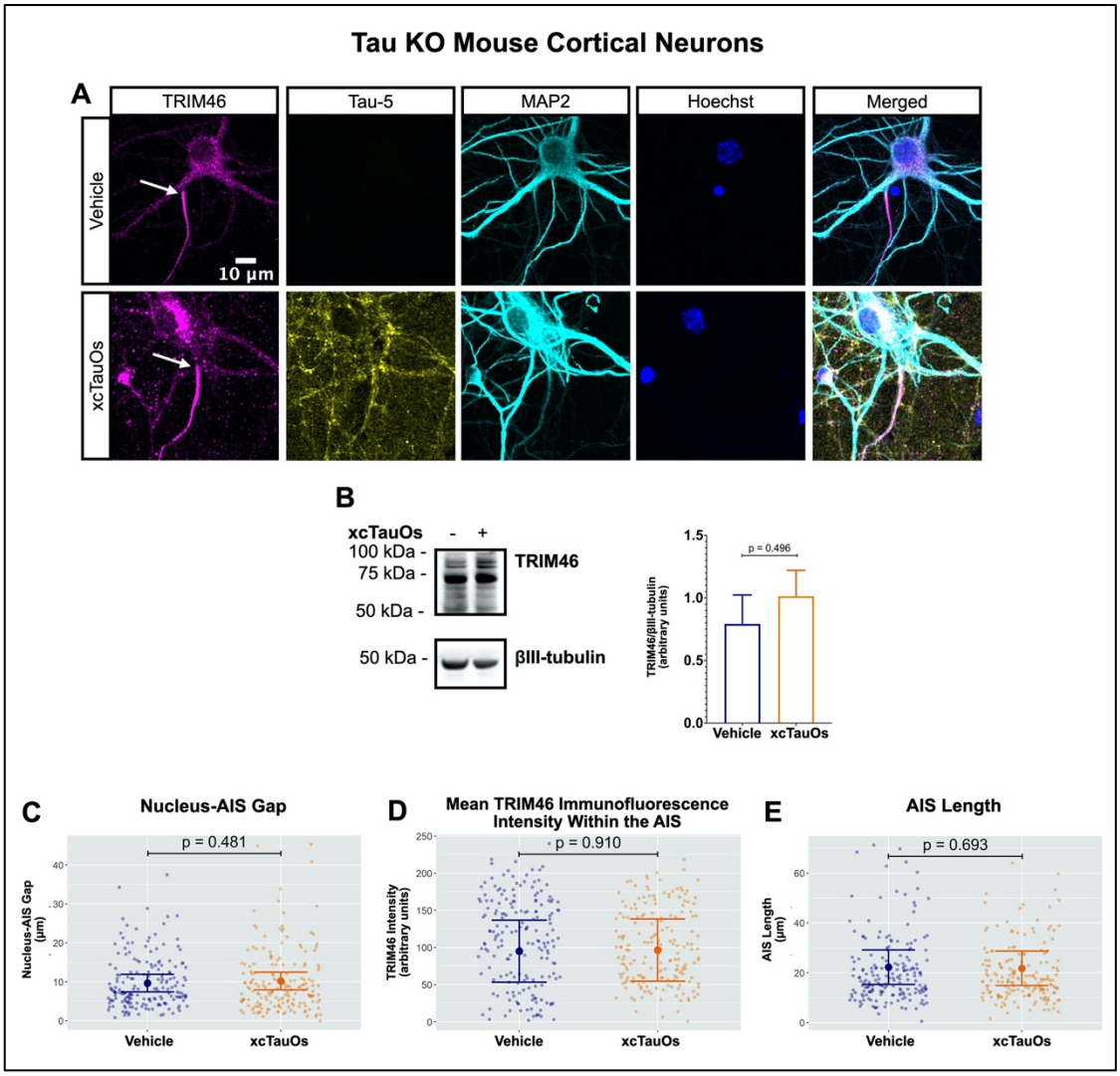

Figure 7. xcTauOs do not affect the AIS in tau KO neurons

(A) Localization of TRIM46 (white arrows indicate proximal AIS ends), tau (Tau-5), somatodendritic compartment (MAP2), and nuclei (Hoechst) in primary tau KO mouse cortical neuron cultures. (B) Quantitative western blotting of unfractionated tau KO cultures probed with anti-TRIM46, and as a loading control, the neuron-specific anti-βIII-tubulin. p-value is based on two-tailed unpaired t-tests, pooled variance. Bar graph with mean and error bars represent ± standard error of the mean. (C-E) Plots of (C) Nucleus-AIS gap; (D) mean TRIM46 immunofluorescence intensity within the AIS, a surrogate measure of TRIM46 concentration; and (E) AIS length. Graph data were measured from 5-6 biological replicates (independent neuronal culture preparations). Immunofluorescence was performed with 1 technical replicate (independent coverslip) each, which accounted for a total of ~184 neurons per treatment condition (vehicle or xcTauOs). p-values from mixed model linear regression are indicated. Large dot indicates the predicted mean and error bars represent the 95% confidence interval.

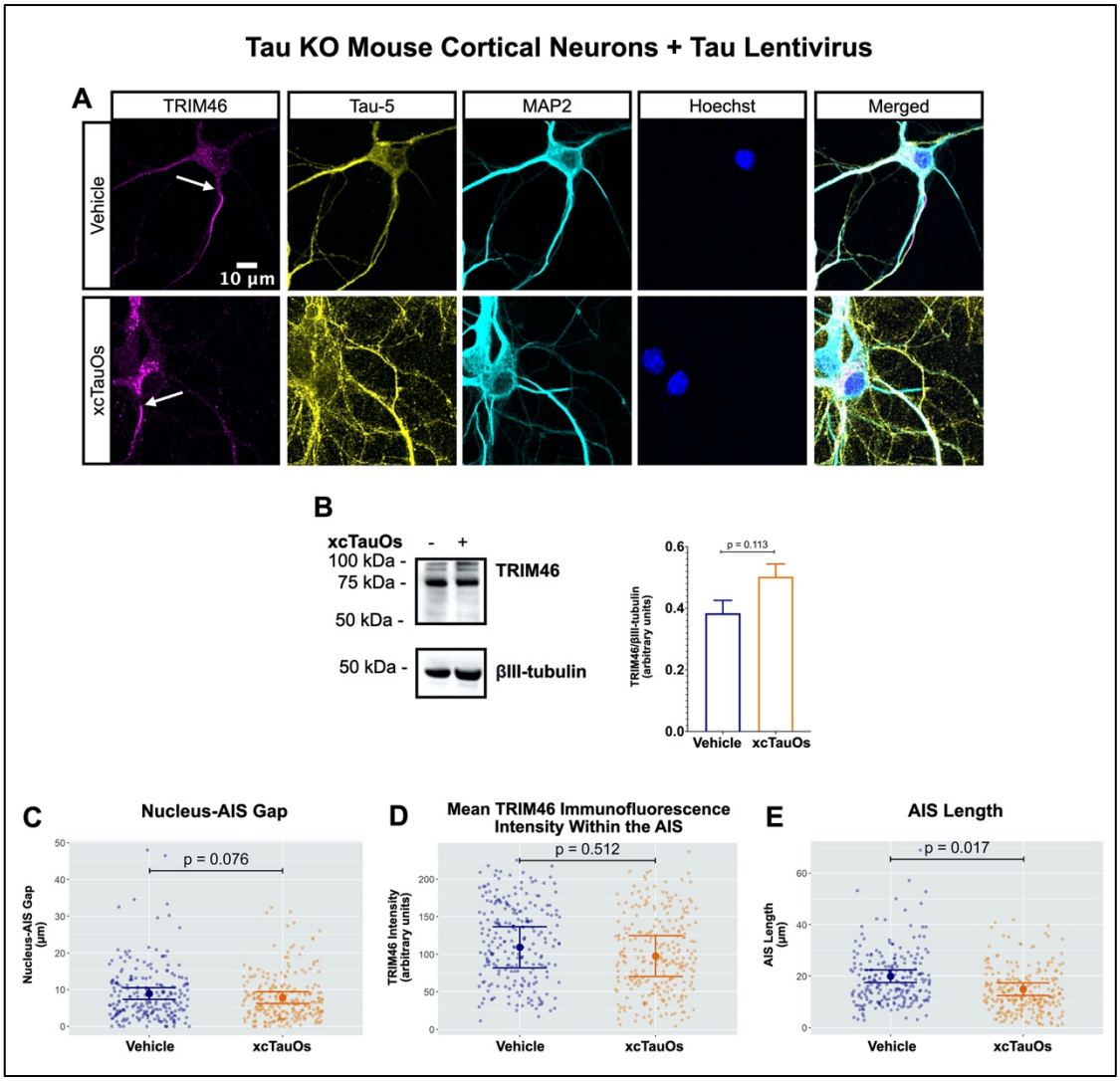

Figure 8. Expression of human tau in tau KO neurons restores AIS length sensitivity to xcTauOs

(A) Localization of TRIM46 (white arrows indicate proximal AIS ends), tau (Tau-5), somatodendritic compartment (MAP2), and nuclei (Hoechst) in primary tau KO mouse cortical neuron cultures expressing lentiviral encoded human 2N4R tau. (B) Quantitative western blotting of unfractionated tau KO cultures with lentiviral tau expression probed with anti-TRIM46, and as a loading control, the neuron-specific anti-βIII-tubulin. p-value is based on two-tailed unpaired t-tests, pooled variance. Bar graph with mean and error bars represent ± standard error of the mean. (C-E) Plots of (C) Nucleus-AIS gap; (D) mean TRIM46 immunofluorescence intensity within the AIS, a surrogate measure of TRIM46 concentration; and (E) AIS length. Graph data were measured from 3-5 biological replicates (independent neuronal culture preparations). Immunofluorescence was performed with 1 technical replicate (independent coverslip) each, which accounted for a total of ~243 neurons per treatment condition (vehicle or xcTauOs). p-values from mixed model linear regression

are indicated. Large dot indicates the predicted mean and error bars represent the 95% confidence interval.

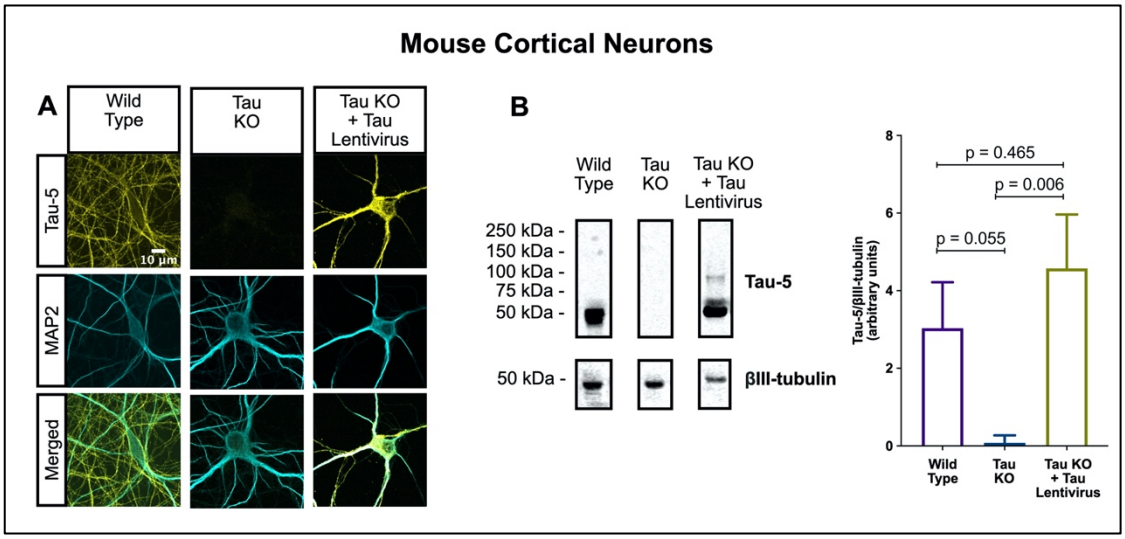

Figure 9. Lentiviral-encoded tau is expressed within normal levels in tau KO neurons

Shown here are detection of lentiviral-encoded human 2N4R tau in cultured tau KO neurons by immunofluorescence microscopy (A) and quantitative western blotting (B). Note that the average human tau expression level was ~30% higher than the endogenous mouse tau expression level in cultured WT neurons, but the difference was not statistically different. Data were obtained from the following number of biological replicates: 3 for Wild Type, 6 for Tau KO and 3 for Tau KO + Tau Lentivirus. p-values are based on two-tailed unpaired t-tests, pooled variance. Error bars on the graph represent ± standard error of the mean.

AIS protein levels are unchanged in human AD hippocampus

A prior study claimed that the levels of two major structural proteins of the AIS, ankyrin-G and βIV-spectrin, are reduced in human AD frontal cortex [54]. To determine if AIS protein loss also occurs elsewhere in human AD brain, we performed western blotting of unfractionated human hippocampal tissue derived from post-mortem AD and age matched non-AD donors (Figure 10). As

expected, most AD samples (8 of 9), but not non-AD samples (1 of 5), were positive for the NFT marker, tau($_{pS202/pT205}$) (Figure 10B-C). In contrast, none of the three AIS proteins that we examined - ankyrin-G, neurofascin-186, or TRIM46 - were reduced in AD versus non-AD brain. In the case of ankyrin-G, there are three major splice isoforms - 190 kDa, 270 kDa and 480 kDa – and only the latter two are highly enriched in the AIS. As shown in Figure 10B and 10D, there were no differences detected in levels of any ankyrin-G isoform between AD and non-AD hippocampus.

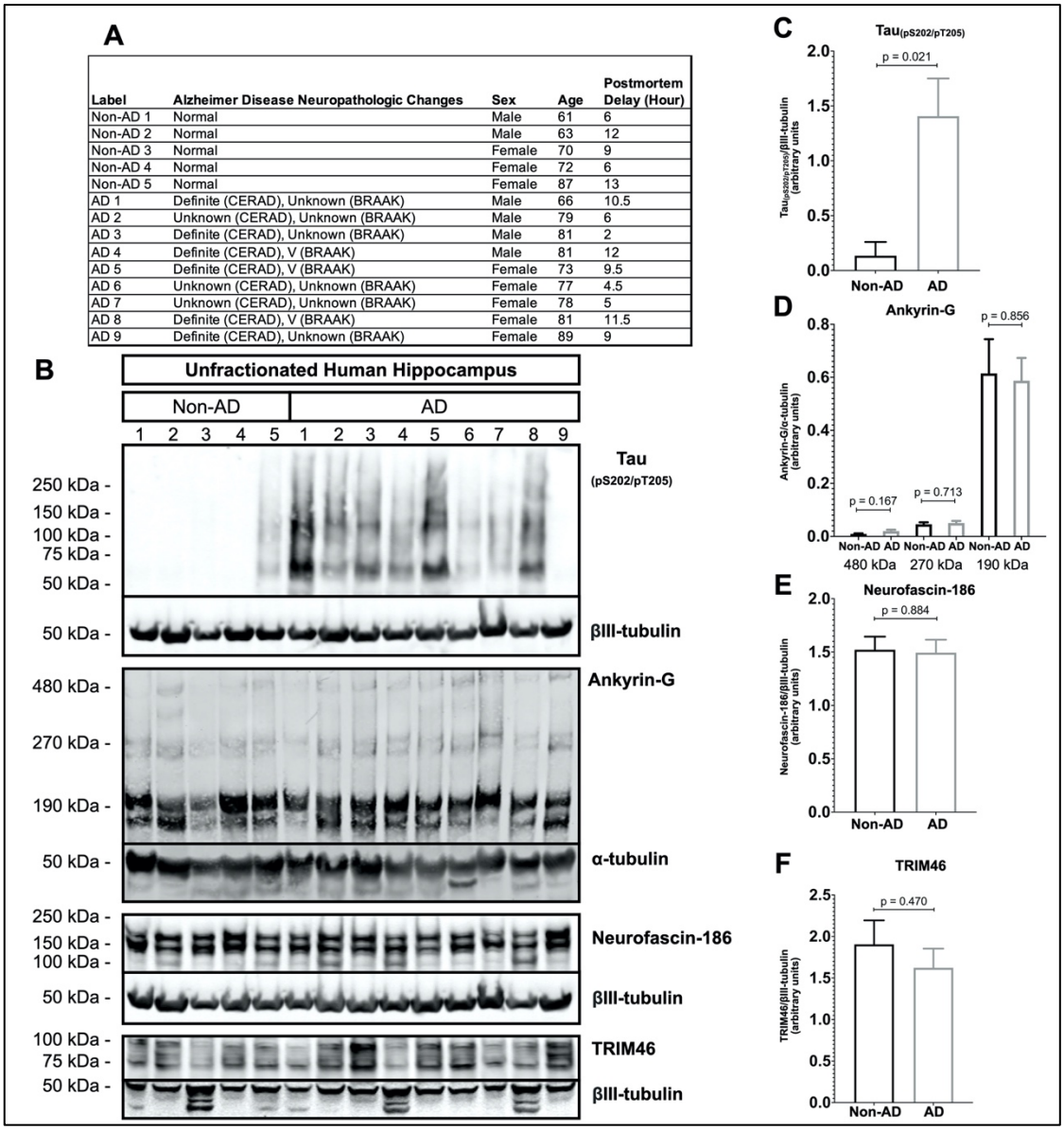

Label	Alzheimer Disease Neuropathologic Changes	Sex	Age	Postmortem Delay (Hour)
Non-AD 1	Normal	Male	61	6
Non-AD 2	Normal	Male	63	12
Non-AD 3	Normal	Female	70	9
Non-AD 4	Normal	Female	72	6
Non-AD 5	Normal	Female	87	13
AD 1	Definite (CERAD), Unknown (BRAAK)	Male	66	10.5
AD 2	Unknown (CERAD), Unknown (BRAAK)	Male	79	6
AD 3	Definite (CERAD), Unknown (BRAAK)	Male	81	2
AD 4	Definite (CERAD), V (BRAAK)	Male	81	12
AD 5	Definite (CERAD), V (BRAAK)	Female	73	9.5
AD 6	Unknown (CERAD), Unknown (BRAAK)	Female	77	4.5
AD 7	Unknown (CERAD), Unknown (BRAAK)	Female	78	5
AD 8	Definite (CERAD), V (BRAAK)	Female	81	11.5
AD 9	Definite (CERAD), Unknown (BRAAK)	Female	89	9

Figure 10. Resident AIS proteins levels are not reduced in AD hippocampus

(A) Clinical characterization of human hippocampus samples used for quantitative western blotting. (B) Western blotting of unfractionated human hippocampus probed with antibodies to tau$_{(pS202/pT205)}$ and the resident AIS proteins, ankyrin-G, neurofascin-186, and TRIM46. Loading controls, βIII-tubulin or α-tubulin, are shown for each of the aforementioned proteins. (C-F) Quantitation of western blots. Graphs were generated from 5-9 biological replicates (independent tissue samples) per blot. p-values are based on two-tailed unpaired t-tests, unpooled variance. Bar graph with mean and error bars represent ± standard error of the mean.

AIS damage in human AD neurons with NFTs

The western blotting results for ankyrin-G, neurofascin-186, and TRIM46 (Figure 10) in human hippocampus resemble the cultured neuron results for TRIM46 (Figures 5 and 8) in the sense that total protein levels were not reduced in AD versus non-AD by xcTauOs i*n vitro*. Because xcTauO treatment of cultured neurons caused AIS shortening and reduced the concentration of TRIM46 by ~60% within the remainder of the AIS (Figure 5), we searched for AIS structural changes in human AD brain. To that end, we performed immunohistochemistry of paraffin-embedded human hippocampal tissue using anti-TRIM46 as an AIS marker and Tau-5 (Figure 11). Eight tissue sections from both AD and age-matched non-AD controls were examined, and individual neurons were classified as “no tau accumulation”, “tau accumulation without NFTs” (see asterisk), or “NFTs present” (see arrowhead). Matching the analysis of cultured neurons shown in Figures 5-8, we measured the nucleus-AIS gap length, mean TRIM46 intensity within the AIS, and AIS length for both AD and non-AD samples. Note that these human brain sections were 4 μm thick, but the AIS typically ranges in length from 20-60 μm, so most length measurements did not account for the entire span of an AIS.

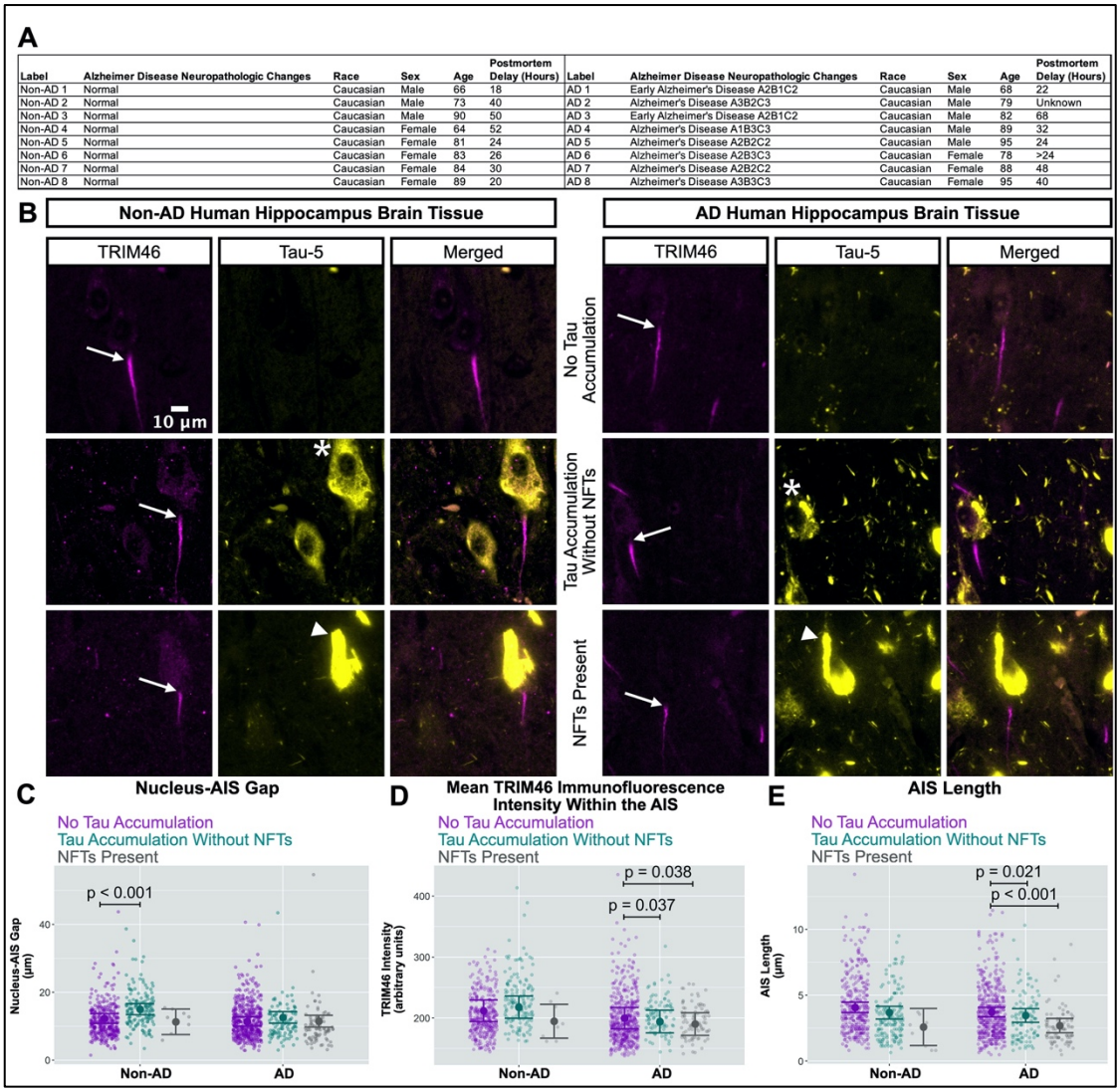

Label	Alzheimer Disease Neuropathologic Changes	Race	Sex	Age	Postmortem Delay (Hours)
Non-AD 1	Normal	Caucasian	Male	66	18
Non-AD 2	Normal	Caucasian	Male	73	40
Non-AD 3	Normal	Caucasian	Male	90	50
Non-AD 4	Normal	Caucasian	Female	64	52
Non-AD 5	Normal	Caucasian	Female	81	24
Non-AD 6	Normal	Caucasian	Female	83	26
Non-AD 7	Normal	Caucasian	Female	84	30
Non-AD 8	Normal	Caucasian	Female	89	20

Label	Alzheimer Disease Neuropathologic Changes	Race	Sex	Age	Postmortem Delay (Hours)
AD 1	Early Alzheimer's Disease A2B1C2	Caucasian	Male	68	22
AD 2	Alzheimer's Disease A3B2C3	Caucasian	Male	79	Unknown
AD 3	Early Alzheimer's Disease A2B1C2	Caucasian	Male	82	68
AD 4	Alzheimer's Disease A1B3C3	Caucasian	Male	89	32
AD 5	Alzheimer's Disease A2B2C2	Caucasian	Male	95	24
AD 6	Alzheimer's Disease A2B3C3	Caucasian	Female	78	>24
AD 7	Alzheimer's Disease A2B2C2	Caucasian	Female	88	48
AD 8	Alzheimer's Disease A3B3C3	Caucasian	Female	95	40

Figure 11. In AD brain, NFTs are associated with reduced clustering of TRIM46 within the AIS and AIS shortening

(A) Clinical characterization of human hippocampus samples used for quantitative immunofluorescence microscopy. (B) Localization of TRIM46 (white arrows indicate proximal AIS ends) and tau (Tau-5, tau accumulation without NFTs = asterisk, NFTs present = white arrowhead) in non-AD and AD hippocampus. (C-E) Plots of (C) Nucleus-AIS gap, (D) mean TRIM46 immunofluorescence intensity within the AIS, a surrogate measure of TRIM46 clustering, and (E) AIS length. Graphs were generated from 8 biological replicates (independent tissue samples), which accounted for a total of ~580 neurons per group (non-AD or AD). p-values from mixed model linear regression are indicated. Large dot indicates the predicted mean and error bars represent the 95% confidence interval.

Interestingly, as shown in Figure 11C, the nucleus-AIS gap in non-AD hippocampus was slightly, but statistically significantly shorter in neurons with "no tau accumulation" compared to neurons with "tau accumulation without NFTs". AIS length and mean TRIM46 intensity within the AIS were not affected by tau aggregation status in non-AD hippocampus, with the caveat that the number of neurons with NFTs that we observed in the non-AD group is small. In the AD samples, however, both mean TRIM46 concentration within the AIS (Figure 11D) and AIS length (Figure 11E) were statistically significantly greater in neurons with "no tau accumulation" compared to neurons with "tau accumulation without NFTs" or with "NFTs present".

Finally, we also analyzed the raw data for nucleus-AIS gap length, mean TRIM46 intensity within the AIS, and AIS length in the context of disease stage without regard for tau aggregation status. As shown in Figure 12, by doing so we could not discriminate early Braak, late Braak and age-matched non-AD from each other by this set of criteria. In other words, decreases in AIS length and TRIM46 concentration within the AIS are correlated with tau aggregation state on a neuron-by-neuron basis, but not with disease stage.

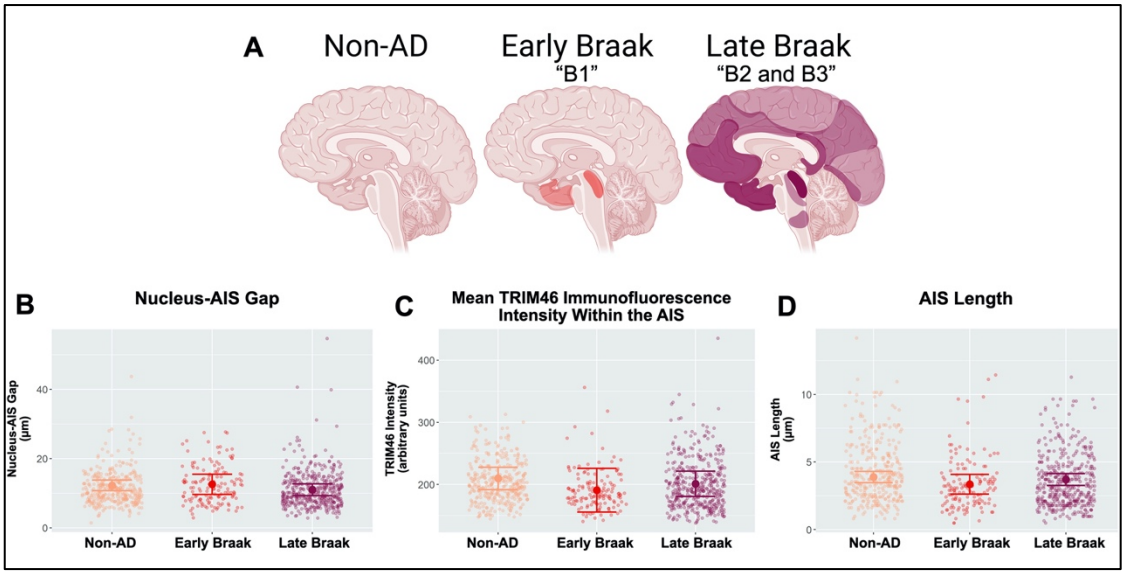

Figure 12. Braak stages do not correlate with changes in the AIS on a tissue wide basis

(A) Schematic of non-AD, early Braak (B1), and late Braak (B2-B3) stages. (B-D) Plots of (B) Nucleus-AIS gap, (C) mean TRIM46 immunofluorescence intensity within the AIS, a surrogate measure of TRIM46 concentration, and (D) AIS length. Graphs were generated from 8 biological replicates (independent tissue samples), which accounted for a total of ~387 neurons per group (non-AD, early Braak, or late Braak). p-values from mixed model linear regression are indicated. Large dot indicates the predicted mean and error bars represent the 95% confidence interval.

Discussion

Neurons are arguably one of the most structurally polarized animal cell types, and the AIS, which is found only in neurons, is essential for organizing neuronal cytoarchitecture. For example, the AIS encompasses a diffusion barrier that helps to segregate axonal from somatodendritic molecules, and it houses tightly packed voltage-gated ion channels that generate action potentials. Given the important functionality of the AIS, it follows naturally that damage of the AIS could have profound negative effects on the structural polarity of neurons, and by extension, on neuronal function.

Several prior studies have revealed AIS damage in neurodegenerative disorders, including AD [43,46,49,51,53,54,59,64,73,74,77,83,85,86,148–150], and there is evidence for possible involvement of amyloid-β oligomers [49] and plaques [43] in triggering that damage. Here we identify xcTauOs, which are hallmarks of AD and other tauopathies, as a potent inducer of AIS damage. Using TRIM46 as an AIS marker, we show that exposure of primary mouse cortical neurons to xcTauOs causes AIS shortening and reduces the concentration of TRIM46 within the remainder of the AIS by more than half (Figure 5A, D, E). The total neuronal protein levels of TRIM46 were not altered by xcTauOs, however, indicating that TRIM46 is redistributed from the AIS to presumably the cytoplasm in response to xcTauO exposure (Figure 5B). Effects of xcTauOs on the AIS were not observed in cultured tau KO neurons (Figure 7) unless human tau was expressed in the cells by lentiviral transduction (Figure 8). xcTauOs thus work in concert with intracellular tau to damage the AIS in cultured neurons.

The in vivo relevance of these cultured neuron findings was established by showing that reduced AIS length and clustering of TRIM46 within the AIS is associated with the presence of NFTs in hippocampal neurons (Figure 11), but that the overall hippocampal levels of TRIM46 and two other AIS proteins, ankyrin-G, and neurofascin-186, are not significantly different in AD versus age-matched tissue without AD (Figure 10). Altogether, these new results establish the AIS as a previously unknown target of xcTauOs, identify intracellular tau as an essential co-factor for the AIS damage induced by xcTauOs, and identify xcTauOs as likely causes of AIS damage in vivo.

Expression of human 2N4R tau in tau KO neurons caused AIS length to be even more sensitive to xcTauOs than in WT neurons that expressed only endogenous mouse tau (Figures 5 and 8). Average AIS shortening after a 24-hour exposure to xcTauOs was statistically significant: 19% in WT neurons and 24% in human tau-expressing tau KO neurons. In contrast, while the intensity of the TRIM46 immunofluorescence signal, a quantitative indicator of TRIM46 concentration, dropped ~60% after xcTauO exposure for WT neurons, it dropped only 10% for tau KO neurons that expressed human tau and that figure did not reach statistical significance.

One possible explanation for the differential AIS sensitivities to xcTauOs in WT versus tau KO neurons expressing human tau concerns intracellular tau isoforms. The WT neurons we used expressed approximately equal levels of 0N3R and 0N4R mouse tau (unpublished observations), whereas the human tau expressed in tau KO neurons was 2N4R, and like all human tau isoforms contains an 11 amino acid sequence, residues 19-29, that is not present in mouse tau. Perhaps species-specific or isoform-specific structural features of intracellular tau influence how the AIS responds to xcTauOs, and to the isoform composition of the xcTauOs as well. Regardless, the AIS shortening we observed in xcTauO-treated tau KO neurons that expressed human tau was slightly greater than that of WT neurons, while the TRIM46 concentration in the remainder of the WT AIS trended lower. While it is clear that AIS sensitivity to xcTauOs requires intracellular tau, the mechanistic basis for this requirement remains to be determined.

We chose to focus on TRIM46 as an indicator of AIS structure for two main reasons. The first was simply practical. Although TRIM46 co-localized in our

experiments with the well-known AIS structural proteins, ankyrin-G, βIV-spectrin and neurofascin-186 (Figure 13), the TRIM46 immunofluorescence signal was observed to be brighter and more confined to the AIS than the signals for the other two proteins. Secondly, TRIM46, which bundles microtubules in the AIS [137,138], has not been extensively studied so we were inspired to investigate it in the context of AD and other tauopathies. That said, it would be interesting to extend the characterization of AIS protein responses to xcTauOs to additional resident AIS proteins.

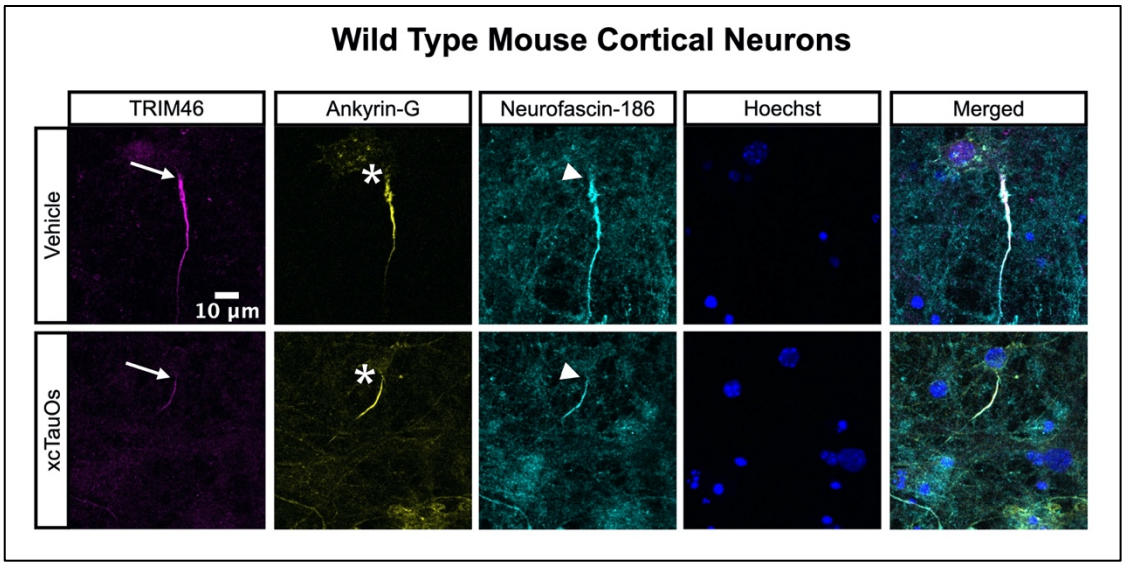

Figure 13. Co-localization of multiple AIS proteins and their sensitivity to xcTauOs

Localization of TRIM46 (arrows), ankyrin-G (asterisks), neurofascin-186 (arrowhead), and nuclei (Hoechst) in primary WT mouse cortical neuron cultures.

A prior report of AIS protein content in human brain by Sohn and colleagues included evidence of a dramatic reduction of ankyrin-G and βIV-spectrin in AD compared to non-AD brain [54], which seems to contradict what we report here for ankyrin-G (no change; see Figure 10). Several factors might account for this discrepancy. Whereas Sohn and colleagues examined RIPA buffer-soluble

extracts of frontal cortex clarified by ultracentrifugation for western blotting and quantified only the 270 kDa isoform of ankyrin-G, for western blotting we used uncentrifuged, SDS-soluble extracts of hippocampus and quantification of the 190 kDa, 270 kDa, and 480 kDa isoforms of ankyrin-G, the latter two of which are highly enriched in the AIS. It is possible that differences in tissue source (frontal cortex versus hippocampus), sample extraction methods and ankyrin-G isoform quantification, alone or in combination, explain why an AD-associated drop in ankyrin-G levels were found by Sohn and colleagues, but not in our study.

Similarly, our data for AIS shortening in human AD hippocampus (Figure 11) are inconsistent with a report by Antón-Fernández and colleagues that the AIS is longer in AD compared to non-AD brain [46]. A few factors might account for this discrepancy. Whereas Antón-Fernández and colleagues examined βIV-spectrin in 50 μm thick frontal cortex, we used TRIM46 as an AIS marker in 4 μm thick sections of hippocampus. It is thus possible that differences in AIS marker (βIV-spectrin versus TRIM46), tissue thickness (50 μm versus 4 μm), and brain region (frontal cortex versus hippocampus), alone or in combination, explain why we observed AIS shortening, and Antón-Fernández and colleagues observed AIS lengthening in AD neurons in vivo.

Notably, our human brain tissue observations were performed only on Caucasian (Figure 11) and indeterminate race (Figure 10) donors. As demonstrated in previous studies, the inclusion of non-Caucasian donors [151–155], particularly non-Hispanic Black groups [155], may increase experimental validity as this group has a higher incidence of AD [156]. Future studies should therefore strive to include individuals from ethnically and racially diverse

populations. This increase in sample size may help untangle the correlation of NFTs with AIS changes statistically.

Acknowledgements

This paper represents partial fulfillment of the Ph.D. requirements for MNB. The authors would like to thank MNB's dissertation committee (Drs. Mark Beenhakker, George Bloom, Thurl Harris, James Mandell, Edward Perez-Reyes, Bettina Winckler, and Scott Zeitlin); Drs. Silvia Blemker, Mete Civelek, Barry Condron, Jasmine Crenshaw, Carl Creutz, Heather Ferris, Gordon Laurie, Yi Hao, Marlit Hayslett, Keisha John, Kimberly Kelly, Joshua Kulas, John Lazo, Sonali Majumdar, Elizabeth Sharlow, Anthony Spano, Ann Sutherland, and Cedric Williams; past and current members of the Bloom lab (Drs. Guillermo Eastman, Shahzad Khan, Erin Kodis, Andrés Norambuena, Evelyn Pardo, Binita Rajbanshi, Lauren Rudenko, Antonia Silva, Eric Swanson and Edward John, Taylor Kim, Lisa Post, Nutan Shivange, Victoria Sun, and Horst Wallrabe); past and current members of the University of Virginia's Advanced Microscopy facility (Stacey Criswall and Natalia Dworak); past and current members of the University of Virginia's Writing Center (Grace Tavakkol, CJ Oswald, and Sydney Anderson), Academic English Now (Dr. Marek Kiczkowiak), and departmental administrators (Phillis Hynes, Sherrie Jones, Antoinette Reid, Deborah Steele, and Carrie Walker) for their support and encouragement.

Funding

This work was supported by NIH Grant AG051085 (GSB); the Owens Family Foundation (GSB); the Cure Alzheimer's Fund (GSB); NIH Training Grant T32GM008715 (MNB); and NSF Training Grant EXPAND Program 2021791 (MNB).

Conflict of interest

George Bloom is an Editorial Board Member of this journal, but was not involved in the peer-review process nor had access to any information regarding its peer-review. All other authors have no conflicts of interest to report.

Datasets/Data availability statement

The data supporting the findings of this study are available on request from the corresponding author.

Chapter Four: Extracellular Tau Oligomers Increase Tripartite Motif-Containing Protein 46 Co-localization with Late Endosomes/Early Lysosomes

Merci N. **Best**[a,b], Angela C.E. **VanTerpool**[a], Yunu **Lim**[a], Nina N. **Ferenc**[a], Nayoung **Kim**[a], Lisa A. **Post**[a,c], Dora **Bigler Wang**[a], Danielle C. **Llanzea**[b], Anna E. **Wasserman**[a], Elizabeth C. **Gonye**[b], Douglas A. **Bayliss**[b], Heather A. **Ferris**[c,d], Elizabeth R. **Sharlow**[b], John S. **Lazo**[b] & George S. **Bloom**[a,c,e]

[a]Department of Biology, University of Virginia, Charlottesville, VA, USA

[b]Department of Pharmacology, University of Michigan, Ann Arbor, MI, USA

[c]Department of Neuroscience, University of Virginia, Charlottesville, VA, USA

[d]Division of Endocrinology and Metabolism, University of Virginia, Charlottesville, VA, USA

[e]Department of Cell Biology, University of Virginia, Charlottesville, VA, USA

Running title: Tau oligomers increase TRIM46 localization

*Correspondence to: George S. Bloom, Department of Biology, University of Virginia, PO Box 400328, Charlottesville, VA 22904-4328, USA; Tel: +1 434 243 3543; E-mail: gsb4g@virginia.edu

Abstract

Background: Tripartite motif-containing protein 46 (TRIM46) is a microtubule-associated protein enriched in the proximal axon and axon initial segment (AIS). TRIM46 has also been described as an E3 ubiquitin ligase that possibly drives neurodegeneration by hindering the degradation, clearance, and removal of misfolded or damaged AIS-enriched proteins. Numerous lysosomal degradation pathways operate in degradation, but few mechanistic pathways involving TRIM46 have been described.

Objective: Test the hypothesis that xcTauOs increase TRIM46 localization near LAMP1$^+$ late endosomes/early lysosomes.

Methods: Cultured 1) NIH/3T3 mouse fibroblast cells, 2) ReNcell VM human neural progenitor cells, 3) human induced pluripotent stem cell-derived neuronal progenitor cells, 4) wild type (WT) mouse neurons, 5) insulin-like growth factor 1 receptor mouse astrocytes and 6) tau knockout (KO) mouse neurons were exposed to xcTauOs and quantitative immunofluorescence microscopy with anti-TRIM46 to monitor protein localization near LAMP1$^+$ organelles. The same method was used to compare TRIM46 and LAMP1 in human hippocampal tissue obtained from AD and age-matched non-AD donors. Additional experiments were performed using a GFP-tagged TRIM46 lentivirus to monitor TRIM46.

Results: xcTauOs increase TRIM46 localization near LAMP1$^+$ organelles that can be attenuated by preincubating with pharmacological inhibition of calpain and Cdk5. Lentivirus TRIM46 expression using GFP-TRIM46, GFP-S106A - phosphorylation null, or GFP-S106D - phosphorylation mimetic constructs drive

a similar localization pattern in the absence and presence of xcTauOs. This localization pattern is also similar in the human AD hippocampus.

Conclusion: xcTauOs may activate Cdk5-phosphorylation of TRIM46 at S106, which likely drives TRIM46 accumulation in late endosomes/early lysosomes.

Keywords

Tripartite motif-containing protein 46, Axon Initial Segment, E3 ubiquitin ligase, lysosome, extracellular tau oligomers

Introduction

Alzheimer's disease, Parkinson's disease, and Frontal temporal dementia with parkinsonism-17, along with 20 other tauopathies, affect over 30 million people [157]. One commonality is the involvement of the microtubule-associated protein, tau [158]. Specifically, these neurological conditions are characterized by tau modifications that alter tau structure and result in the production of tau oligomers and paired helical filaments that assemble into neurofibrillary tangles commonly found in tauopathy post-mortem brain tissue [159]. Synthetic tau oligomers are commonly used in *in vitro* experiments to better understand tau aggregation and toxicity [44,104,112,145,160–164]. In a previous study on the effect of extracellular tau oligomers (xcTauOs) on the axon initial segment (AIS), xcTauOs were found to reduce AIS intensity and shorten the length. Under vehicle treated conditions, TRIM46 – the AIS protein examined in the study is enriched in the AIS [44]. In contrast, xcTauOs cause a robust accumulation of TRIM46 in the somatodendritic compartment of neurons and in the cell body of astrocytes [44]. The purpose of this study was to explore this result by exploring a potential mechanism.

Cyclin-dependent kinase 5 (Cdk5), another AIS-enriched protein, has been implicated in the transport of TRIM46 [165]. Cdk5 is a proline-directed serine/threonine-protein that, among other roles, phosphorylates TRIM46 [138]. Cdk5 is activated by the calcium-dependent protease, calpain [166,167]. Cdk5 also maintains lysosomal homeostasis by regulating lysosome biogenesis [168]. Accordingly, we decided to address the following questions: 1) Do xcTauOs increase TRIM46 localization in other cultured cells? 2) Does TRIM46

co-localize with LAMP1$^+$ organelles? 3) Can pharmacological inhibitors attenuate xcTauO-mediated TRIM46 localization? 4) Does lentiviral driven TRIM46 expression increase TRIM46 and LAMP1 co-localization? 5) Does TRIM46 and LAMP1 co-localization have human relevance?

To address these questions, we observed antibody-based TRIM46 localization in NIH/3T3 fibroblast cells, ReNcell® VM human neural progenitor cells, human induced pluripotent stem cell-derived neural progenitor cells, wild type (WT) and tau knockout (KO) mouse neurons, and insulin-like growth factor 1 receptor (IGF-1R) mouse astrocyte cultures, and human hippocampus brain tissue using immunofluorescence microscopy. We also observed lentivirus-driven expression of GFP-TRIM46 in WT and tau KO mouse neurons. For NIH/3T3 fibroblast cells, ReNcell® VM human neural progenitor cells, human induced pluripotent stem cell-derived neural progenitor cells we found that xcTauOs cause an increase of TRIM46 localization near LAMP1$^+$ late endosomes and early lysosomes. For xcTauO treated wild type neurons and IGF-1R mouse astrocytes, we found an increase in TRIM46 and LAMP1 co-localization that could be attenuated by calpain or Cdk5 pharmacological inhibitors. GFP-TRIM46 also cause TRIM46 and LAMP1 co-localization. Similarly, in human AD hippocampus brain tissue TRIM46 and LAMP1 co-localized. Collectively, these findings prompt the hypothesis that xcTauOs activate calpain-mediated Cdk5 phosphorylation of TRIM46 that leads to its degradation in the lysosomal pathway.

Materials and methods

Purification and oligomerization of recombinant human tau

1N4R and 2N4R tau were purified and oligomerized as previously described [44].

Cultured NIH-3T3 fibroblasts cells

NIH3T3 fibroblast cells were cultured as previously described [169,170].

Cultured ReNcell VM

ReNcell VM were cultured as previously described [171].

Cultured neural progenitor cells

Human induced pluripotent stem cell-derived neural progenitor cells were cultured as previously described [172].

Mice

WT and TKO mice were used as previously described [44]. In this study, IGF-1R mice were also used.

Cultured neurons

WT and TKO mouse neurons were cultured as previously described [44].

Cultured astrocytes

IGF-1R mouse astrocytes was cultured as previously described [173,174].

Pharmacology

Primary cortical neurons and astrocytes were preincubated at 9-15 days *in vitro* with the indicated pharmacological inhibitor or vehicle equivalent at a final concentration of 10 nM - 100 uM total MDL28170 Calpain Inhibitor III (Cayman, #14283) or E-64 (Cayman, #10007963) or Roscovitine (Cayman, #10009569) for 1 hour.

GFP-TRIM46 lentivirus

In collaboration with SynBio Technologies, GFP-TRIM46 was inserted into a neuron-specific promoter. We also collaborated with SynBio Technologies to conduct mutagenesis of the site serine 106 (S106). To test the necessity of phosphorylation of TRIM46 at S106, we created a phosphorylation null construct, by mutating the serine to an alanine to inhibit the ability of Cdk5 to phosphorylate TRIM46 at that site. To test the sufficiency of phosphorylation of TRIM46 at S106, we created a phosphorylation mimetic construct, by mutating the serine to an aspartic acid to constitutively activate Cdk5 phosphorylation of

TRIM46 at that site. Using these constructs lentiviruses were created using previously published protocols [44].

Immunofluorescence microscopy

Immunofluorescence was performed as previously described [44].

Table 8. Primary and secondary antibodies used in chapter four

Antigen	*Host/ Label*	*Application(s)*	*Stock Concentration*	*Dilution(s)*	*Source/ Catalog #*
Primary Antibodies Used For This Study					
Lysosomal-Associated Membrane Protein (LAMP1)	Mouse (Monoclonal)	IHC	0.2 mg/mL	1-400	Santa Cruz/ sc-20011
LAMP1	Rat	ICC	0.1 mg/mL	1-400	abcam/ Ab25245
TRIM46	Rabbit	ICC, IHC	500 ug/mL	1-500	Proteintech/ 21026-1-AP
MAP2	Chicken	ICC, IHC	Not Reported	1-2000	Abcam/ Ab92434
Secondary Antibodies Used For This Study (Made in Goats)					
Mouse-IgG	Alexa FluorTM 488	IHC	2 mg/mL	1-1000	Invitrogen/ A-11029
Rabbit-IgG	Alexa FluorTM 647	ICC, IHC	2 mg/mL	1-1000	Invitrogen/ A-21244
Rat-IgG	Alexa FluorTM 488	ICC	2 mg/mL	1-1000	Invitrogen/ A-11006
Rat-IgG	Alexa FluorTM 647	ICC	2 mg/mL	1-1000	Invitrogen/ A-21247
Chicken-IgG	Alexa FluorTM 568	ICC, IHC	2 mg/mL	1-1000	Invitrogen/ A-11041
ICC: Immunocytochemistry (Cultured Cells), IHC: Immunohistochemistry (Brain)					

Pearson correlation coefficient

Co-localization of TRIM46 with LAMP1 was quantified by the Pearson's correlation coefficient plugin for ImageJ.

Statistics

T-test were performed as previously described [44].

Results

xcTauOs cause increased TRIM46 localization in cultured cells

xcTauOs cause partial loss of TRIM46 from the AIS and a corresponding appearance of somatodendritic puncta in neurons and perinuclear puncta of TRIM46 in the astrocytes [44]. We tested the hypothesis that xcTauOs alter TRIM46 localization in other cultured cells. We exposed NIH/3T3 fibroblast cells to xcTauOs made from recombinant human 1N4R or 2N4R tau and used immunofluorescence microscopy as quantitative morphometric readouts to monitor the effects on TRIM46 localization. With vehicle treatment, there was no immunofluorescence labelling of NIH/3T3 fibroblast cells with anti-TRIM46 (Figure 14). Exposing NIH/3T3 fibroblast cells to xcTauOs at a total tau concentration of 125 nM for 24 hours resulted in robust accumulation of punctuate structures recognized by the TRIM46 antibody in the cytoplasm. Thus, we conclude that xcTauOs cause increased TRIM46 localization in NIH/3T3 fibroblast cells.

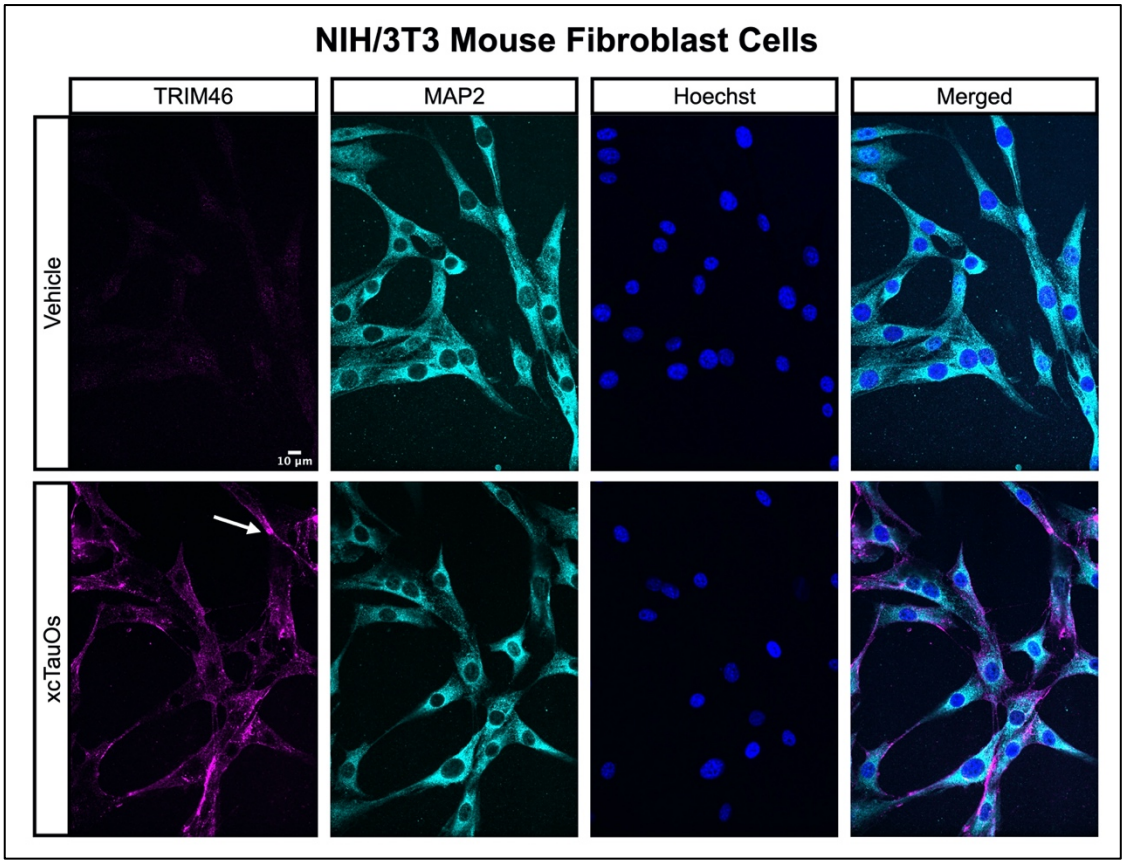

Figure 14. xcTauOs increase TRIM46 localization in NIH/3T3 fibroblast cells

Localization of TRIM46 puncta (white arrows), fibroblast cell body (MAP2), and nuclei (Hoechst) in NIH/3T3 fibroblast cells.

We performed additional experiments with two human neuron cell lines ReNcell® VM human neural progenitor cells, which have the ability to differentiate into neurons and glia (Figure 15). Importantly, extracellular tau monomers (xcTauMs) did not cause this effect, emphasizing that this process is driven by xcTauOs (Figure 16). Similar results occurred with human induced pluripotent stem cell-derived neuronal progenitor cells (Figure 17). These data are the first report of a similar accumulation of punctuate TRIM46 in NIH/3T3 fibroblast cells and the somatodendritic compartment of these human neurons

ReNcell® VM human neural progenitor cells and human induced pluripotent stem cell-derived neuronal progenitor cells.

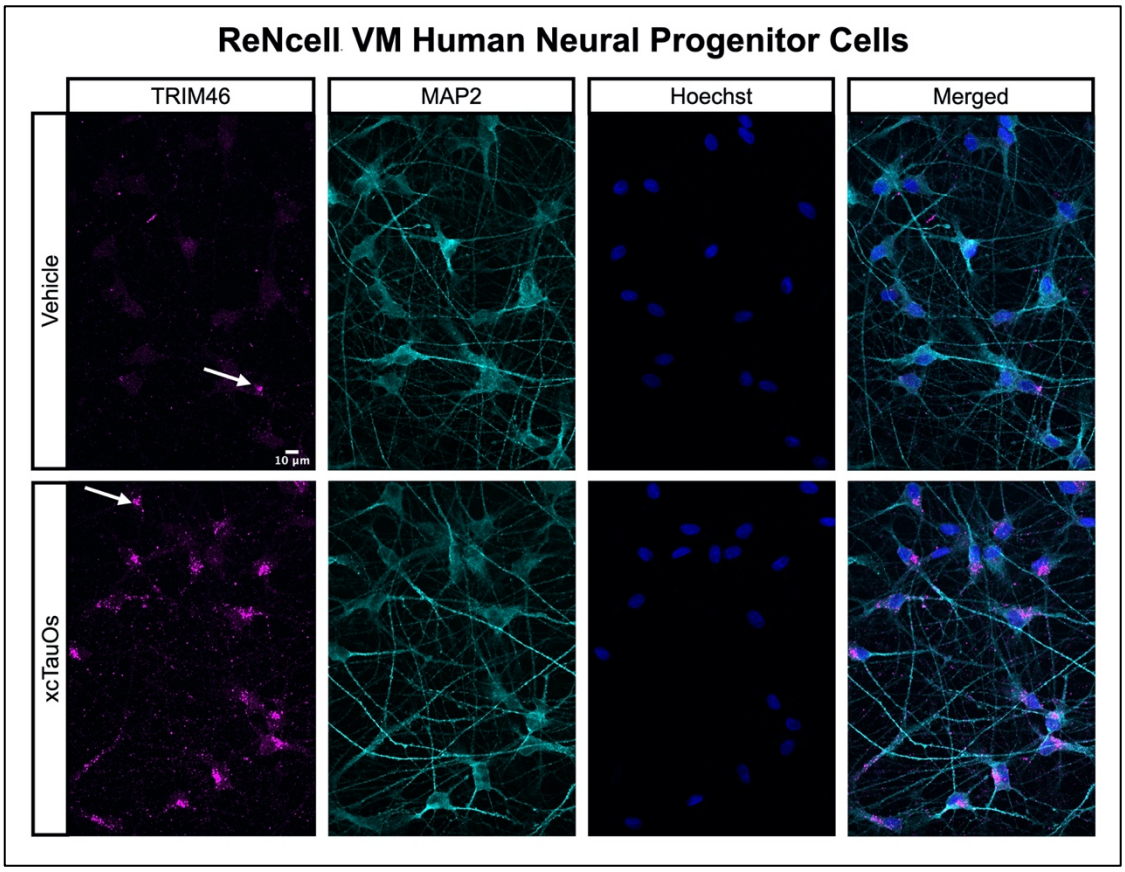

Figure 15. xcTauOs increase TRIM46 localization in ReNcell VM human NPCs

Localization of TRIM46 puncta (white arrows), neuronal somatodendritic compartment (MAP2), and nuclei (Hoechst) in ReNcell® VM human neural progenitor cells.

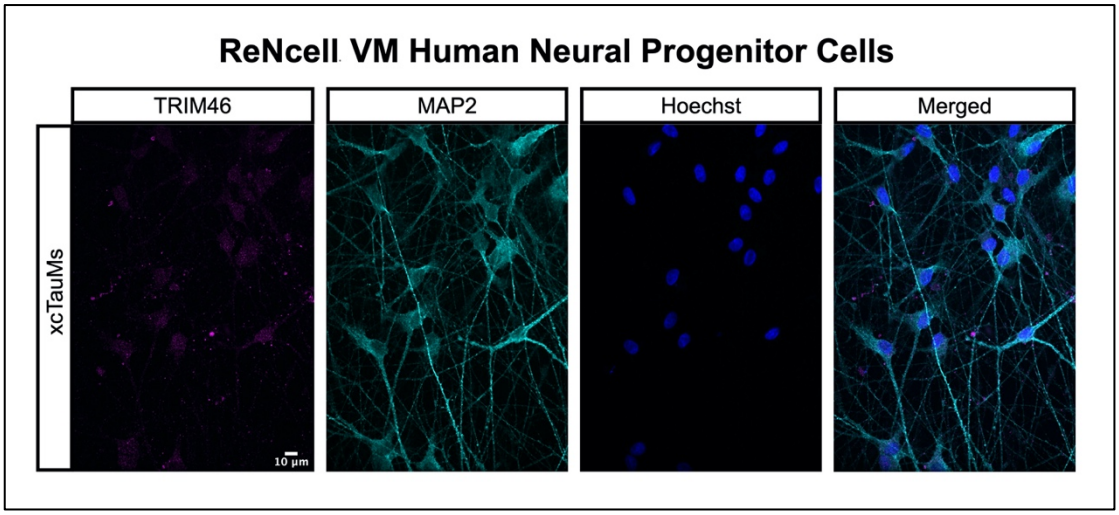

Figure 16. xcTauMs have no effect on TRIM46 localization in ReNcell VM human NPCs

Absence of TRIM46, neuronal somatodendritic compartment (MAP2), and nuclei (Hoechst) in ReNcell® VM human neural progenitor cells.

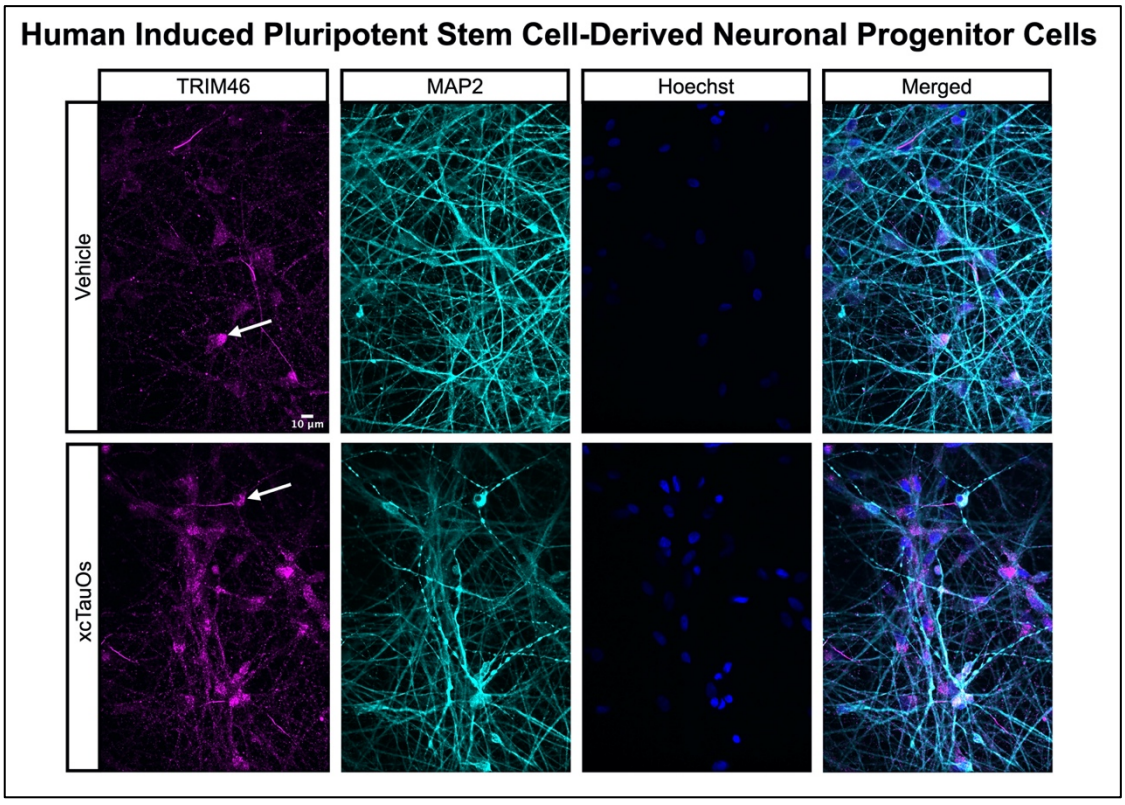

Figure 17. xcTauOs increase TRIM46 localization in human iPSC-derived NPCs

Localization of TRIM46 puncta (white arrows), neuronal somatodendritic compartment (MAP2), and nuclei (Hoechst) in human induced pluripotent stem cell-derived neural progenitor cells.

xcTauOs cause TRIM46 and LAMP1 co-localization in cultured neurons and astrocytes

The localization pattern of TRIM46 is reminiscent of lysosomes [175]. We therefore hypothesized that xcTauOs cause TRIM46 to accumulate in late endosomes/early lysosomes. To test our hypothesis, we performed experiments using primary cortical neurons derived from WT mice. As shown in Figure 18, treatment of WT neurons with xcTauOs significantly increased TRIM46 and LAMP1 co-localization in the somatodendritic compartment. We observed similar co-localization in the astrocytes co-cultured alongside the neurons (Figure 18).

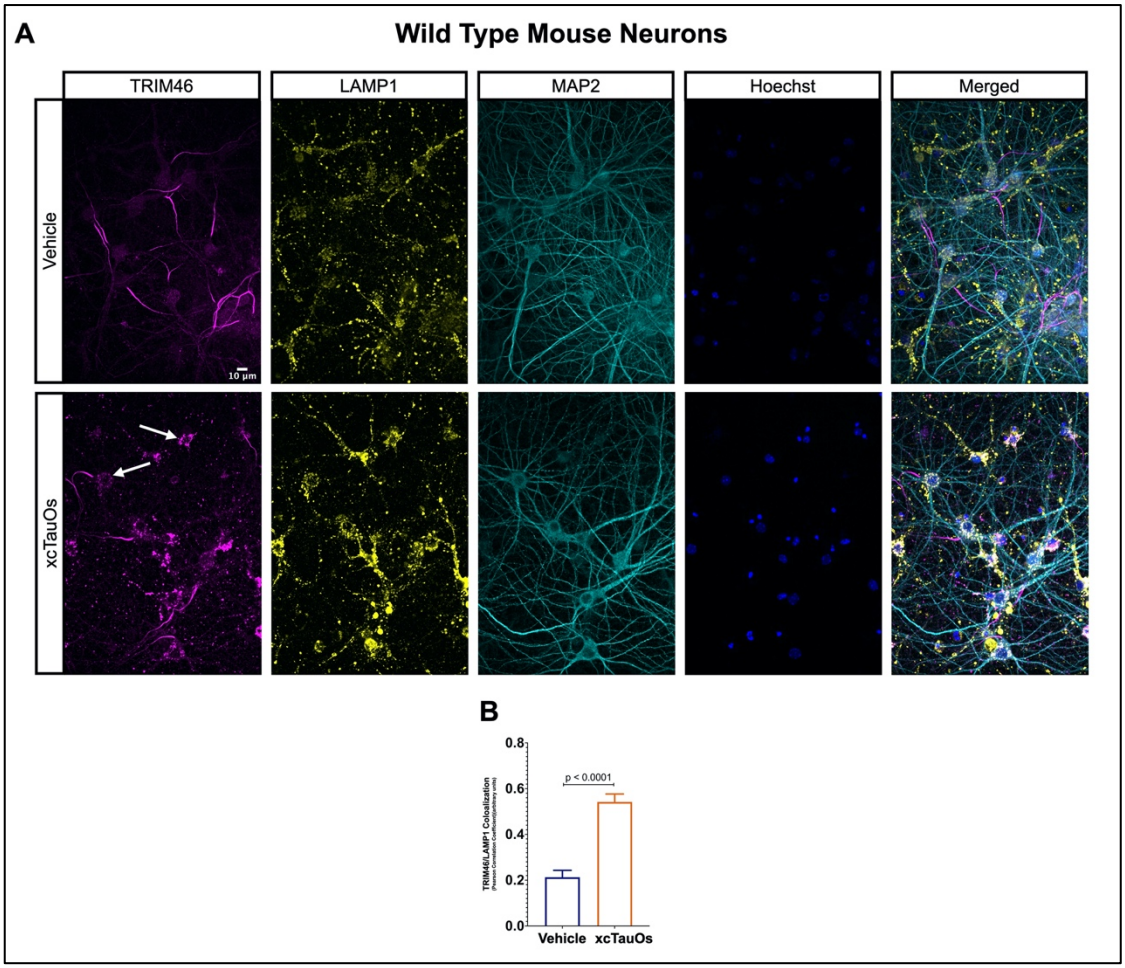

Figure 18. xcTauOs increase TRIM46 and LAMP1 co-localization in WT mouse neurons

Localization of TRIM46 puncta (white arrows), late endosomes/early lysosomes (LAMP1), neuronal somatodendritic compartment (MAP2), and nuclei (Hoechst) in primary WT mouse cortical neuron cultures. (B) Quantification of the Pearson's correlation coefficient between TRIM46 and LAMP1. Graph was generated from 5 biological replicates. p-values are based on two-tailed unpaired t-tests, pooled variance. Error bars on the graph represent ± standard error of the mean.

To determine whether this TRIM46 originates in neurons, we performed experiments using primary astrocytes derived from IGF-1R mice (Figure 19). In the absence of neurons, we observed TRIM46 and LAMP1 co-localization in mouse astrocytes exposed to xcTauOs (Figure 19). This effect is specific to

xcTauOs and does not occur in xcTauM treated mouse astrocytes (Figure 20).

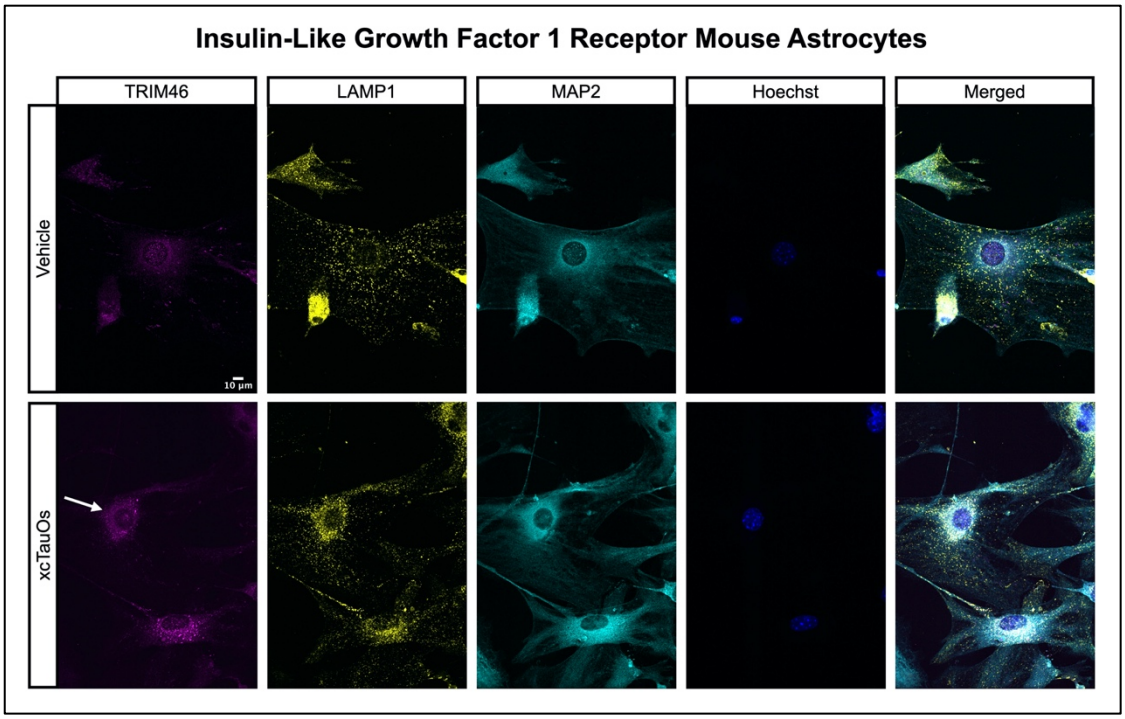

Figure 19. xcTauOs increase TRIM46 and LAMP1 co-localization in IGF-1R mouse astrocytes

Localization of TRIM46 puncta (white arrow), late endosomes/early lysosomes (LAMP1), astrocyte cell body (MAP2), and nuclei (Hoechst) in primary insulin-like growth factor 1 receptor mouse astrocyte cultures.

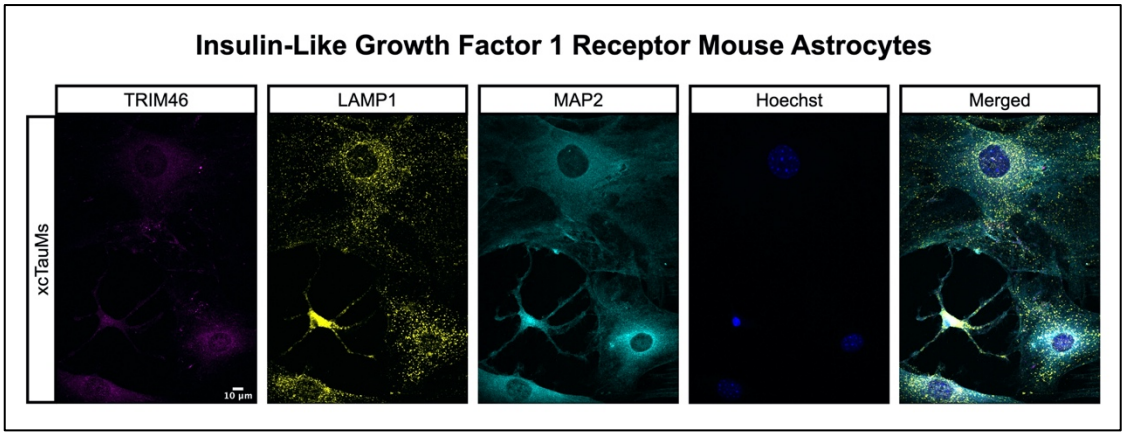

Figure 20. xcTauMs have no effect on TRIM46 and LAMP1 co-localization in IGF-1R mouse astrocytes

Absence of TRIM46 puncta (white arrow), late endosomes/early lysosomes (LAMP1), astrocyte cell body (MAP2), and nuclei (Hoechst) in primary insulin-like growth factor 1 receptor mouse astrocyte cultures.

Calpain and Cdk5 inhibitors may attenuate TRIM46 and LAMP1 co-localization

Next, we set out to test whether the pathway of TRIM46 accumulation in lysosome was phosphorylation of TRIM46 at S106 through calpain activation of Cdk5. We used two inhibitors of calpain that were cell permeable – E-64 and MDL-28170 (Figure 21). While preincubation attenuated TRIM46 and LAMP1 co-localization, the MAP2 also appeared to be reduced (Figure 21). We also used Roscovitine - the cell permeable inhibitor of Cdk5 is. At 100 uM 1-hour preincubation before 24-hour xcTauO treatment attenuated TRIM46 and LAMP1 co-localization. Importantly DMSO had no effect on TRIM46 and LAMP1 co-localization in the somatodendritic compartment of neurons. These findings were similar in mouse astrocytes (Figure 22).

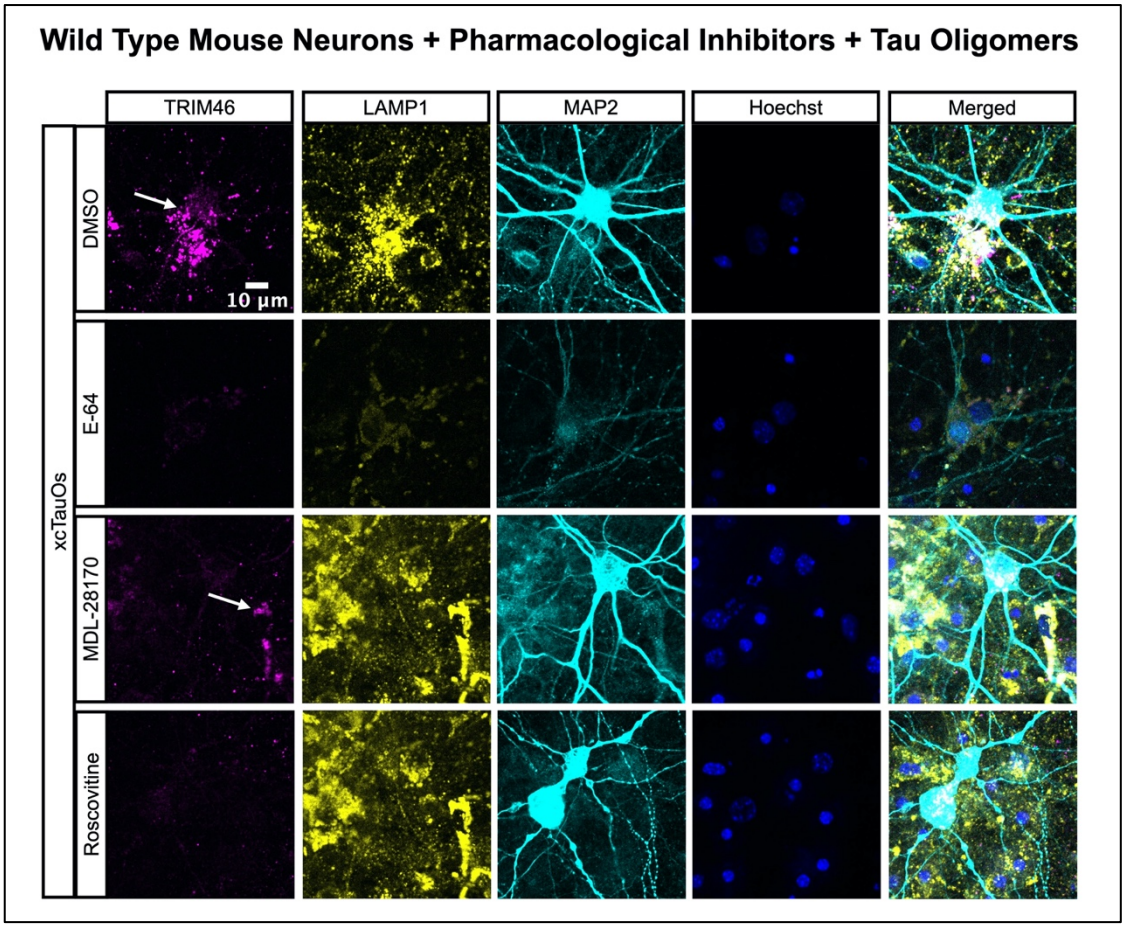

Figure 21. Pharmacological inhibition of calpain or Cdk5 attenuate TRIM46 and LAMP1 co-localization in WT mouse neurons

Localization of TRIM46 puncta (white arrows), late endosomes/early lysosomes (LAMP1), neuronal somatodendritic compartment (MAP2), and nuclei (Hoechst) in primary WT mouse cortical neuron cultures preincubated for 1 hour with pharmacological inhibitors of calpain (E-64 and MDL-28170) and Cdk5 (Roscovitine).

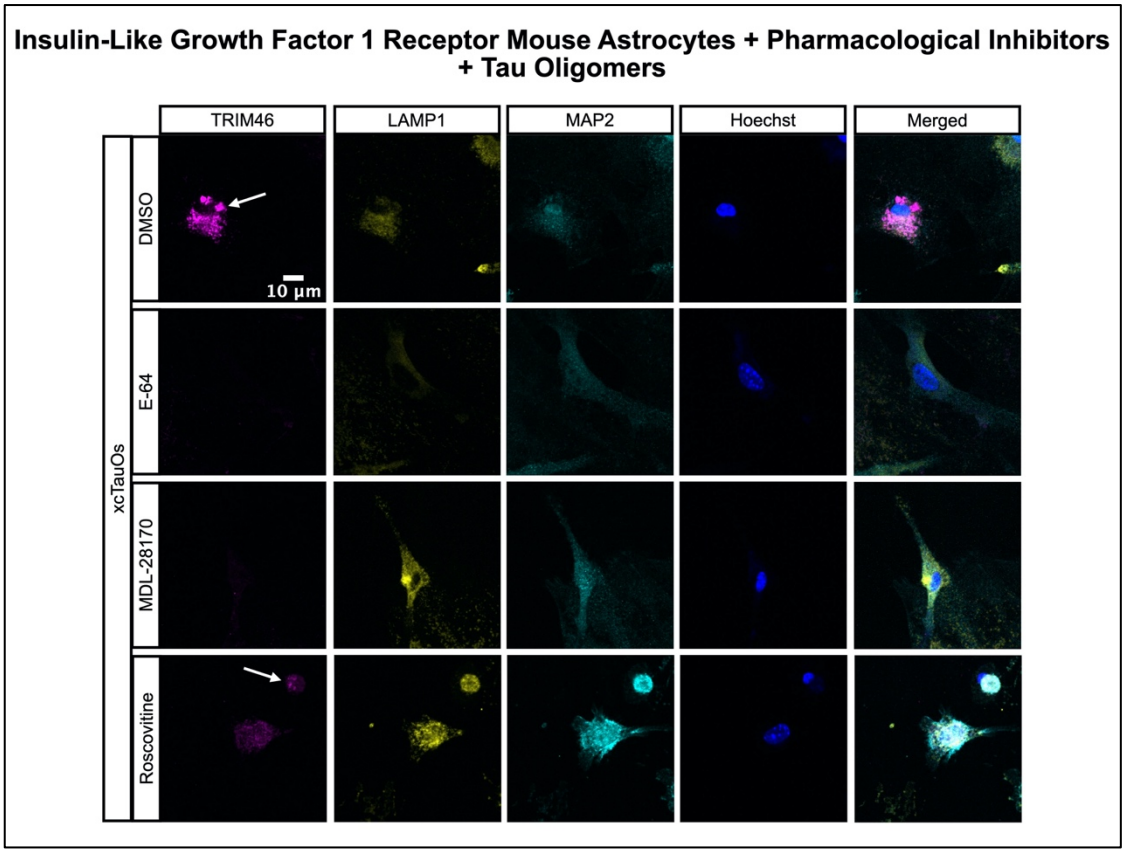

Figure 22. Pharmacological inhibition of calpain or Cdk5 attenuate TRIM46 and LAMP1 co-localization in IGF-1R mouse neurons

Localization of TRIM46 puncta (white arrows), late endosomes/early lysosomes (LAMP1), neuronal somatodendritic compartment (MAP2), and nuclei (Hoechst) in primary insulin-like growth factor 1 receptor mouse cortical astrocyte cultures preincubated for 1 hour with pharmacological inhibitors of calpain (E-64 and MDL-28170) and Cdk5 (Roscovitine).

Expression of GFP-TRIM46 from a lentiviral vector induces TRIM46 and LAMP1 co-localization in cultured neurons

Reliance on antibody reagents presents the concern that the fluorescence observed may not represent TRIM46 protein. Therefore, we collaborated with SynBio Technologies to develop the GFP-TRIM46 lentivirus (Figure 23A). We

confirmed that GFP-TRIM46 is present in the AIS of WT mouse neurons and serves as a label of the AIS (Figure 23B).

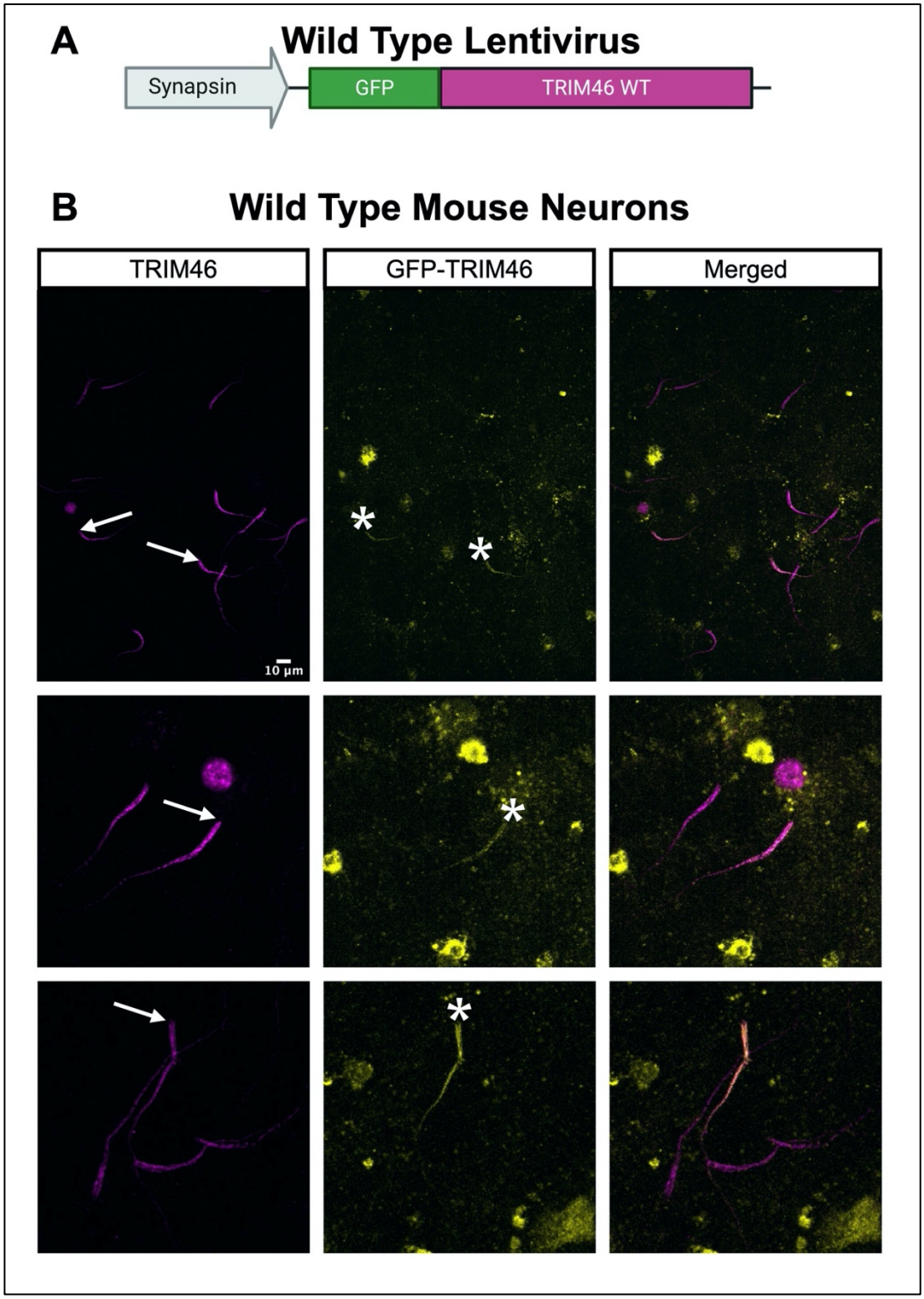

Figure 23. GFP-TRIM46 labels the AIS

(A) Schematic of wild type GFP-tagged TRIM46 lentivirus. (B) Localization of TRIM46 (white arrows) and GFP-TRIM46 (white asterisks) in primary WT mouse cortical neuron cultures.

We also performed mutagenesis to create two lentiviruses with single-site point mutants that inactivate or activate TRIM46 phosphorylation. The first GFP-S106A, where the ability of Cdk5 is prevented from phosphorylating TRIM46 at S106 (Figure 24A). The other was GFP-S106D, where TRIM46 phosphorylation by Cdk5 at S106 is mimic (Figure 24A). GFP-TRIM46 lentiviruses expressed in the AIS of WT neurons vehicle and xcTauO treated cells, while GFP-S106A and GFP-S106D only expressed in the AIS of WT neurons treated with vehicle (Figure 24B). All lentivirus increased TRIM46 and LAMP1 co-localization, irrespective of treatment (Figure 24B). In tau KO neurons, all except GFP-S106D vehicle expressed TRIM46 in the AIS (Figure 24C). Similar to the WT neurons, the TRIM46 and LAMP1 co-localization was consistent in the vehicle and xcTauO treated neurons.

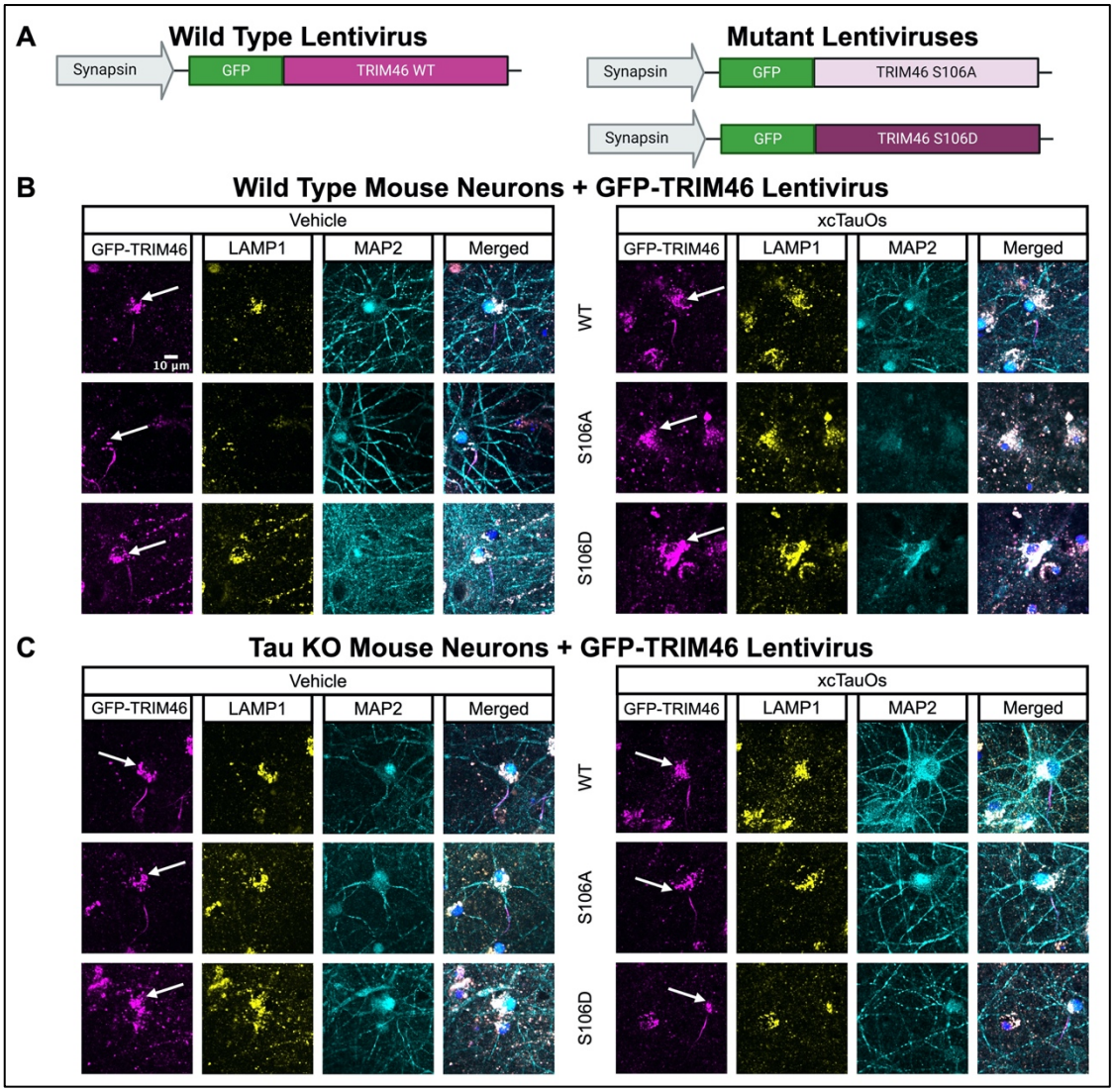

Figure 24. GFP-TRIM46 increase TRIM46 and LAMP1 co-localization in cultured neurons

(A) Schematic of wild type GFP- TRIM46 lentivirus and two mutations, a phosphorylation null mutation (GFP-S106A) and a phosphorylation mimetic mutation (GFP-S106D). (B) Localization of TRIM46 puncta (white arrows), late endosomes/early lysosomes (LAMP1) and neuronal somatodendritic compartment (MAP2) in primary wild type mouse cortical neuron cultures. (C) Localization of TRIM46 puncta (white arrows), late endosomes/early lysosomes (LAMP1) and neuronal somatodendritic compartment (MAP2) in primary Tau knockout mouse cortical neuron cultures.

TRIM46 and LAMP1 co-localize in human AD neurons

Finally, we set out to determine human relevance of the findings in cultured cells. Therefore, we tested the hypothesis that TRIM46 and LAMP1 co-localize in the AD human brain. While TRIM46 labels the AIS in non-AD brain tissue, the only TRIM46 labelling in AD brain tissue was punctuated staining in the somatodendritic compartment. These findings raise the possibility that TRIM46 association with late endosomes/early lysosomes occurs in AD following disruption of the AIS.

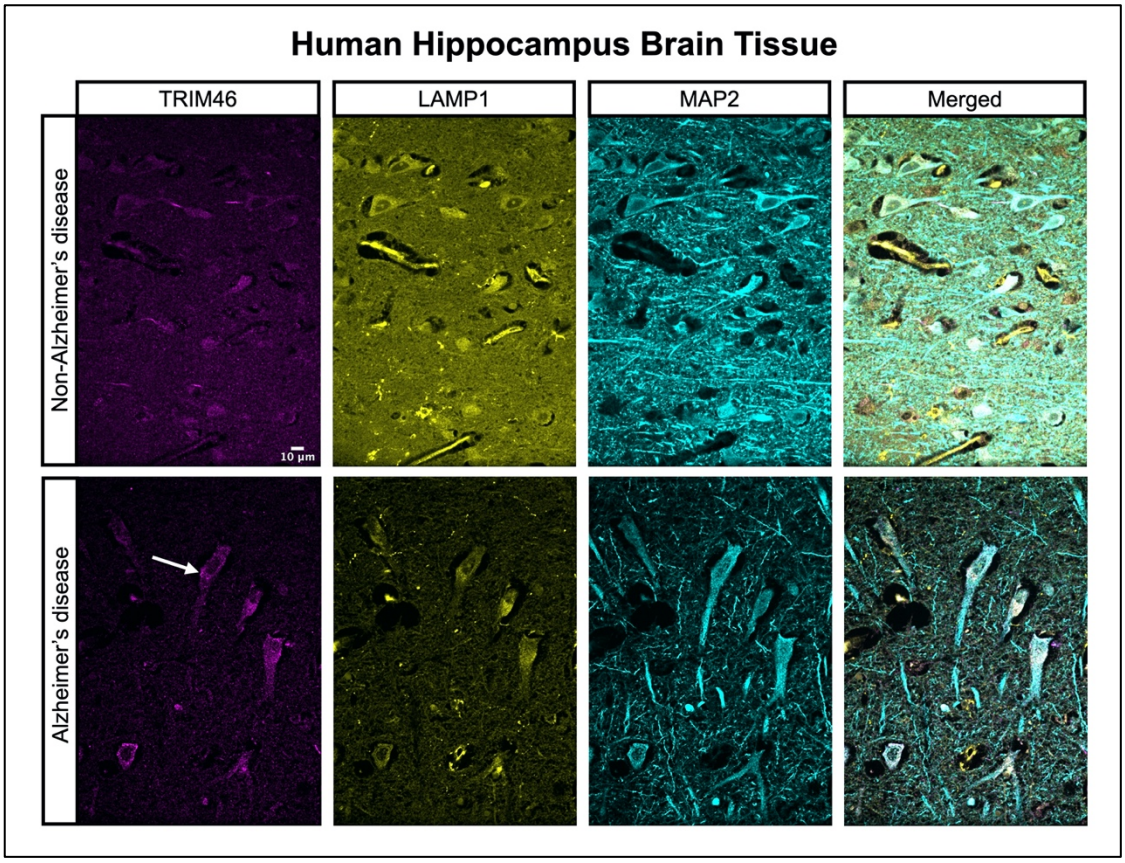

Figure 25. TRIM46 and LAMP1 co-localize in post-mortem human AD brain

Localization of TRIM46 puncta (white arrow), late endosomes/early lysosomes (LAMP1), and neuronal somatodendritic compartment (MAP2) in human hippocampus brain tissue.

Discussion

Here we identify that a hallmark of AD and other tauopathies, xcTauOs, induce re-distribution of TRIM46, which is normally in the AIS into the somatodendritic compartment of neurons. This localization pattern was similar to previous published reports of lysosomes in the pre-axonal region [175]. Our studies with LAMP1 staining confirm that the TRIM46 localization is near LAMP1$^+$ organelles, likely late endosomes/early lysosomes. Most xcTauO-driven processes work through intracellular tau, so it was surprising that xcTauO increases TRIM46 localization with LAMP1$^+$ organelles in WT, tau KO, and tau lentivirus + tau KO neurons.

This study underscores the involvement of calpain/Cdk5 cascade in xcTauO-mediated induction of TRIM46 in astrocytes. In this study, calpain antagonist (MDL2870) blocked the activation of calpain and inhibited xcTauO-induced astrocyte cytoplasmic TRIM46 activation. Similarly, the Cdk5 antagonist (Roscovitine) blocked the activation of Cdk5 and inhibited xcTauO-induced astrocyte cytoplasmic TRIM46 activation. These data lend credence to the previous reports that the administration of MDL2870 significantly decreased (Schafer et al.,2009). Also, there was a previous report that administration of Roscovitine significantly decreased AIS length [22]. This effect of Roscovitine contradicts our hypothesis that this mechanism is in alignment with the effect of xcTauOs on AIS length. We can conclude that suppressing Cdk5 or its activator calpain can lead to a reduction of cytoplasmic TRIM46. We also develop three novel GFP-TRIM46 constructs that drive TRIM46 and LAMP1 co-

localization and thereby provide us with further mechanistic insight towards understanding the effect of xcTauOs on TRIM46 localization.

The in vivo relevance of these cultured cell findings was established by sowing that increased TRIM46 and LAMP1 co-localization that differed between non-AD and AD. Altogether, these new results establish TRIM46 phosphorylation as a relevant mechanism. However, the biological relevance of these findings has yet to be determined as it is unknown whether TRIM46 and LAMP1 co-localization drives neurodegeneration by hindering the degradation, clearance, and removal of misfolded or damaged AIS-enriched proteins. is featured by the landing of the kinesin-1 motor on stable MTs, where it is required for lysosome and ER tubule translocation into the axon [8,129,137,176]. This is similar to previous reports that xcTauOs disrupt axonal transport [112].

TRIM46 is the first AIS-enriched protein that has been implicated as an E3 ubiquitin ligase. E3 ubiquitin ligases are known for their ability to recognize a target protein and degrade it through the ubiquitin pathway [177]. While other TRIM family members have E3 ubiquitin ligase activity it is yet to be widely accepted that the same holds true for TRIM46 [137,178]. TRIM46 may be an unusual C-I TRIM subfamily member that not necessarily exhibits E3 ubiquitin ligase activity [137].

Together, our findings implicate xcTauO-induced phosphorylation of TRIM46 by Cdk5 at S106 as a novel driver of the appearance of cytoplasmic TRIM46, independent of intracellular tau. More broadly, our results suggest that xcTauOs may be functionally connected with Cdk5 dysregulation in AD. This work emphasizes the utility of TRIM46 as a molecular target. By using multiple

cell lines, we were able to uncover the robust effect of xcTauOs. Taken together, our results confirmed the significance of TRIM46 in xcTauO-induced activation of TRIM46 expression in astrocytes and revealed that TRIM46 may serve as a potential target to develop new therapeutic agents for neurodegenerative disorders.

Most of the findings presented here are preliminary and will require the performance of additional experiments to perform robust statistical analysis. Therefore, the future directions of this research include determining whether the exploratory findings are reproducible. If so, additional mechanistic studies could be performed to determine whether xcTauOs activate Cdk5. The next step would be determining whether this pathway leads to Cdk5 phosphorylation of tau, TRIM46, or both. Finally, whether this phosphorylation event is required for the appearance of TRIM46 puncta would conclude this project. Given the validation that the tools developed to express fluorescently tagged TRIM46 and its phosphorylation null and constituently active forms in both neurons and non-neuronal cells work– the completion of these experiments should be feasible.

Acknowledgements

This paper represents partial fulfillment of the Ph.D. requirements for MNB. The authors would like to thank MNB's dissertation committee (Drs. Mark Beenhakker, George Bloom, Thurl Harris, James Mandell, Edward Perez-Reyes, Bettina Winckler, and Scott Zeitlin); Drs. Silvia Blemker, Mete Civelek, Barry Condron, Jasmine Crenshaw, Carl Creutz, Heather Ferris, Gordon Laurie, Yi Hao, Marlit Hayslett, Keisha John, Kimberly Kelly, Joshua Kulas,

John Lazo, Sonali Majumdar, Elizabeth Sharlow, Anthony Spano, Ann Sutherland, and Cedric Williams; past and current members of the Bloom lab (Drs. Guillermo Eastman, Shahzad Khan, Erin Kodis, Andrés Norambuena, Evelyn Pardo, Binita Rajbanshi, Lauren Rudenko, Antonia Silva, Eric Swanson and Edward John, Taylor Kim, Lisa Post, Nutan Shivange, Victoria Sun, and Horst Wallrabe); past and current members of the University of Virginia's Advanced Microscopy facility (Stacey Criswall and Natalia Dworak); past and current members of the University of Virginia's Writing Center (Grace Tavakkol, CJ Oswald, and Sydney Anderson), Academic English Now (Dr. Marek Kiczkowiak), and departmental administrators (Phillis Hynes, Sherrie Jones, Antoinette Reid, Deborah Steele, and Carrie Walker) for their support and encouragement.

Funding

This work was supported by NIH Grant AG051085 (GSB); the Owens Family Foundation (GSB); the Cure Alzheimer's Fund (GSB); NIH Training Grant T32GM008715 (MNB); and NSF Training Grant EXPAND Program 2021791 (MNB).

Conflict of interest

All authors have no conflicts of interest to report.

Datasets/Data availability statement

The data supporting the findings of this study are available on request from the corresponding author.

Chapter Five: Conclusion

The main topic of this dissertation was axon initial segment (AIS) damage in neurodegenerative diseases (NDs). As the number of individuals with NDs increase, we must design effective therapeutics to treat the aging populations. One method is through studying commonalities among ND, like AIS damage. Before this dissertation there were no 1) literature reviews on AIS damage in NDs, 2) research studies on the effect of extracellular tau oligomers (xcTauOs) on the AIS. Forty-two papers quantified the AIS structure and function in NDs. The studies that do this find contradictory results creating a lack of understanding on whether systematic damage to the AIS is a unifying feature of NDs.

To address the first gap, a systematic literature review was performed using the 42 papers. We identified 14 AIS structural parameters and two AIS functional parameters. Although, there was no consensus of whether the AIS parameters do not change, decrease, or increase, we conclude that AIS damage is a unifying feature among Alzheimer's disease (AD), amyotrophic lateral sclerosis, frontotemporal dementia, multiple sclerosis, and Parkinson's disease. To address the second gap, two research papers identified that xcTauOs cause a decrease in AIS immunofluorescent intensity as a semi-quantitative measurement of localized protein abundance and a reduction in AIS length. We also found that xcTauOs increase AIS protein, tripartite motif-containing protein 46 (TRIM46) and late endosome/early lysosome LAMP1 co-localization. These results find that xcTauOs are a novel mechanism of AIS damage in AD.

The organizational structure of chapter one was an introduction. Chapter two was a systematic literature review with five themes. The third and fourth chapters are research papers. Finally, chapter five was a conclusion.

The practical implications of the findings will benefit other scientist studying cellular structures that are linear like the AIS. Our AIS analyzer open access quantitative image analysis tool can be used to help standardize measurements of AIS structural parameters in the field. Also, our GFP-TRIM46 tools can be used in other research fields to study TRIM46 localization in real-time.

To acknowledge the limitations in this study, first in chapter two we identified 14 AIS structural and two AIS functional parameters, but there are several other parameters that could also be interrogated. A limitation in chapter three is that we only analyzed three AIS structural parameters. In chapter four, we only analyze one additional AIS structural parameter. In chapter three, while access to human brain tissue was a limitation, this study was able to identify a correlation between neurofibrillary tangles and AIS damage in AD. Finally, in chapter four, the use of immunofluorescence-based Pearson's correlation coefficient is not the most robust analysis. The results of this chapter remain unclear as to why TRIM46 and LAMP1 co-localize and its biological relevance.

These limitations lead directly to the suggestions for future research. Considering this dissertation in its entirety, future studies should make every effort to address the following research questions. First, does structural damage to the AIS correlate with functional damage? Second, does AIS damage cause neurodegeneration? Third, is AIS damage found in Black Americans with AD? Fourth, is TRIIM46 and LAMP1 co-localization reflective of AIS damage? And

if so, is the mechanism xcTauO-induced activation of calpain-mediated cyclin-dependent kinase five phosphorylation of TRIM46 at serine 106?

References

[1] Niotis K, Akiyoshi K, Carlton C, Isaacson R (2022) Dementia Prevention in Clinical Practice. *Semin Neurol* **42**, 525–548.

[2] Gorman AM (2008) Neuronal cell death in neurodegenerative diseases: recurring themes around protein handling. *J Cell Mol Med* **12**, 2263.

[3] Gao HM, Hong JS (2008) Why neurodegenerative diseases are progressive: uncontrolled inflammation drives disease progression. *Trends Immunol* **29**, 357.

[4] Nagappan PG, Chen H, Wang DY (2020) Neuroregeneration and plasticity: a review of the physiological mechanisms for achieving functional recovery postinjury. *Mil Med Res* **7**,.

[5] Winckler B, Forscher P, Mellman I (1999) A diffusion barrier maintains distribution of membrane proteins in polarized neurons. *Nature* **397**, 698–701.

[6] Leterrier C (2018) *The Axon Initial Segment: An Updated Viewpoint*.

[7] Foust A, Popovic M, Zecevic D, McCormick DA (2010) Action Potentials Initiate in the Axon Initial Segment and Propagate through Axon Collaterals Reliably in Cerebellar Purkinje Neurons. *Journal of Neuroscience* **30**, 6891–6902.

[8] Bentley M, Banker G (2016) The cellular mechanisms that maintain neuronal polarity. *Nat Rev Neurosci* **17**, 611–622.

[9] Rasband MN (2010) The axon initial segment and the maintenance of neuronal polarity. *Nature Reviews Neuroscience 2010 11:8* **11**, 552–562.

[10] Saxena S, Caroni P (2011) Selective Neuronal Vulnerability in Neurodegenerative Diseases: from Stressor Thresholds to Degeneration. *Neuron* **71**, 35–48.

[11] Donato A, Kagias K, Zhang Y, Hilliard MA (2019) Neuronal sub-compartmentalization: a strategy to optimize neuronal function. *Biol Rev Camb Philos Soc* **94**, 1023.

[12] Jones SL, Svitkina TM (2016) Axon Initial Segment Cytoskeleton: Architecture, Development, and Role in Neuron Polarity. *Neural Plast* **2016**,.

[13] Moore FB, Baleja JD (2012) Molecular remodeling mechanisms of the neural somatodendritic compartment. *Biochimica et Biophysica Acta (BBA) - Molecular Cell Research* **1823**, 1720–1730.

[14] Leterrier C, Clerc N, Rueda-Boroni F, Montersino A, Dargent B, Castets F (2017) Ankyrin G Membrane Partners Drive the Establishment and Maintenance of the Axon Initial Segment. *Front Cell Neurosci* **11**, 6.

[15] Huang YM, Rasband MN (2016) Organization of the axon initial segment: Actin like a fence. *Journal of Cell Biology* **215**,.

[16] Raghuram V, Werginz P, Fried SI (2019) Scaling of the AIS and Somatodendritic Compartments in α S RGCs. *Front Cell Neurosci* **13**,.

[17] Hamdan H, Lim BC, Torii T, Joshi A, Konning M, Smith C, Palmer DJ, Ng P, Leterrier C, Oses-Prieto JA, Burlingame AL, Rasband MN (2020) Mapping axon initial segment structure and function by multiplexed proximity biotinylation. *Nat Commun* **11**, 1–17.

[18] Grubb MS, Burrone J (2010) Activity-dependent relocation of the axon initial segment fine-tunes neuronal excitability. *Nature* **465**, 1070–1074.

[19] Evans MD, Sammons RP, Lebron S, Dumitrescu AS, Watkins TBK, Uebele VN, Renger JJ, Grubb MS (2013) Calcineurin signaling mediates activity-dependent relocation of the Axon Initial segment. *Journal of Neuroscience* **33**, 6950–6963.

[20] Chand AN, Galliano E, Chesters RA, Grubb MS (2015) A distinct subtype of dopaminergic interneuron displays inverted structural plasticity at the axon initial segment. *Journal of Neuroscience* **35**, 1573–1590.

[21] Yamada R, Kuba H (2016) Structural and Functional Plasticity at the Axon Initial Segment. *Front Cell Neurosci* **10**,.

[22] Evans MD, Dumitrescu AS, Kruijssen DLH, Taylor SE, Grubb MS (2015) Rapid Modulation of Axon Initial Segment Length Influences Repetitive Spike Firing. *Cell Rep* **13**, 1233–1245.

[23] Huang CYM, Rasband MN (2018) Axon initial segments: structure, function, and disease. *Ann N Y Acad Sci* **1420**, 46.

[24] Hernández F, Llorens-Martín M, Bolós M, Pérez M, Cuadros R, Pallas-Bazarra N, Zabala JC, Avila J (2018) New Beginnings in Alzheimer's Disease: The Most Prevalent Tauopathy. *Journal of Alzheimer's Disease* **64**, S529–S534.

[25] Alzheimer's Disease Fact Sheet , Last updated July 8, 2021, Accessed on July 8, 2021.

[26] Leng K, Li E, Eser R, Piergies A, Sit R, Tan M, Neff N, Li SH, Rodriguez RD, Suemoto CK, Leite REP, Ehrenberg AJ, Pasqualucci CA, Seeley WW, Spina S, Heinsen H, Grinberg LT, Kampmann M (2021) Molecular

characterization of selectively vulnerable neurons in Alzheimer's disease. *Nature Neuroscience 2021 24:2* **24**, 276–287.

[27] Jackson WS (2014) Selective vulnerability to neurodegenerative disease: the curious case of Prion Protein. *Dis Model Mech* **7**, 21–29.

[28] Fu H, Hardy J, Duff KE (2018) Selective vulnerability in neurodegenerative diseases. *Nat Neurosci* **21**, 1350.

[29] Roussarie JP, Yao V, Rodriguez-Rodriguez P, Oughtred R, Rust J, Plautz Z, Kasturia S, Albornoz C, Wang W, Schmidt EF, Dannenfelser R, Tadych A, Brichta L, Barnea-Cramer A, Heintz N, Hof PR, Heiman M, Dolinski K, Flajolet M, Troyanskaya OG, Greengard P (2020) Selective Neuronal Vulnerability in Alzheimer's Disease: A Network-Based Analysis. *Neuron* **107**, 821-835.e12.

[30] Sharma A, Kumar Y (2019) Nature's Derivative(s) as Alternative Anti-Alzheimer's Disease Treatments. *J Alzheimers Dis Rep* **3**, 279.

[31] Bloom GS (2014) Amyloid-β and tau: the trigger and bullet in Alzheimer disease pathogenesis. *JAMA Neurol* **71**, 505–508.

[32] Alois Alzheimer (1907) Über eine eigenartige Erkrankung der Hirnrinde. *Allgemeine Zeitschrift fur Psychiatrie und Psychisch-gerichtliche Medizin* **64**, 146–8.

[33] Fuller SC (2006) A STUDY OF THE NEUROFIBRILS IN DEMENTIA PARALYTICA, DEMENTIA SENILIS, CHRONIC ALCOHOLISM, CEREBRAL LUES AND MICROCEPHALIC IDIOCY. *https://doi.org/101176/ajp634415* **63**, 415-468–13.

[34] Fuller SC (2006) A STUDY OF THE MILIARY PLAQUES FOUND IN BRAINS OF THE AGED. *https://doi.org/101176/ajp682147* **68**, 147-220–16.

[35] Armstrong RA (2019) Risk factors for Alzheimer's disease. *Folia Neuropathol* **57**, 87–105.

[36] *FDA-approved treatments for Alzheimer's*.

[37] Ma F, Akolkar H, Xu J, Liu Y, Popova D, Xie J, Youssef MM, Benosman R, Hart RP, Herrup K (2023) The Amyloid Precursor Protein Modulates the Position and Length of the Axon Initial Segment. *Journal of Neuroscience* **43**, 1830–1844.

[38] Ferreira da Silva T, Granadeiro LS, Bessa-Neto D, Luz LL, Safronov B V., Brites P (2021) Plasmalogens regulate the AKT-ULK1 signaling pathway to control the position of the axon initial segment. *Prog Neurobiol* **205**,.

[39] Sun Z, Wang B, Chen C, Li C, Zhang Y (2021) 5-HT6R null mutatrion induces synaptic and cognitive defects. *Aging Cell* **20**,.

[40] Martinsson I, Quintino L, Garcia MG, Konings SC, Torres-Garcia L, Svanbergsson A, Stange O, England R, Deierborg T, Li JY, Lundberg C, Gouras GK (2022) Aβ/Amyloid Precursor Protein-Induced Hyperexcitability and Dysregulation of Homeostatic Synaptic Plasticity in Neuron Models of Alzheimer's Disease. *Front Aging Neurosci* **14**,.

[41] Chen Z, Peng L, Zhao M, Tao L, Zou P, Zhang Y (2021) Axon Initial Segment Pathology in Alzheimer's Disease Mouse Model Disturbs the Action Potential Initiation and Propagation.

[42] Thi Huong Luu Le L, Lee J, Im D, Park S, Hwang K-D, Hoon Lee J, Jiang Y, Lee Y-S, Ho Suh Y, Kim HI, Jae Lee M Self-aggregating Tau Fragments Recapitulate Pathologic Phenotypes and Neurotoxicity of Alzheimer's Disease in Mice.

[43] Marin MA, Ziburkus J, Jankowsky J, Rasband MN (2016) Amyloid-β Plaques Disrupt Axon Initial Segments. *Exp Neurol* **281**, 93–98.

[44] Best MN, Lim Y, Ferenc NN, Kim N, Min L, Bigler Wang D, Sharifi K, Wasserman AE, McTavish SA, Siller K, Jones MK, Jenkins PM, Mandell JW, Bloom GS (2023) Extracellular Tau Oligomers Damage the Axon Initial Segment. *J Alzheimers Dis*.

[45] Tsushima H, Emanuele M, Polenghi A, Esposito A, Vassalli M, Barberis A, Difato F, Chieregatti E (2015) HDAC6 and RhoA are novel players in Abeta-driven disruption of neuronal polarity. *Nat Commun* **6**, 7781.

[46] Antón-Fernández A, León-Espinosa G, DeFelipe J, Muñoz A (2022) Pyramidal cell axon initial segment in Alzheimer´s disease. *Scientific Reports 2022 12:1* **12**, 1–11.

[47] Hu L, Wang B, Zhang Y (2017) Serotonin 5-HT6 receptors affect cognition in a mouse model of Alzheimer's disease by regulating cilia function. *Alzheimers Res Ther* **9**,.

[48] Hsu WCJ, Wildburger NC, Haidacher SJ, Nenov MN, Folorunso O, Singh AK, Chesson BC, Franklin WF, Cortez I, Sadygov RG, Dineley KT, Rudra JS, Taglialatela G, Lichti CF, Denner L, Laezza F (2017) PPARgamma agonists rescue increased phosphorylation of FGF14 at S226 in the Tg2576 mouse model of Alzheimer's disease. *Exp Neurol* **295**, 1–17.

[49] Zempel H, Dennissen F, Kumar Y, Luedtke J, Biernat J, Mandelkow E-M, Mandelkow E (2017) Axodendritic sorting and pathological missorting of Tau is isoform specific and determined by axon initial segment architecture. *Journal of Biological Chemistry* **292**, 12192–12207.

[50] Wang X, Zhang XG, Zhou TT, Li N, Jang CY, Xiao ZC, Ma QH, Li S (2016) Elevated neuronal excitability due to modulation of the voltage-gated sodium channel Nav1.6 by Aβ1-42. *Front Neurosci* **10**, 94.

[51] Sun X, Wu Y, Gu M, Zhang Y (2014) miR-342-5p Decreases Ankyrin G Levels in Alzheimer's Disease Transgenic Mouse Models. *Cell Rep* **6**, 264–270.

[52] Santuccione AC, Merlini M, Shetty A, Tackenberg C, Bali J, Ferretti MT, McAfoose J, Kulic L, Bernreuther C, Welt T, Grimm J, Glatzel M, Rajendran L, Hock C, Nitsch RM (2013) Active vaccination with ankyrin G reduces β-amyloid pathology in APP transgenic mice. *Mol Psychiatry* **18**, 358–368.

[53] Sun X, Wu Y, Gu M, Liu Z, Ma Y, Li J, Zhang Y (2014) Selective filtering defect at the axon initial segment in Alzheimer's disease mouse models. *Proceedings of the National Academy of Sciences* **111**, 14271–14276.

[54] Sohn PD, Tracy TE, Son H-I, Zhou Y, Leite REP, Miller BL, Seeley WW, Grinberg LT, Gan L (2016) Acetylated tau destabilizes the cytoskeleton in the axon initial segment and is mislocalized to the somatodendritic compartment. *Mol Neurodegener* **11**, 47.

[55] Sanchez-Mut J V., Aso E, Panayotis N, Lott I, Dierssen M, Rabano A, Urdinguio RG, Fernandez AF, Astudillo A, Martin-Subero JI, Balint B,

Fraga MF, Gomez A, Gurnot C, Roux JC, Avila J, Hensch TK, Ferrer I, Esteller M (2013) DNA methylation map of mouse and human brain identifies target genes in Alzheimer's disease. *Brain* **136**, 3018–3027.

[56] Sos KE, Mayer MI, Takács VT, Major A, Bardóczi Z, Beres BM, Szeles T, Saito T, Saido TC, Mody I, Freund TF, Nyiri G (2020) Amyloid β induces interneuron-specific changes in the hippocampus of APPNL-F mice. *PLoS One* **15**,.

[57] Stroobants S, D'Hooge R, Damme M (2021) Aged Tmem106b knockout mice display gait deficits in coincidence with Purkinje cell loss and only limited signs of non-motor dysfunction. *Brain Pathol* **31**, 223–238.

[58] Butler VJ, Salazar DA, Soriano-Castell D, Alves-Ferreira M, Dennissen FJA, Vohra M, Oses-Prieto JA, Li KH, Wang AL, Jing B, Li B, Groisman A, Gutierrez E, Mooney S, Burlingame AL, Ashrafi K, Mandelkow EM, Encalada SE, Kao AW (2019) Tau/MAPT disease-associated variant A152T alters tau function and toxicity via impaired retrograde axonal transport. *Hum Mol Genet* **28**, 1498.

[59] Li X, Kumar Y, Zempel H, Mandelkow E-M, Biernat J, Mandelkow E (2011) Novel diffusion barrier for axonal retention of Tau in neurons and its failure in neurodegeneration. *EMBO J* **30**, 4825–37.

[60] Wang Y, Guan M, Wang H, Li Y, Zhanghao K, Xi P, Zhang Y (2021) The largest isoform of Ankyrin-G is required for lattice structure of the axon initial segment. *Biochem Biophys Res Commun* **578**, 28–34.

[61] Zarei S, Carr K, Reiley L, Diaz K, Guerra O, Altamirano PF, Pagani W, Lodin D, Orozco G, Chinea A (2015) A comprehensive review of amyotrophic lateral sclerosis. *Surg Neurol Int* **6**,.

[62] Hulisz D (2018) Amyotrophic lateral sclerosis: disease state overview. *Am J Manag Care* **24**, S320–S326.

[63] Yu Y, Su FC, Callaghan BC, Goutman SA, Batterman SA, Feldman EL (2014) Environmental Risk Factors and Amyotrophic Lateral Sclerosis (ALS): A Case-Control Study of ALS in Michigan. *PLoS One* **9**, 101186.

[64] Jørgensen HS, Jensen DB, Dimintiyanova KP, Bonnevie VS, Hedegaard A, Lehnhoff J, Moldovan M, Grondahl L, Meehan CF (2021) Increased Axon Initial Segment Length Results in Increased Na+ Currents in Spinal Motoneurones at Symptom Onset in the G127X SOD1 Mouse Model of Amyotrophic Lateral Sclerosis. *Neuroscience* **468**, 247–264.

[65] Mejzini R, Flynn LL, Pitout IL, Fletcher S, Wilton SD, Akkari PA (2019) ALS Genetics, Mechanisms, and Therapeutics: Where Are We Now? *Front Neurosci* **13**,.

[66] Taylor CP, Traynelis SF, Siffert J, Pope LE, Matsumoto RR (2016) Pharmacology of dextromethorphan: Relevance to dextromethorphan/quinidine (Nuedexta®) clinical use. *Pharmacol Ther* **164**, 170–182.

[67] Cai M, Yang EJ (2019) Complementary and alternative medicine for treating amyotrophic lateral sclerosis: a narrative review. *Integr Med Res* **8**, 234–239.

[68] Genç B, Gautam M, Helmold BR, Koçak N, Günay A, Goshu GM, Silverman RB, Hande Ozdinler P (2022) NU-9 improves health of hSOD1G93A mouse upper motor neurons in vitro, especially in

combination with riluzole or edaravone. *Scientific Reports 2022 12:1* **12**, 1–11.

[69] Smerdon JW (2019) Axon Initial Segment Plasticity in Mouse Models of Amyotrophic Lateral Sclerosis. *Columbia University*.

[70] Kiryu-Seo S, Matsushita R, Tashiro Y, Yoshimura T, Iguchi Y, Katsuno M, Takahashi R, Kiyama H (2022) Impaired disassembly of the axon initial segment restricts mitochondrial entry into damaged axons. *EMBO J* **41**, e110486.

[71] Harley P, Neves G, Riccio F, Machado CB, Cheesbrough A, R'Bibo L, Burrone J, Lieberam I (2022) Pathogenic TDP-43 Disrupts Axon Initial Segment Structure and Neuronal Excitability in a Human iPSC Model of ALS. *bioRxiv* 2022.05.16.492186.

[72] Bos R, Rihan K, Quintana P, El-Bazzal L, Bernard-Marissal N, Da Silva N, Jabbour R, Mégarbané A, Bartoli M, Brocard F, Delague V (2022) Altered action potential waveform and shorter axonal initial segment in hiPSC-derived motor neurons with mutations in VRK1. *Neurobiol Dis* **164**, 105609.

[73] Bonnevie VS, Dimintiyanova KP, Hedegaard A, Lehnhoff J, Grøndahl L, Moldovan M, Meehan CF (2020) Shorter axon initial segments do not cause repetitive firing impairments in the adult presymptomatic G127X SOD-1 Amyotrophic Lateral Sclerosis mouse. *Sci Rep* **10**, 1–16.

[74] Sasaki S, Maruyama S (1992) Increase in diameter of the axonal initial segment is an early change in amyotrophic lateral sclerosis. *J Neurol Sci* **110**, 114–120.

[75] Sasaki S, Maruyama S, Yamane K, Sakuma H, Takeishi M (1990) Ultrastructure of swollen proximal axons of anterior horn neurons in motor neuron disease. *J Neurol Sci* **97**, 233–240.

[76] Sasaki S, Iwata M (2007) Mitochondrial alterations in the spinal cord of patients with sporadic amyotrophic lateral sclerosis. *J Neuropathol Exp Neurol* **66**, 10–16.

[77] Sasaki S, Warita H, Abe K, Iwata M (2005) Impairment of axonal transport in the axon hillock and the initial segment of anterior horn neurons in transgenic mice with a G93A mutant SOD1 gene. *Acta Neuropathol* **110**, 48–56.

[78] Pîrşcoveanu DFV, Pirici I, Tudorică V, Bălşeanu TA, Albu VC, Bondari S, Bumbea AM, Pîrşcoveanu M (2017) Tau protein in neurodegenerative diseases - a review. *Rom J Morphol Embryol* **58**, 1141–1150.

[79] Olney NT, Spina S, Miller BL (2017) Frontotemporal Dementia. *Neurol Clin* **35**, 339.

[80] Frontotemporal dementia - Symptoms and causes, Last updated 2021, Accessed on 2021.

[81] Tsai RM, Boxer AL (2014) Treatment of frontotemporal dementia. *Curr Treat Options Neurol* **16**, 1–14.

[82] Caselli RJ, Yaari R (2007) Medical management of frontotemporal dementia. *Am J Alzheimers Dis Other Demen* **22**, 489–498.

[83] Lüningschrör P, Werner G, Stroobants S, Kakuta S, Dombert B, Sinske D, Wanner R, Lüllmann-Rauch R, Wefers B, Wurst W, D'Hooge R, Uchiyama Y, Sendtner M, Haass C, Saftig P, Knöll B, Capell A, Damme

M (2020) The FTLD Risk Factor TMEM106B Regulates the Transport of Lysosomes at the Axon Initial Segment of Motoneurons. *Cell Rep* **30**, 3506–3519.

[84] Feng T, Mai S, Roscoe JM, Sheng RR, Ullah M, Zhang J, Katz II, Yu H, Xiong W, Hu F (2020) Loss of TMEM106B and PGRN leads to severe lysosomal abnormalities and neurodegeneration in mice. *EMBO Rep* **21**,.

[85] Sohn PD, Huang CT-L, Yan R, Fan L, Tracy TE, Camargo CM, Montgomery KM, Arhar T, Mok S-A, Freilich R, Baik J, He M, Gong S, Roberson ED, Karch CM, Gestwicki JE, Xu K, Kosik KS, Gan L (2019) Pathogenic Tau Impairs Axon Initial Segment Plasticity and Excitability Homeostasis. *Neuron* **104**, 458–470.

[86] Hatch RJ, Wei Y, Xia D, Götz J (2017) Hyperphosphorylated tau causes reduced hippocampal CA1 excitability by relocating the axon initial segment. *Acta Neuropathol* **133**, 717–730.

[87] Ghasemi N, Razavi S, Nikzad E (2017) Multiple Sclerosis: Pathogenesis, Symptoms, Diagnoses and Cell-Based Therapy. *Cell Journal (Yakhteh)* **19**, 1.

[88] Goldenberg MM (2012) Multiple Sclerosis Review. *Pharmacy and Therapeutics* **37**, 175.

[89] Murray TJ (2005) Multiple Sclerosis: A History of a Disease. *J R Soc Med* **98**,.

[90] Hamada MS, Kole MHP (2015) Myelin loss and axonal ion channel adaptations associated with gray matter neuronal hyperexcitability. *Journal of Neuroscience* **35**, 7272–7286.

[91] Senol AD, Pinto G, Beau M, Guillemot V, Dupree JL, Stadelmann C, Ranft J, Lubetzki C, Davenne M (2022) Alterations of the axon initial segment in multiple sclerosis. *bioRxiv* 2022.03.07.483302.

[92] Thummala SK (2015) Axon Initial Segment Stability in Multiple Sclerosis.

[93] Mathey EK, Derfuss T, Storch MK, Williams KR, Hales K, Woolley DR, Al-Hayani A, Davies SN, Rasband MN, Olsson T, Moldenhauer A, Velhin S, Hohlfeld R, Meinl E, Linington C (2007) Neurofascin as a novel target for autoantibody-mediated axonal injury. *J Exp Med* **204**, 2363–2372.

[94] Armstrong MJ, Okun MS (2020) Diagnosis and Treatment of Parkinson Disease: A Review. *JAMA* **323**, 548–560.

[95] Radulovic J, Ivkovic S, Adzic M (2022) From chronic stress and anxiety to neurodegeneration: Focus on neuromodulation of the axon initial segment. *Handb Clin Neurol* **184**, 481–495.

[96] Poewe W, Seppi K, Tanner CM, Halliday GM, Brundin P, Volkmann J, Schrag AE, Lang AE (2017) Parkinson disease. *Nature Reviews Disease Primers 2017 3:1* **3**, 1–21.

[97] Jankovic J, Tan EK (2020) Parkinson's disease: etiopathogenesis and treatment. *J Neurol Neurosurg Psychiatry* **91**, 795–808.

[98] Andorfer C, Kress Y, Espinoza M, De Silva R, Tucker KL, Barde YA, Duff K, Davies P (2003) Hyperphosphorylation and aggregation of tau in mice expressing normal human tau isoforms. *J Neurochem* **86**, 582–590.

[99] Bennett DA, Schneider JA, Wilson RS, Bienias JL, Arnold SE (2004) Neurofibrillary Tangles Mediate the Association of Amyloid Load With Clinical Alzheimer Disease and Level of Cognitive Function. *Arch Neurol* **61**, 378–384.

[100] Lacosta AM, Insua D, Badi H, Pesini P, Sarasa M (2017) Neurofibrillary Tangles of Aβx-40 in Alzheimer's Disease Brains. *Journal of Alzheimer's Disease* **58**, 661–667.

[101] Iqbal K, Gong C-X, Liu F (2013) Hyperphosphorylation-induced tau oligomers. *Front Neurol* **4**, 1–9.

[102] Holmes BB, Furman JL, Mahan TE, Yamasaki TR, Mirbaha H, Eades WC, Belaygorod L, Cairns NJ, Holtzman DM, Diamond MI (2014) Proteopathic tau seeding predicts tauopathy in vivo. *Proc Natl Acad Sci U S A* **111**, 4376–4385.

[103] Frost B, Diamond MI (2010) *Prion-like Mechanisms in Neurodegenerative Diseases*.

[104] Holmes BB, Diamond MI (2014) Prion-like Properties of Tau Protein: The Importance of Extracellular Tau as a Therapeutic Target. *Journal of Biological Chemistry* **289**, 19855–19861.

[105] Mirbaha H, Chen D, Mullapudi V, Terpack SJ, White CL, Joachimiak LA, Diamond MI (2022) Seed-competent tau monomer initiates pathology in a tauopathy mouse model. *Journal of Biological Chemistry* **298**, 1–9.

[106] Karch CM, Jeng AT, Goate AM (2013) Calcium phosphatase calcineurin influences tau metabolism. *Neurobiol Aging* **34**, 374–386.

[107] Bright J, Hussain S, Dang V, Wright S, Cooper B, Byun T, Ramos C, Singh A, Parry G, Stagliano N, Griswold-Prenner I (2015) Human secreted tau increases amyloid-beta production. *Neurobiol Aging* **36**, 693–709.

[108] Kanmert D, Cantlon A, Muratore CR, Jin M, O'Malley TT, Lee G, Young-Pearse TL, Selkoe DJ, Walsh DM (2015) C-terminally truncated forms of tau, but not full-length tau or its C-terminal fragments, are released from neurons independently of cell death. *Journal of Neuroscience* **35**, 10851–10865.

[109] Chai X, Dage JL, Citron M (2012) Constitutive secretion of tau protein by an unconventional mechanism. *Neurobiol Dis* **48**, 356–366.

[110] Yamada K, Cirrito JR, Stewart FR, Jiang H, Finn MB, Holmes BB, Binder LI, Mandelkow EM, Diamond MI, Lee VMY, Holtzman DM (2011) In vivo microdialysis reveals age-dependent decrease of brain interstitial fluid tau levels in P301S human tau transgenic mice. *Journal of Neuroscience* **31**, 13110–13117.

[111] Magnoni S, Esparza TJ, Conte V, Carbonara M, Carrabba G, Holtzman DM, Zipfel GJ, Stocchetti N, Brody DL (2012) Tau elevations in the brain extracellular space correlate with reduced amyloid-β levels and predict adverse clinical outcomes after severe traumatic brain injury. *Brain* **135**, 1268–1280.

[112] Swanson E, Breckenridge L, McMahon L, Som S, McConnell I, Bloom GS (2017) Extracellular Tau Oligomers Induce Invasion of Endogenous Tau into the Somatodendritic Compartment and Axonal Transport Dysfunction. *Journal of Alzheimer's Disease* **58**, 803–820.

[113] Li C, Götz J (2017) Somatodendritic accumulation of Tau in Alzheimer's disease is promoted by Fyn-mediated local protein translation. *EMBO J* **36**, 3120–3138.

[114] Kobayashi S, Tanaka T, Soeda Y, Almeida OFX, Takashima A (2017) Local Somatodendritic Translation and Hyperphosphorylation of Tau Protein Triggered by AMPA and NMDA Receptor Stimulation. *EBioMedicine* **20**, 120–126.

[115] Ittner A, Ittner LM (2018) Dendritic Tau in Alzheimer's Disease. *Neuron* **99**, 13–27.

[116] Ittner LM, Ke YD, Delerue F, Bi M, Gladbach A, van Eersel J, Wölfing H, Chieng BC, Christie MJ, Napier IA, Eckert A, Staufenbiel M, Hardeman E, Götz J (2010) Dendritic function of tau mediates amyloid-beta toxicity in Alzheimer's disease mouse models. *Cell* **142**, 387–397.

[117] Usenovic M, Niroomand S, Drolet RE, Yao L, Gaspar RC, Hatcher NG, Schachter J, Renger JJ, Parmentier-Batteur S (2015) Internalized Tau Oligomers Cause Neurodegeneration by Inducing Accumulation of Pathogenic Tau in Human Neurons Derived from Induced Pluripotent Stem Cells. *Journal of Neuroscience* **35**, 14234–14250.

[118] Hill E, Karikari TK, Moffat KG, Richardson MJE, Wall MJ (2019) Introduction of Tau Oligomers into Cortical Neurons Alters Action Potential Dynamics and Disrupts Synaptic Transmission and Plasticity. *eNeuro* **6**, 1–20.

[119] Sobotzik JM, Sie JM, Politi C, Del Turco D, Bennett V, Deller T, Schultz C (2009) AnkyrinG is required to maintain axo-dendritic polarity in vivo. *Proc Natl Acad Sci U S A* **106**, 17564–17569.

[120] Zonta B, Desmazieres A, Rinaldi A, Tait S, Sherman DL, Nolan MF, Brophy PJ (2011) A Critical Role for Neurofascin in Regulating Action Potential Initiation through Maintenance of the Axon Initial Segment. *Neuron* **69**, 945–956.

[121] Gulledge AT, Bravo JJ (2016) Neuron Morphology Influences Axon Initial Segment Plasticity. *eNeuro* **3**, 255–265.

[122] Höfflin F, Jack A, Riedel C, Mack-Bucher J, Roos J, Corcelli C, Schultz C, Wahle P, Engelhardt M (2017) Heterogeneity of the axon initial segment in interneurons and pyramidal cells of rodent visual cortex. *Front Cell Neurosci* **11**, 1–17.

[123] Nelson AD, Caballero-Florán RN, Rodríguez Díaz JC, Hull JM, Yuan Y, Li J, Chen K, Walder KK, Lopez-Santiago LF, Bennett V, McInnis MG, Isom LL, Wang C, Zhang M, Jones KS, Jenkins PM (2020) Ankyrin-G regulates forebrain connectivity and network synchronization via interaction with GABARAP. *Mol Psychiatry* **25**, 2800–2817.

[124] Jenkins PM, Kim N, Jones SL, Tseng WC, Svitkina TM, Yin HH, Bennett V (2015) Giant ankyrin-G: A critical innovation in vertebrate evolution of fast and integrated neuronal signaling. *Proc Natl Acad Sci U S A* **112**, 957–964.

[125] Zhou D, Lambert S, Malen PL, Carpenter S, Boland LM, Bennett V (1998) AnkyrinG is required for clustering of voltage-gated Na channels at axon initial segments and for normal action potential firing. *Journal of Cell Biology* **143**, 1295–1304.

[126] Kordeli E, Lambert S, Bennett V (1995) AnkyrinG: A new ankyrin gene with neural-specific isoforms localized at the axonal initial segment and node of Ranvier. *Journal of Biological Chemistry* **270**, 2352–2359.

[127] Hedstrom KL, Ogawa Y, Rasband MN (2008) AnkyrinG is required for maintenance of the axon initial segment and neuronal polarity. *Journal of Cell Biology* **183**, 635–640.

[128] Salzer JL (2019) An unfolding role for ankyrin-G at the axon initial segment. *Proc Natl Acad Sci U S A* **116**, 19228–19230.

[129] Farías GG, Fréal A, Tortosa E, Stucchi R, Pan X, Portegies S, Will L, Altelaar M, Hoogenraad CC (2019) Feedback-Driven Mechanisms between Microtubules and the Endoplasmic Reticulum Instruct Neuronal Polarity. *Neuron* **102**, 184–201.

[130] Berghs S, Aggujaro D, Dirkx R, Maksimova E, Stabach P, Hermel JM, Zhang JP, Philbrick W, Slepnev V, Ort T, Solimena M, Solimena M (2000) βiv Spectrin, a New Spectrin Localized at Axon Initial Segments and Nodes of Ranvier in the Central and Peripheral Nervous System. *Journal of Cell Biology* **151**, 985–1002.

[131] Yang Y, Ogawa Y, Hedstrom KL, Rasband MN (2007) βIV spectrin is recruited to axon initial segments and nodes of Ranvier by ankyrinG. *Journal of Cell Biology* **176**, 509–519.

[132] Komada M, Soriano P (2002) βIV-spectrin regulates sodium channel clustering through ankyrin-G at axon initial segments and nodes of Ranvier. *Journal of Cell Biology* **156**, 337–348.

[133] Yang Y, Lacas-Gervais S, Morest DK, Solimena M, Rasband MN (2004) βIV Spectrins Are Essential for Membrane Stability and the Molecular

Organization of Nodes of Ranvier. *Journal of Neuroscience* **24**, 7230–7240.

[134] Fréal A, Rai D, Tas RP, Pan X, Katrukha EA, van de Willige D, Stucchi R, Aher A, Yang C, Altelaar AFM, Vocking K, Post JA, Harterink M, Kapitein LC, Akhmanova A, Hoogenraad CC (2019) Feedback-Driven Assembly of the Axon Initial Segment. *Neuron* **104**, 305–321.

[135] Alpizar SA, Baker AL, Gulledge AT, Hoppa MB (2019) Loss of Neurofascin-186 Disrupts Alignment of AnkyrinG Relative to Its Binding Partners in the Axon Initial Segment. *Front Cell Neurosci* **13**, 1–15.

[136] Hedstrom KL, Xu X, Ogawa Y, Frischknecht R, Seidenbecher CI, Shrager P, Rasband MN (2007) Neurofascin assembles a specialized extracellular matrix at the axon initial segment. *Journal of Cell Biology* **178**, 875–886.

[137] Van Beuningen SFB, Will L, Harterink M, Chazeau A, Van Battum EY, Frias CP, Franker MAM, Katrukha EA, Stucchi R, Vocking K, Antunes AT, Slenders L, Doulkeridou S, Sillevis Smitt P, Altelaar AFM, Post JA, Akhmanova A, Pasterkamp RJ, Kapitein LC, de Graaff E, Hoogenraad CC (2015) TRIM46 Controls Neuronal Polarity and Axon Specification by Driving the Formation of Parallel Microtubule Arrays. *Neuron* **88**, 1208–1226.

[138] Harterink M, Vocking K, Pan X, Soriano Jerez EM, Slenders L, Fréal A, Tas RP, van de Wetering WJ, Timmer K, Motshagen J, van Beuningen SFB, Kapitein LC, Geerts WJC, Post JA, Hoogenraad CC (2019) TRIM46 Organizes Microtubule Fasciculation in the Axon Initial Segment. *Journal of Neuroscience* **39**, 4864–4873.

[139] Ichinose S, Ogawa T, Jiang X, Hirokawa N (2019) The Spatiotemporal Construction of the Axon Initial Segment via KIF3/KAP3/TRIM46 Transport under MARK2 Signaling. *Cell Rep* **28**, 2413–2426.

[140] León-Espinosa G, DeFelipe J, Muñoz A (2012) Effects of Amyloid-β Plaque Proximity on the Axon Initial Segment of Pyramidal Cells. *Journal of Alzheimer's Disease* **29**, 841–852.

[141] Kaech S, Banker G (2006) Culturing hippocampal neurons. *Nat Protoc* **1**, 2406–2415.

[142] Seward ME, Swanson E, Norambuena A, Reimann A, Cochran JN, Li R, Roberson ED, Bloom GS (2013) Amyloid-β signals through tau to drive ectopic neuronal cell cycle re-entry in Alzheimer's disease. *J Cell Sci* **126**, 1278–1286.

[143] Combs B, Tiernan CT, Hamel C, Kanaan NM (2017) Production of recombinant tau oligomers in vitro. *Methods Cell Biol* **141**, 45–64.

[144] Jenkins PM, Vasavda C, Hostettler J, Davis JQ, Abdi K, Bennett V (2013) E-cadherin Polarity Is Determined by a Multifunction Motif Mediating Lateral Membrane Retention through Ankyrin-G and Apical-lateral Transcytosis through Clathrin. *Journal of Biological Chemistry* **288**, 14018–14031.

[145] Patterson KR, Remmers C, Fu Y, Brooker S, Kanaan NM, Vana L, Ward S, Reyes JF, Philibert K, Glucksman MJ, Binder LI (2011) Characterization of Prefibrillar Tau Oligomers in Vitro and in Alzheimer Disease. *Journal of Biological Chemistry* **286**, 23063–23076.

[146] Kuba H, Oichi Y, Ohmori H (2010) Presynaptic activity regulates Na(+) channel distribution at the axon initial segment. *Nature* **465**, 1075–1078.

[147] Dawson HN, Ferreira A, Eyster M V., Ghoshal N, Binder LI, Vitek MP (2001) Inhibition of neuronal maturation in primary hippocampal neurons from tau deficient mice. *J Cell Sci* **114**, 1179–1187.

[148] León-Espinosa G, Defelipe J, Muoz A (2012) Effects of amyloid-β plaque proximity on the axon initial segment of pyramidal cells. *Journal of Alzheimer's Disease* **29**, 841–852.

[149] Meza RC, López-Jury L, Canavier CC, Henny P (2018) Role of the Axon Initial Segment in the Control of Spontaneous Frequency of Nigral Dopaminergic Neurons In Vivo. *Journal of Neuroscience* **38**, 733–744.

[150] Martínez-Silva M de L, Imhoff-Manuel RD, Sharma A, Heckman CJ, Shneider NA, Roselli F, Zytnicki D, Manuel M (2018) Hypoexcitability precedes denervation in the large fast-contracting motor units in two unrelated mouse models of ALS. *Elife* **7**, 1–26.

[151] Elliott CL, Ryan L, Silverberg N (2021) Building Inclusive and Open Alzheimer Disease and Alzheimer Disease–Related Dementias Research Programs. *JAMA Neurol* **78**, 1177–1178.

[152] Raman R, Quiroz YT, Langford O, Choi J, Ritchie M, Baumgartner M, Rentz D, Aggarwal NT, Aisen P, Sperling R, Grill JD (2021) Disparities by Race and Ethnicity Among Adults Recruited for a Preclinical Alzheimer Disease Trial. *JAMA Netw Open* **4**, 1–12.

[153] Dilworth-Anderson P (2011) Introduction to the science of recruitment and retention among ethnically diverse populations. *Gerontologist* **51**, 1–4.

[154] Dilworth-Anderson P, Cohen MD (2010) Beyond diversity to inclusion: recruitment and retention of diverse groups in Alzheimer research. *Alzheimer Dis Assoc Disord* **24**, 14–18.

[155] Deters KD, Napolioni V, Sperling RA, Greicius MD, Mayeux R, Hohman T, Mormino EC (2021) Amyloid PET Imaging in Self-Identified Non-Hispanic Black Participants of the Anti-Amyloid in Asymptomatic Alzheimer's Disease (A4) Study. *Neurology* **96**, 1491–1500.

[156] Plassman BL, Langa KM, Fisher GG, Heeringa SG, Weir DR, Ofstedal MB, Burke JR, Hurd MD, Potter GG, Rodgers WL, Steffens DC, Willis RJ, Wallace RB (2007) Prevalence of Dementia in the United States: The Aging, Demographics, and Memory Study. *Neuroepidemiology* **29**, 125–132.

[157] Chang H-Y, Sang T-K, Chiang A-S (2018) Untangling the Tauopathy for Alzheimer's disease and parkinsonism. *J Biomed Sci* **25**, 54.

[158] Weingarten MD, Lockwood AH, Hwo S-Y, Kirschner MW (1975) *A Protein Factor Essential for Microtubule Assembly (tau factor/tubulin/electron microscopy/phosphocellulose)*.

[159] Iba M, Guo JL, McBride JD, Zhang B, Trojanowski JQ, Lee VMY (2013) Synthetic Tau Fibrils Mediate Transmission of Neurofibrillary Tangles in a Transgenic Mouse Model of Alzheimer's-Like Tauopathy. *The Journal of Neuroscience* **33**, 1024.

[160] C A, CM A, Y K, PR H, K D, P D (2005) Cell-cycle reentry and cell death in transgenic mice expressing nonmutant human tau isoforms. *J Neurosci* **25**, 5446–5454.

[161] Brunden KR, Trojanowski JQ, Lee VM-Y (2008) Evidence That Non-Fibrillar Tau Causes Pathology Linked To Neurodegeneration And Behavioral Impairments. *J Alzheimers Dis* **14**, 393.

[162] Lasagna-Reeves CA, Castillo-Carranza DL, Sengupta U, Clos AL, Jackson GR, Kayed R (2011) Tau oligomers impair memory and induce synaptic and mitochondrial dysfunction in wild-type mice. *Mol Neurodegener* **6**,.

[163] Bloom GS (2014) Amyloid-β and Tau. *JAMA Neurol* **71**, 505.

[164] Guo JL, Lee VMY (2014) Cell-to-cell transmission of pathogenic proteins in neurodegenerative diseases. *Nat Med* **20**, 130.

[165] Trunova S, Baek B, Giniger E (2011) Cdk5 regulates the size of an axon initial segment-like compartment in mushroom body neurons of the Drosophila central brain. *Journal of Neuroscience* **31**, 10451–10462.

[166] Allnutt AB, Waters AK, Kesari S, Yenugonda VM (2020) Physiological and Pathological Roles of Cdk5: Potential Directions for Therapeutic Targeting in Neurodegenerative Disease. *ACS Chem Neurosci* **11**, 1218–1230.

[167] Liu SL, Wang C, Jiang T, Tan L, Xing A, Yu JT (2016) The Role of Cdk5 in Alzheimer's Disease. *Mol Neurobiol* **53**, 4328–4342.

[168] Ishii S, Matsuura A, Itakura E (2019) Identification of a factor controlling lysosomal homeostasis using a novel lysosomal trafficking probe. *Sci Rep* **9**,.

[169] Xu K, Rubin H (1990) Cell transformation as aberrant differentiation: Environmentslly dependent spontaneous transformation of NIH 3T3 cells. *Cell Res* **1**, 197–206.

[170] Rahimi AM, Cai M, Hoyer-Fender S (2022) Heterogeneity of the NIH3T3 Fibroblast Cell Line. *Cells* **11**, 1–19.

[171] Norambuena A, Wallrabe H, Cao R, Wang DB, Silva A, Svindrych Z, Periasamy A, Hu S, Kim DY, Tanzi RE, Bloom GS (2018) A Novel Lysosome-to-Mitochondria Signaling Pathway Disrupted by Amyloid--Oligomers. *EMBO J* 1–18.

[172] Sharlow ER, Llaneza DC, Grever WE, Mingledorff GA, Mendelson AJ, Bloom GS, Lazo JS (2022) High content screening miniaturization and single cell imaging of mature human feeder layer-free iPSC-derived neurons. *SLAS Discovery*.

[173] Cibelli A, Veronica Lopez-Quintero S, Mccutcheon S, Scemes E, Spray DC, Stout RF, Suadicani SO, Thi MM, Urban-Maldonado M (2021) Generation and Characterization of Immortalized Mouse Cortical Astrocytes From Wildtype and Connexin43 Knockout Mice. *Front Cell Neurosci* **15**, 1–18.

[174] Schildge S, Bohrer C, Beck K, Schachtrup C (2013) Isolation and Culture of Mouse Cortical Astrocytes. *JoVE* e50079.

[175] Özkan N, Koppers M, van Soest I, van Harten A, Jurriens D, Liv N, Klumperman J, Kapitein LC, Hoogenraad CC, Farías GG (2021) ER – lysosome contacts at a pre-axonal region regulate axonal lysosome availability. *Nature Communications 2021 12:1* **12**, 1–18.

[176] Farías GG, Guardia CM, Britt DJ, Guo X, Bonifacino JS (2015) Sorting of Dendritic and Axonal Vesicles at the Pre-axonal Exclusion Zone. *Cell Rep* **13**, 1221–1232.

[177] Potjewyd FM, Axtman AD (2021) Exploration of Aberrant E3 Ligases Implicated in Alzheimer's Disease and Development of Chemical Tools to Modulate Their Function. *Front Cell Neurosci* **15**, 477.

[178] Courtois-Cox S, Genther Williams SM, Reczek EE, Johnson BW, McGillicuddy LT, Johannessen CM, Hollstein PE, MacCollin M, Cichowski K (2006) A negative feedback signaling network underlies oncogene-induced senescence. *Cancer Cell* **10**, 459–472.